UCLA
UCLA Electronic Theses and Dissertations

Title
Characterization of the role of ephrinB2 in human embryonic stem cell fate

Permalink
https://escholarship.org/uc/item/96q7f2ft

Author
Palomares, Karina

Publication Date
2012

Peer reviewed|Thesis/dissertation

eScholarship.org Powered by the California Digital Library
University of California

UNIVERSITY OF CALIFORNIA

Los Angeles

Characterization of the role of ephrinB2 in human embryonic stem cell fate

A dissertation submitted in partial satisfaction of the
requirements for the degree Doctor of Philosophy
in Microbiology, Immunology, and Molecular Genetics

by

Karina Palomares

2013

ABSTRACT OF THE DISSERTATION

Characterization of the role of ephrinB2 in human embryonic stem cell fate

by

Karina Palomares
Doctor of Philosophy in Microbiology, Immunology, and Molecular Genetics
University of California, Los Angeles, 2013
Professor Benhur Lee, Chair

Human embryonic stem cells (hESCs) have great potential for use in regenerative medicine due to their indefinite capacity for self-renewal and their ability to differentiate into cell types derived from all three embryonic germ layers. An important step toward advancing their use in cell-based therapies is development of methods for directed differentiation into specific lineages. Understanding the signaling pathways that underlie hESC differentiation is critical if we are to achieve the full potential of these cells.

EphrinB-ephB receptor interactions are a common regulator of multiple somatic stem cells, including neural stem cells (NSCs) and hematopoietic stem cells (HSCs). EphrinB2, in particular, has been identified as a molecular stem cell marker shared in mouse embryonic stem cells (ESCs), NSCs, and HSCs. Its receptor, ephB4, has also been implicated in playing a role in ESC differentiation. Despite evidence that the ephrinB2-ephB4 axis may be involved in ESC fate, this axis has not been carefully studied in hESCs due to a lack of highly specific reagents

to interrogate ephrinB2-ephB4 interactions. Here, we characterized the role of ephrinB2 in hESC fate.

First, we developed a novel method to specifically tag ephrinB2 hESCs. We showed that we could efficiently pseudotype a lentiviral vector with the Nipah virus (NiV) envelope that could efficiently target ephrinB2+ cells *in vitro*. These NiV pseudotyped particles specifically transduced a sub-population of hESCs. Next, we sought to further characterize these ephrinB2+ hESCs by FACS-sorting the NiV-transduced GFP+ cells and examining their properties in culture. Passaging of the sorted cells revealed that ephrinB2 does not mark for a stable population of cells, but may be an intrinsic marker of heterogeneity. The ephrinB2+ hESCs demonstrated the abilities to self-renew *in vitro*, to differentiate into the three germ layers *in vitro*, and to form teratomas *in vivo*.

Lastly, to further examine the role of ephrinB2 in hESC fate, we generated a hESC line stably expressing an shRNA against ephrinB2 (shEFNB2). Real-time PCR analysis and microarray analysis of embryoid bodies (EBs) derived from shEFNB2 cells demonstrated a severe deficiency in neuro-ectoderm gene expression and an up-regulation of genes involved in mesendoderm specification. Further, functional mesoderm-directed differentiation assays revealed that shEFNB2 hESCs have an increased propensity to differentiate into one specific sub-type of mesenchymal cells. In sum, the findings of this dissertation suggest that the heterogeneity of ephrinB2 expression and perturbation of ephrinB2 signaling may both be manipulated to enhance directed differentiation of hESCs *in vitro*.

The dissertation of Karina Palomares is approved

April Dawn Pyle

Hanna K.A. Mikkola

Otoniel M. Martinez

Benhur Lee, Committee Chair

University of California, Los Angeles

2013

I dedicate this work to my mother, Josefina, and my father, Manuel.

Their unconditional love and support have made it possible for me to obtain this degree.

TABLE OF CONTENTS

LIST OF FIGURES

CHAPTER 1

CHAPTER 2

CHAPTER 3

CHAPTER 4

LIST OF TABLES

CHAPTER 2

CHAPTER 3

ACKNOWLEDGEMENTS

First and foremost, I would like to thank my thesis advisor and mentor, Dr. Benhur Lee. His constant enthusiasm and excitement for science is truly inspirational and uplifting. He gave me the opportunity to work on a very exciting, yet challenging, project. Although at times I was frustrated, he helped me develop into the scientist I am today. I would especially like to thank my second mentor, Dr. April Pyle. I cannot adequately express my gratitude for her constant support as I transitioned into a new field. Benhur and April were the perfect balance I needed to progress through my graduate career, and I honestly cannot imagine better mentors. In addition, I would like to thank my committee members, Dr. Hanna Mikkola and Dr. Oto Martinez-Maza, for their invaluable guidance throughout the years.

I would like to acknowledge all the past and present members of the Lee lab for their support, collaboration, and most importantly, their friendship. They all contributed to a great lab environment, marked by high productivity but very fun moments as well. I am very lucky to have worked with very talented post-docs and students that contributed to my work and scientific development. Thank you Patrick Hong, Hector Aguilar, Frederic Vigant, Mickey Pentecost, Olivier Pernet, Yao Wang, Arnold Park, and Nic Webb. I am especially grateful to Ruixue Zhang, who contributed her vast expertise and technical support to advancement of my stem cell project. I would also like to thank Kelechi Chikere- my classmate, labmate, and now great friend. We started in the lab at the same time, planned all our committee meetings back to back, and are now graduating at the same time. I would have never come this far without his support and friendship during our long journey in the Lee lab.

I would also like to acknowledge my outstanding scientific collaborators at UCLA. Dr. Koki Morizono provided the rigorous training I needed to undertake my lentiviral project as a first year. Advancement of my stem cell project required collaborations with various stem cell experts, including Dr. Sean Sherman, Dr. Jackelyn Alva, Dr. Ben Van Handel, Dr. Michaela

Patterson, and Dr. Mirko Corselli. I am especially grateful to members of the Pyle lab for all their advice, support, and acceptance into their lab.

Last, but definitely not least, I would like to thank all my friends and family. I have met some of the most amazing people while in graduate school, and have developed long-lasting, meaningful friendships. Thank you Akanksha, Gabriela, Jemima, John, Lynn, Kaushali, Jackie, Faith, Eugene, Michaela, Ben, Mirko, Joey, Aakriti, Adriana, and Ashish. Words cannot express my gratitude to Sean, who was there for me from the beginning and is still here for me now. Finally, I am extremely grateful for the unconditional love and support from my parents throughout the years. I will be forever indebted to them both.

Chapter 2 was recently published in *Journal of Virology*: **Palomares K**, Vigant F, Van Handel B, Pernet O, Chikere K, Hong P, Sherman SP, Patterson M, An DS, Lowry WE, Mikkola HKA, Morizono K, Pyle AD, Lee B. (2012). Nipah virus envelope pseudotyped lentiviruses efficiently target ephrinB2+ stem cell populations *in vitro* and bypass the liver sink when administered *in vivo*. *Journal of Virology*. (Epub ahead of print). It is reprinted here with permission from American Society for Microbiology and all co-authors. The work presented in **Chapter 3** is currently in preparation for a manuscript. The work presented in this dissertation was supported in part by a California Institute for Regenerative Medicine grant RB2-01571 and by NIH grant AI069317-06.

VITA

2004	NSF-REU Undergraduate Research Fellowship University of Notre Dame
2004	Bachelor of Science, Biological Sciences University of Notre Dame
2006-2007	Minority Biomedical Research Support- Research Initiative For Scientific Enhancement (MBRS-RISE) Program Fellowship California State University, Los Angeles
2006-2007	Teaching Assistant Department of Biological Sciences California State University, Los Angeles
2007	Master of Science, Biological Sciences California State University, Los Angeles
2007-2008	Eugene V. Cota-Robles Fellowship University of California, Los Angeles
2009- 2010	Teaching Assistant Department of Microbiology, Immunology and Molecular Genetics University of California, Los Angeles
2011-2012	Graduate Student Mentorship Fellowship University of California, Los Angeles

PUBLICATIONS AND PRESENTATIONS

Palomares K, Vigant F, Van Handel B, Pernet O, Chikere K, Hong P, Sherman SP, Patterson M, An DS, Lowry WE, Mikkola HKA, Morizono K, Pyle AD, Lee B. (2012). Nipah virus envelope pseudotyped lentiviruses efficiently target ephrinB2+ stem cell populations *in vitro* and bypass the liver sink when administered *in vivo*. *Journal of Virology* (In press).

Palomares K, Zhang R, Alva J, Sherman S, Pyle A, Lee B. "EphrinB2 is an intrinsic marker of hESC heterogeneity." 2nd annual Tri-Institutional (UCLA, UCSF, USC) Stem Cell Retreat. Asilomar, CA. 2012. (poster)

Palomares K, Pernet O, Hong P, Morizono K, Pyle A, Chen I, Lee B. "Nipah virus envelope pseudotyped lentiviruses offer novel strategies for targeted gene therapy and efficiently targets ephrinB2+ cells in vitro and in vivo." Keystone Symposia: Cell Biology of Virus Entry, Replication and Pathogenesis. Whistler, British Columbia. 2012. (poster)

Palomares K, Pernet O, Lee B**. "**Nipah Virus Envelope Pseudotyped Lentiviruses and Methods of Use Therefor". U.S. Provisional Application Serial No 61/615,534. Filed 03/2012.

Palomares K, Alva J, Sherman S, Zhang R, Pyle A, Lee B. "EphrinB2 is an intrinsic marker of hESC heterogeneity, and identifies a subset of cells with reduced self-renewal capacity." 2011 CIRM Grantee Meeting. San Francisco, CA. 2011. (poster)

Palomares K., Lee B. "Nipah virus envelope pseudotyped lentiviruses offer novel routes for targeted gene therapy." American Society for Virology 28th Annual Meeting. Vancouver, British Columbia. 2009. (oral presentation)

CHAPTER 1

Introduction

Human embryonic stem cells

Embryonic stem cells (ESCs) are derived from the inner cell mass (ICM) of a preimplantation embryo and are defined by two hallmark characteristics: the ability to self-renew in an undifferentiated state *in vitro* indefinitely; and the potential to differentiate into lineages derived from the three embryonic germ layers *in vitro* and *in vivo*. ESCs were first isolated from a mouse blastocyst in 1981 [1,2], and then derived from a human blastocyst in 1998 [3]. Since ESCs can serve as an unlimited source of any cell type in the body, human ESCs (hESCs) could potentially provide a renewable source of cells for use in transplantation therapy. Thus, hESCs hold great promise for regenerative medicine [4].

hESCs grow as flat, tightly compacted colonies with distinct borders on a mitotically inactivated mouse embryonic fibroblast (MEF) feeder layer. The cells have a high ratio of nucleus to cytoplasm and prominent nucleoli [3]. hESCs express several cell-surface markers that are characteristic of the undifferentiated state, including stage-specific embryonic antigen 3 and 4 (SSEA-3 and SSEA-4) [5], the tumor-recognition antigens (TRA-1-60 and TRA-1-81) [6], and alkaline phosphatase [3]. Although mESCs are maintained in the undifferentiated state in media supplemented with leukemia inhibitory factor (LIF) [7], hESCs do not respond to LIF and require the addition of bFGF for long-term maintenance [8]. Upon the removal of bFGF and cultivation in suspension, hESCs differentiate efficiently *in vitro* and give rise to a differentiated cell mass called embryoid bodies (EBs) [9]. Although EBs are far less complex than the actual embryo, they can partially mimic the spatial organization in the embryo. Thus, hESCs also provide a unique resource for understanding early human development.

Expression of a core set of transcription factors is necessary to maintain the pluripotent state of hESCs. Oct4, Nanog, and Sox2 have been identified as the master regulators that induce and maintain the undifferentiated state [10]. Genome-wide location analysis revealed that these factors co-occupy the promoters of pluripotency genes that are maintained in an active state, as well as the promoters of lineage-specific genes that are repressed but remain poised

for subsequent expression during differentiation [11]. The three factors bind the genes at overlapping sites, suggesting that they act collaboratively to maintain the transcriptional program required for pluripotency. The importance of Oct4, Nanog, and Sox2 was further highlighted by their induction of pluripotency in fibroblasts [12].

hESC differentiation

In order to create renewable sources of cells and tissues for regenerative medicine, hESC differentiation must be controlled to direct cells along specific pathways. Basic developmental biology research has made significant progress in elucidating the molecular basis of gastrulation in the mouse, which can be applied to directed differentiation of hESCs into endoderm, mesoderm, and ectoderm derivatives (reviewed in [13]). Although mouse and human ESCs exhibit some different requirements for growth and maintenance in culture [3], the signaling pathways that regulate mouse epiblast stem cells and hESC differentiation are similar [14].

During embryogenesis, the process of gastrulation generates the 3 germ layers: ectoderm, mesoderm, and endoderm (Fig. 1-1). In the mouse, gastrulation begins with the formation of the primitive streak (PS) [15]. Uncommitted epiblast cells undergo an epithelial-to-mesenchymal transition (EMT), mobilize, traverse the PS, and emerge as either mesoderm or definitive endoderm derivatives based on temporal and spatial factors. Cells that pass through the most posterior end of the PS give rise to the extraembryonic mesoderm, which forms hematopoietic, endothelial, and vascular smooth muscle cells. Cells that migrate through the most anterior end of the PS generate definitive endoderm. Lastly, ectoderm develops from the anterior region of the epiblast that does not enter the PS. Expression analyses of the various regions of the PS have indicated that the Wnt, Nodal, bone morphogenic protein (BMP), and FGF signaling pathways control germ layer development, and thereby the induction of specific lineages (reviewed in [16]).

Manipulation of the BMP, Wnt, Nodal, and FGF pathways with agonists or inhibitors can thus be used to alter lineage specification *in vitro* (Fig. 1-2). Cells progressing through a PS stage are marked by Brachyury or Mixl1 expression, and is dependent on a combination of BMP, Wnt and Nodal signaling. Following this mesoderm induction, further manipulation of the different signaling pathways will generate different subpopulations of mesoderm. Induction with BMP4 leads to an increase in Brachyury and Mixl1 expression, and subsequent formation of KDR+ and PDGFR+ mesoderm, which gives rise to hemangioblasts, precursors with both hematopoietic and endothelial potential [17]. For specification of cardiac mesoderm, transient inhibition of the Wnt pathway is required [18]. Activation of the Nodal signaling pathway with activin efficiently induces definitive endoderm formation in hESCs, marked by expression of the Sox17 and FoxA2 transcription factors [19]. If no serum or other PS inducers are added to cultures, the "default" pathway will follow and neuro-ectoderm will develop, specifically marked by Sox1 expression. Studies in mESCs demonstrated that induction of neuro-ectoderm is dependent on both the inhibition of BMP, Wnt, and activin signaling, as well as the presence of FGF signals endogenously produced by the differentiating cells [20]. Thus, modeling the early steps of embryonic development *in vitro* may provide the best approach for achieving specification of hESCs into the appropriate germ layer and tissue derivatives.

hESC heterogeneity

Although hESCs share basic stem cell characteristics, they also demonstrate a high degree of heterogeneity. Cultures usually contain both undifferentiated stem cells and spontaneously arising differentiated progeny. However, even within colonies, marker expression is heterogeneous. Various studies have shown that different subpopulations can be identified on the basis of their expression of stem-cell surface antigens. For example, for subpopulations isolated on SSEA-3 expression, only the SSEA-3+ cells had clonogenic capacity *in vitro*, and expressed higher levels of Nanog and Oct4 than SSEA-3- cells, but the SSEA-3-

cells still expressed higher levels of these transcription factors than fully differentiated cells [21,22]. These results suggested that SSEA-3- cells are in an intermediate state between the pluripotent state and the fully committed state. Fractionation of hESCs based on expression of two other pluripotency cell-surface markers, GCTM2 and CD9, identified 4 subpopulations that exhibited a quantitative continuous gradient of these markers [12]. The population of cells with the highest level of surface antigen expression also demonstrated the highest levels of pluripotency genes, such as Oct4. Interestingly, cells in the middle of the gradient co-expressed pluripotency and lineage-specific genes, suggesting that some cells are primed for differentiation. Subsequent single-cell transcript analysis further demonstrated that cells expressing the highest levels of pluripotency genes had the greatest capacity for self-renewal [23]. Taken together, the findings of these studies suggest that in early development, the process of lineage commitment begins before loss of all stem cell maintenance factors. If lineage priming does occur, hESC heterogeneity could also potentially be exploited to promote the propagation and directed differentiation of cells *in vitro*.

Genes that contribute to "stemness"

Currently, there is much effort focused on improving protocols to produce enriched populations of differentiated cells for therapeutic applications. However, the mechanisms regulating self-renewal versus differentiation are still poorly understood. Global gene expression profiling may provide an insight into the genes involved in maintaining pluripotency and genes that are modulated during differentiation. Several groups have used high throughput techniques to identify genes only expressed in stem cells but not in mature cells and defined them as "stemness" genes [24,25]. Microarray analysis was used to establish the transcriptional profiles of mouse ESCs, NSCs, and HSCs, and found over 200 genes enriched in all three groups. Gene products included transcription factors, proteins involved in intracellular signaling, cell-surface receptors, and ligands. Specifically, ephrinB2 was found to be expressed in all

three stem cell populations [24]. This was the first study that indicated that the ephrin-eph signaling axis might be involved in the ability of stem cells to balance self-renewal versus differentiation pathways.

Eph-ephrin interactions and signaling

Eph receptors constitute the largest family of receptor tryrosine kinases (RTKs). The receptors are divided on the basis of sequence homology and ligand affinity into the A-subclass (EphA1-EphA8) and the B-subclass (EphB1-EphB4, EphB6). The ephrins, their ligands, are divided into the A-subclass (ephrinA1-A5), which are tethered to the cell membrane by a glycosylphosphatidylinositol (GPI) anchor, and the B-subclass (ephrinB1-ephrinB3), which have a transmembrane domain with a short cytoplasmic tail. A-type receptor bind to A-type ligands, while B-type receptors bind to B-type ligands, with the exception of EphA4, which can bind both A-type and B-type ligands (Fig. 1-3).

Eph receptors are activated when they are bound by clustered ephrin ligands. Since both eph receptors and ephrin ligands are membrane-bound, binding and activation of signaling requires cell-cell contact. Ligand binding induces "forward signaling." Ephrins can also signal, resulting in "reverse signaling." Thus, ephrin-eph interactions activate bi-directional signaling, so that the cytoplasmic domains of both, the receptor and ligand, become phosphorylated on tyrosine residues. Depending on the cell type, ephrin-eph activation can lead to repulsion of neighboring cells or increased adhesion/attraction. Many of the signaling pathways downstream of ephrins and ephs converge to regulate adhesion and organization of the actin cytoskeleton [26]. Thus, eph-ephrin interactions have important roles in several biological functions, including vascular development, tissue-border formation, cell migration and adhesion, and axon guidance.

EphrinB-ephB interactions regulate the formation of the vascular network

Ephrins and ephs play a critical role in the formation of vascular networks. During embryonic development, the first step of blood vessel formation consists of the differentiation of primitive mesodermal cells into vascular endothelial cells. "Vasculogenesis" refers to the formation of the primary capillary network from a dispersed population of endothelial cell precursors (angioblasts), including the primary capillary plexus and the yolk sac of the embryo (reviewed in [27]). During "angiogenesis," the primary vascular network is remodeled into a hierarchical network of small and large vessels through sprouting of new vessels, splitting of existing vessels, and sprouting (reviewed in [28]). EphrinB2 is a very early marker of arterial endothelial cells, whereas its receptor, ephB4, marks venous endothelial cells. It was proposed that the repulsive nature of ephrinB2-ephB4 interactions may form a boundary between arterial and venous endothelial cells, preventing cell intermixing, but also resulting in the formation of a capillary network [29]. EphrinB2 was shown to be required for the remodeling of the embryonic vascular system [30]. *EphrinB2*$^{-/-}$ mice die on embryonic day 9.5 (E9.5), due to severe defects in the angiogenic processes necessary for remodeling of the capillary plexus into properly branched structures. *EphB4*$^{-/-}$ mice also show angiogenic defects identical to those in *ephrinB2*$^{-/-}$ [31]. However, while ephB4 expression is restricted to the cardiovascular system, ephrinB2 is also expressed by several other non-vascular tissues, including the surrounding mesenchymal cells, pericytes, and smooth muscle cells [32]. Thus, the role of ephrinB2 extends from arterial/venous specification to regulating endothelial-smooth muscle interactions involved in the development of the arterial muscle wall. Continued expression of ephrins and ephs in the adult indicate further functions in therapeutic and pathological angiogenesis [26].

EphrinB-ephB interactions regulate boundary formation

Ephrin-eph bi-directional signaling is also important for boundary formation [33]. Studies with animal caps of zebrafish embryos first demonstrated that complementary expression of eph

receptors and ephrins resulted in bidirectional activation and mutual repulsion that restricted the movement of each population into the other [34]. When ephrinB2 was expressed in one animal cap and ephB2 or ephB4 in another, few cells crossed into the adjacent territory and a clear border was visible. If either the ephrin or eph was omitted from one population, cell intermingling occurred, suggesting that ephrinB-ephB interactions at the interface of two cell populations restricted cell intermingling.

EphrinB-ephB interactions regulate neural development

Ephrins and ephs are highly expressed in the nervous system, where they play a role in migration of neural crest cells (reviewed in [26]). Neural crest cells form at the dorsolateral edge of the neural epithelium, and then migrate to specific destinations where they can differentiate into neurons and glia of the peripheral nervous system, connective and skeletal tissue of the head, and melanocytes of the skin. In *ephrinB2*$^{-/-}$ mice, neural crest cells expressing ephA4, ephB1, and ephB3 scattered and migrated in a more diffuse pattern instead of following their typical route along the edge of the branchial arch.

Ephrins and ephs also play a role in axon guidance (reviewed in [35]). Following differentiation at appropriate locations, neurons extend axons tipped by a growth cone to a specific target area. Ephrins and ephs restrict neuronal growth cone movement, preventing cells or axons from migrating across their expression boundaries. This repulsive behavior is thought to be mediated by rearrangements in the cytoskeleton that lead to the collapse of the growth cones.

EphrinB-EphB interactions regulate stem cell fate

Eph signaling also regulates the balance between stem cell renewal versus differentiation (reviewed in [36]). In the small intestine, ephrinB and ephB expression determine proper positioning of epithelial cells along the crypt/villus axis [37]. At the bottom of the crypt,

stem cells give rise to progeny that proliferate and commit to different cell lineages during their migration toward the lumen. Absorptive, enteroendocrine, and goblet cells migrate toward the villus, while Paneth cells migrate to the bottom of the crypts. Opposing gradients of ephB2/ephB3 expression at the bottom of the crypt and ephrinB1/ephrinB2 expression at the surface epithelium restrict cell intermingling. In *ephB2/ephB3*$^{-/-}$ mice, the proliferative and differentiated populations intermingle, suggesting that ephB may restrict the potential positions adopted by cells expressing different levels of ephrinB.

Ephrin-eph signaling was also found to regulate the proliferation of neural stem cells [38]. In the adult mammalian brain, neurogenesis occurs in the subventricular zone (SVZ) of the lateral ventricles. In the mouse, SVZ astrocytes are the multipotential stem cells that give rise to neuroblasts that migrate to the olfactory bulb for differentiation [39]. Cells of the SVZ express ephB receptors and ephrinB ligands, with ephrins specifically localizing to astrocytes. Perturbation of ephrinB-ephB signaling resulted in increased proliferation of astrocytes and disruption of neuroblast chain migration. This finding suggested that ephs and ephrins are important mediators of cell proliferation in the brain.

Lastly, ephB4 regulates the differentiation of ESCs towards mesodermal lineages. Overexpression of ephB4 in human umbilical cord blood CD34+ cells enhanced the differentiation of these primitive stem cells into the megakaryocytic and erythroid lineages [40]. Conversely, in *ephb4*$^{-/-}$ mouse ESCs (mESCs), hemangioblast, hematopoietic, endothelial, cardiomyocyte differentiation were impaired [41]. Microarray analysis of EBs derived from the *ephB4*$^{-/-}$ ESCs confirmed that mesoderm-associated genes were downregulated, while neuro-ectoderm-associated genes were upregulated, suggesting a potential role for ephB4 in affecting germ layer choice. These studies raise the possibility that manipulation of ephB4 signaling can be used to alter the differentiation of stem cell populations toward desired lineages. Reagents that selectively modulate ephrin-eph signaling are necessary for future studies on the role of this signaling axis in stem cell fate determination.

EphrinB2 is the Nipah virus receptor

Nipah virus (NiV) is a single-stranded, negative-sense RNA virus belonging to the *Henipavirus* genus of the *Paramyxoviridae*. NiV emerged in Malyasia in 1998 in the form of respiratory illness in pigs and fatal encephalitis in humans [42]. The primary host was identified as the fruit bat of the genus *Pteropus* [43], and pigs were shown to serve as intermediate amplifying hosts for NiV, transmitting the virus from bats to humans [44]. However, direct bat-to-human and human-to-human transmission occurred in later outbreaks in Bangladesh [45]. NiV infection typically leads to death from fatal encephalitis, with a 70% mortality rate in the Bangladesh outbreak [46]. Human autopsies showed that the endothelial cells lining blood vessels were severely affected [47]. Multinucleated, giant endothelial cells were observed most prominently in the blood vessels in the central nervous system (CNS), but also in the vasculature of many other organs, including the lung, heart, and kidney. Due to its extreme pathogenicity, high mortality, potential respiratory transmission, and lack of effective therapeutics, NiV is designated a Category C priority pathogen in the NIAID Biodefense Research Agenda and is handled under Biosafety Level 4 (BSL-4) conditions.

The observed tropism of NiV for the endothelium and the central nervous system (CNS) is concordant with the tissue expression of ephrinB2 and B3 [47-49]. Our group identified the receptor for NiV entry as ephrinB2 [50,51], and showed that ephrinB3 could serve as an alternate receptor [52]. NiV entry into permissive cells requires coordinated action of the attachment viral envelope glycoprotein (NiV-G) and the viral fusion protein (NiV-F). Binding of NiV-G to ephrinB2 induces triggering of NiV-F, which results in a conformational change that leads to viral-cell membrane fusion [53]. Compared to ephB4, NiV-G has a ~ten-fold higher affinity for ephrinB2. Soluble NiV-G binds ephrinB2-expressing cells with a K_D of 0.27nM [52]. Thus, NiV-G could potentially be used to block endogenous ephrinB2-ephB4 interactions, and would serve as a great tool for interrogating the role that the ephrinB2-ephB4 axis plays in regulating developmental fate decisions in hESCs.

Specific aims of the dissertation

Aim I: Generation of a tool to specifically target ephrinB2+ hESCs.

In **Chapter 2** of this dissertation, I present our work on successfully engineering the NiV envelope glycoproteins to be efficiently pseudotyped onto lentiviral vectors and subsequent specific targeting to ephrinB2+ populations *in vitro*. We demonstrated that not only could the NiV pseudotyped particles efficiently transduce hESCs, but hNSCs and a small population of CD34+ hHSCs as well. Interestingly, additional experiments suggested that NiVpp could be potentially targeting the "true" HSCs within the CD90+CD34+CD38- population of fetal liver. This chapter was recently published in *Journal of Virology* (in press).

Aim II: Characterization of ephrinB2+ hESCs.

The first part of **Chapter 3** focuses on characterizing the population of hESCs transduced by NiV pseudotyped particles. Our results suggested that ephrinB2 does not mark for an independent, phenotypically stable population of cells, but may be an intrinsic marker of stem cell heterogeneity. Nevertheless, characterization of the NiV-transduced hESCs indicated that the cells demonstrate the basic properties of stem cells: they self-renew *in vitro*; and they differentiate into derivatives of the three germ layers *in vitro* and *in vivo*.

Aim III: Characterization of ephrinB2-knockdown hESCs.

The second part of **Chapter 3** consists of characterizing hESCs stably expressing a shRNA against ephrinB2. We found that although the ephrinB2-knockdown cells demonstrated proper self-renewal *in vitro*, neuro-ectoderm differentiation was severely impaired. In addition, genes involved in mesoderm induction and endoderm development were significantly up-regulated, suggesting that ephrinB2 knockdown enhances the formation of mesendoderm progenitors. This chapter is currently in preparation for a manuscript.

Figure 1-1

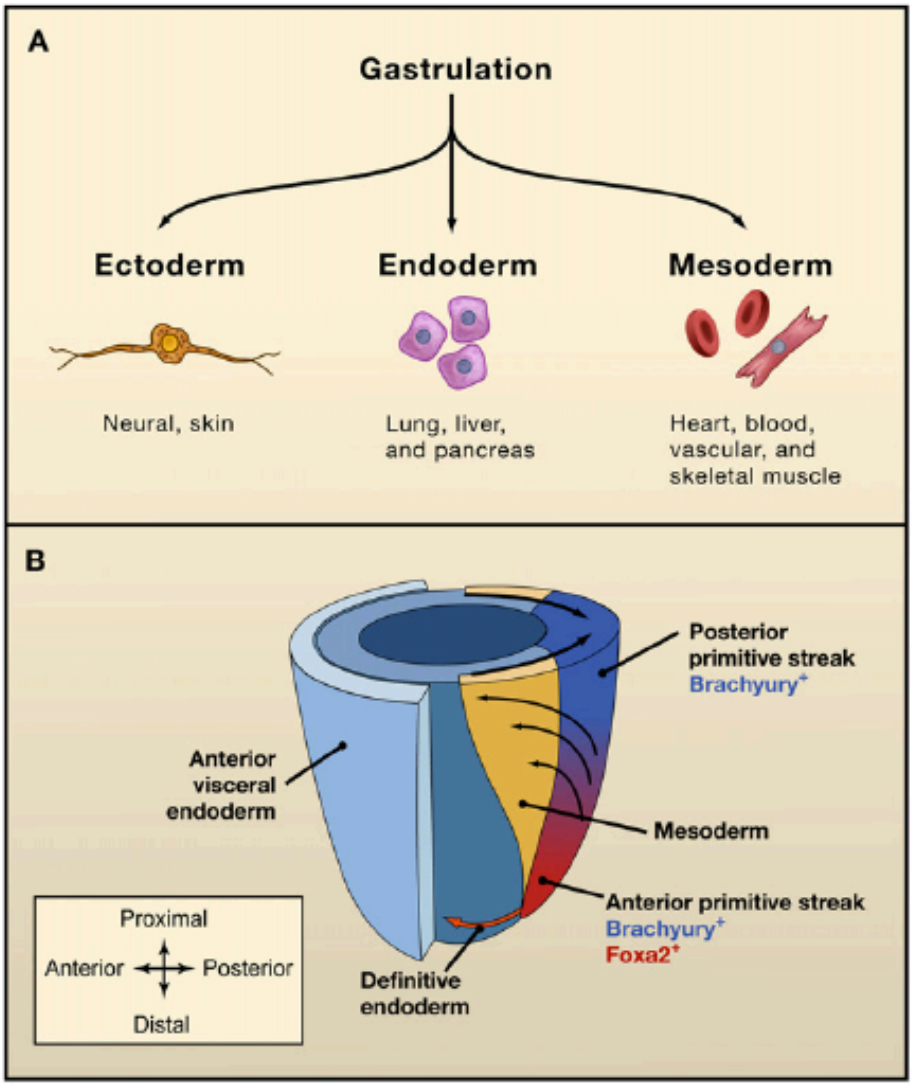

Figure 1-1. Mouse gastrulation and germ layer formation. (A) During embryogenesis, the process of gastrulation generates the 3 germ layers: ectoderm, mesoderm, and endoderm **(B)** In the mouse, gastrulation begins with the formation of the primitive streak (PS). Uncommitted epiblast cells undergo an epithelial-to-mesenchymal transition (EMT), mobilize, and traverse the PS. Cells that pass through the most posterior end of the PS give rise to the extraembryonic mesoderm. Cells that migrate through the most anterior end of the PS generate definitive endoderm. Lastly, ectoderm develops from the anterior region of the epiblast that does not enter the PS. This figure was adapted from Murray and Keller [13], with permission from Elsevier.

Figure 1-2

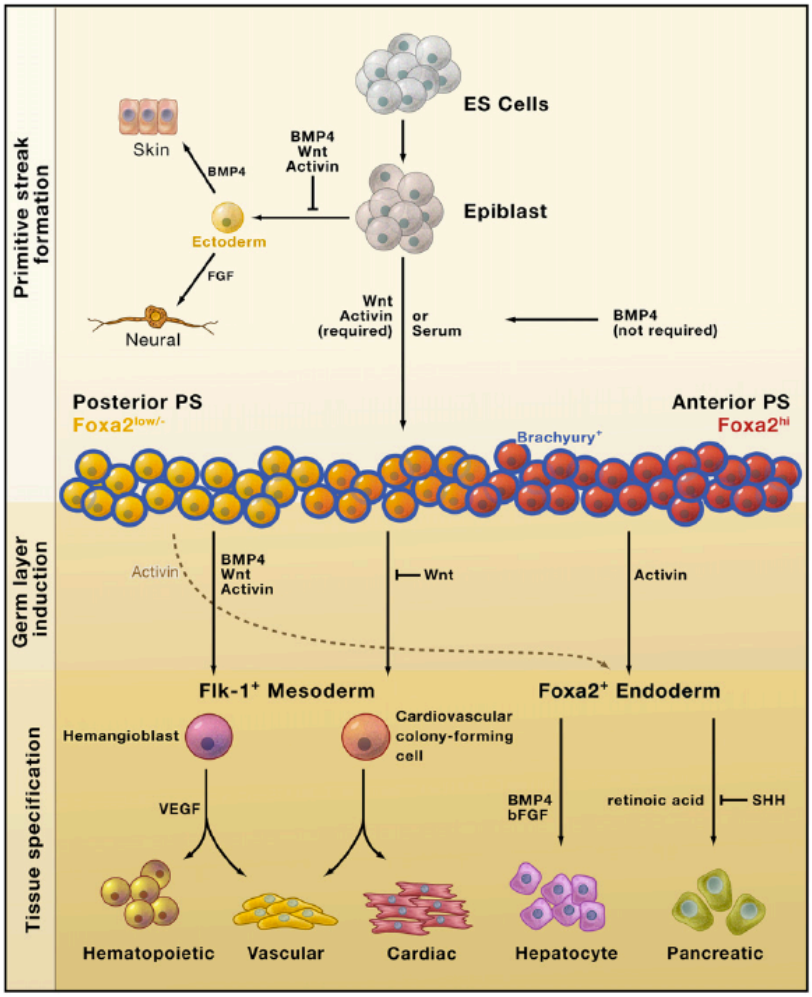

Figure 1-2. Directed differentiation of hESCs. hESCs can be directed to differentiate into all cell types through the addition or repression of growth factors at specific time windows. This figure was adapted from Murray and Keller [13], with permission from Elsevier.

Figure 1-3

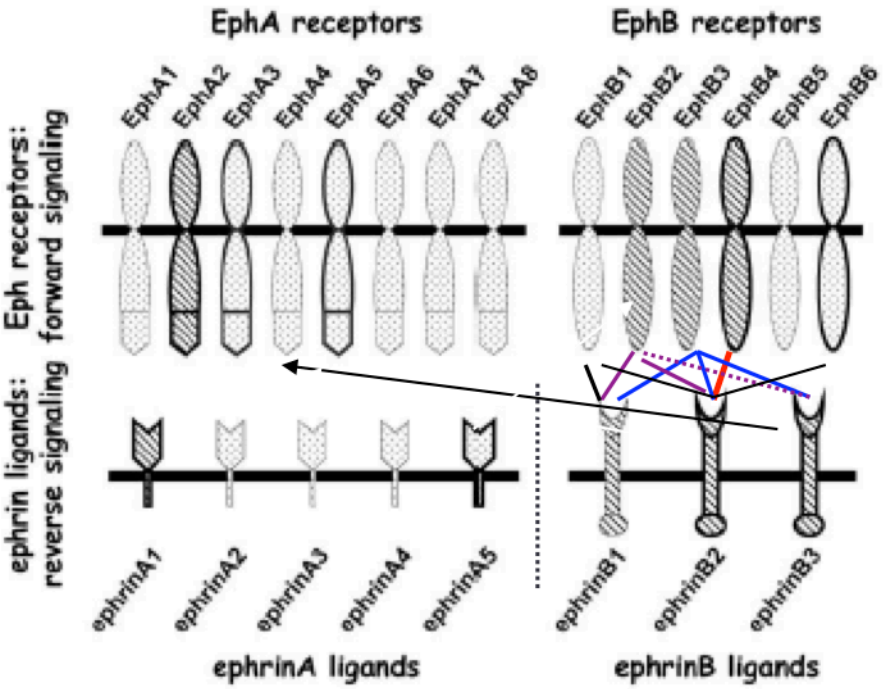

Figure 1-3. The eph receptor and ephrin ligand families. The eph receptors are divided into the A-subclass (EphA1-EphA8) and the B-subclass (EphB1-EphB4, EphB6). The ephrins, their ligands, are divided into the A-subclass (ephrinA1-A5), which are tethered to the cell membrane by a GPI anchor, and the B-subclass (ephrinB1-ephrinB3), which have a transmembrane domain with a short cytoplasmic tail. The lines show the interactions between the receptors and ligands. A-type receptor bind to A-type ligands, while B-type receptors bind to B-type ligands, with the exception of EphA4, which can bind both A-type and B-type ligands.

References

1 Evans, M. J. & Kaufman, M. H. Establishment in culture of pluripotential cells from mouse embryos. *Nature* **292**, 154-156 (1981).

2 Martin, G. R. Isolation of a pluripotent cell line from early mouse embryos cultured in medium conditioned by teratocarcinoma stem cells. *Proc Natl Acad Sci U S A* **78**, 7634-7638 (1981).

3 Thomson, J. A. *et al.* Embryonic stem cell lines derived from human blastocysts. *Science* **282**, 1145-1147 (1998).

4 Weissman, I. L. Translating stem and progenitor cell biology to the clinic: barriers and opportunities. *Science* **287**, 1442-1446 (2000).

5 Kannagi, R. *et al.* Stage-specific embryonic antigens (SSEA-3 and -4) are epitopes of a unique globo-series ganglioside isolated from human teratocarcinoma cells. *EMBO J* **2**, 2355-2361 (1983).

6 Andrews, P. W., Banting, G., Damjanov, I., Arnaud, D. & Avner, P. Three monoclonal antibodies defining distinct differentiation antigens associated with different high molecular weight polypeptides on the surface of human embryonal carcinoma cells. *Hybridoma* **3**, 347-361 (1984).

7 Williams, R. L. *et al.* Myeloid leukaemia inhibitory factor maintains the developmental potential of embryonic stem cells. *Nature* **336**, 684-687, doi:10.1038/336684a0 (1988).

8 Amit, M. *et al.* Clonally derived human embryonic stem cell lines maintain pluripotency and proliferative potential for prolonged periods of culture. *Dev Biol* **227**, 271-278, doi:10.1006/dbio.2000.9912 (2000).

9 Itskovitz-Eldor, J. *et al.* Differentiation of human embryonic stem cells into embryoid bodies compromising the three embryonic germ layers. *Mol Med* **6**, 88-95 (2000).

10 Jaenisch, R. & Young, R. Stem cells, the molecular circuitry of pluripotency and nuclear reprogramming. *Cell* **132**, 567-582, doi:10.1016/j.cell.2008.01.015 (2008).

11 Boyer, L. A. *et al.* Core transcriptional regulatory circuitry in human embryonic stem cells. *Cell* **122**, 947-956, doi:10.1016/j.cell.2005.08.020 (2005).

12 Laslett, A. L. *et al.* Transcriptional analysis of early lineage commitment in human embryonic stem cells. *BMC Dev Biol* **7**, 12, doi:10.1186/1471-213x-7-12 (2007).

13 Murry, C. E. & Keller, G. Differentiation of embryonic stem cells to clinically relevant populations: lessons from embryonic development. *Cell* **132**, 661-680, doi:10.1016/j.cell.2008.02.008 (2008).

14 Vallier, L. *et al.* Early cell fate decisions of human embryonic stem cells and mouse epiblast stem cells are controlled by the same signalling pathways. *PLoS One* **4**, e6082, doi:10.1371/journal.pone.0006082 (2009).

15 Tam, P. P. & Behringer, R. R. Mouse gastrulation: the formation of a mammalian body plan. *Mech Dev* **68**, 3-25 (1997).

16 Gadue, P., Huber, T. L., Nostro, M. C., Kattman, S. & Keller, G. M. Germ layer induction from embryonic stem cells. *Exp Hematol* **33**, 955-964, doi:10.1016/j.exphem.2005.06.009 (2005).

17 Davis, R. P. *et al.* Targeting a GFP reporter gene to the MIXL1 locus of human embryonic stem cells identifies human primitive streak-like cells and enables isolation of primitive hematopoietic precursors. *Blood* **111**, 1876-1884, doi:10.1182/blood-2007-06-093609 (2008).

18 Naito, A. T. *et al.* Developmental stage-specific biphasic roles of Wnt/beta-catenin signaling in cardiomyogenesis and hematopoiesis. *Proc Natl Acad Sci U S A* **103**, 19812-19817, doi:10.1073/pnas.0605768103 (2006).

19 D'Amour, K. A. *et al.* Efficient differentiation of human embryonic stem cells to definitive endoderm. *Nat Biotechnol* **23**, 1534-1541, doi:10.1038/nbt1163 (2005).

20 Ying, Q. L., Stavridis, M., Griffiths, D., Li, M. & Smith, A. Conversion of embryonic stem cells into neuroectodermal precursors in adherent monoculture. *Nat Biotechnol* **21**, 183-186, doi:10.1038/nbt780 (2003).

21 Enver, T. *et al.* Cellular differentiation hierarchies in normal and culture-adapted human embryonic stem cells. *Hum Mol Genet* **14**, 3129-3140, doi:10.1093/hmg/ddi345 (2005).

22 Stewart, M. H. *et al.* Clonal isolation of hESCs reveals heterogeneity within the pluripotent stem cell compartment. *Nat Methods* **3**, 807-815, doi:10.1038/nmeth939 (2006).

23 Hough, S. R., Laslett, A. L., Grimmond, S. B., Kolle, G. & Pera, M. F. A continuum of cell states spans pluripotency and lineage commitment in human embryonic stem cells. *PLoS One* **4**, e7708, doi:10.1371/journal.pone.0007708 (2009).

24 Ivanova, N. B. *et al.* A stem cell molecular signature. *Science* **298**, 601-604, doi:10.1126/science.1073823 (2002).

25 Ramalho-Santos, M., Yoon, S., Matsuzaki, Y., Mulligan, R. C. & Melton, D. A. "Stemness": transcriptional profiling of embryonic and adult stem cells. *Science* **298**, 597-600, doi:10.1126/science.1072530 (2002).

26 Kullander, K. & Klein, R. Mechanisms and functions of Eph and ephrin signalling. *Nat Rev Mol Cell Biol* **3**, 475-486, doi:10.1038/nrm856 (2002).

27 Risau, W. & Flamme, I. Vasculogenesis. *Annu Rev Cell Dev Biol* **11**, 73-91, doi:10.1146/annurev.cb.11.110195.000445 (1995).

28 Risau, W. Mechanisms of angiogenesis. *Nature* **386**, 671-674, doi:10.1038/386671a0 (1997).

29 Yancopoulos, G. D., Klagsbrun, M. & Folkman, J. Vasculogenesis, angiogenesis, and growth factors: ephrins enter the fray at the border. *Cell* **93**, 661-664 (1998).

30 Wang, H. U., Chen, Z. F. & Anderson, D. J. Molecular distinction and angiogenic interaction between embryonic arteries and veins revealed by ephrin-B2 and its receptor Eph-B4. *Cell* **93**, 741-753 (1998).

31 Gerety, S. S., Wang, H. U., Chen, Z. F. & Anderson, D. J. Symmetrical mutant phenotypes of the receptor EphB4 and its specific transmembrane ligand ephrin-B2 in cardiovascular development. *Mol Cell* **4**, 403-414 (1999).

32 Gale, N. W. *et al.* Ephrin-B2 selectively marks arterial vessels and neovascularization sites in the adult, with expression in both endothelial and smooth-muscle cells. *Dev Biol* **230**, 151-160, doi:10.1006/dbio.2000.0112 (2001).

33 Klein, R. Bidirectional signals establish boundaries. *Curr Biol* **9**, R691-694 (1999).

34 Mellitzer, G., Xu, Q. & Wilkinson, D. G. Eph receptors and ephrins restrict cell intermingling and communication. *Nature* **400**, 77-81, doi:10.1038/21907 (1999).

35 Wilkinson, D. G. Multiple roles of EPH receptors and ephrins in neural development. *Nat Rev Neurosci* **2**, 155-164, doi:10.1038/35058515 (2001).

36 Pasquale, E. B. Eph receptor signalling casts a wide net on cell behaviour. *Nat Rev Mol Cell Biol* **6**, 462-475, doi:10.1038/nrm1662 (2005).

37 Batlle, E. *et al.* Beta-catenin and TCF mediate cell positioning in the intestinal epithelium by controlling the expression of EphB/ephrinB. *Cell* **111**, 251-263 (2002).

38 Conover, J. C. *et al.* Disruption of Eph/ephrin signaling affects migration and proliferation in the adult subventricular zone. *Nat Neurosci* **3**, 1091-1097, doi:10.1038/80606 (2000).

39 Doetsch, F., Caille, I., Lim, D. A., Garcia-Verdugo, J. M. & Alvarez-Buylla, A. Subventricular zone astrocytes are neural stem cells in the adult mammalian brain. *Cell* **97**, 703-716 (1999).

40 Wang, Z. *et al.* Receptor tyrosine kinase, EphB4 (HTK), accelerates differentiation of select human hematopoietic cells. *Blood* **99**, 2740-2747 (2002).

41 Wang, Z. *et al.* Ephrin receptor, EphB4, regulates ES cell differentiation of primitive mammalian hemangioblasts, blood, cardiomyocytes, and blood vessels. *Blood* **103**, 100-109, doi:10.1182/blood-2003-04-1063 (2004).

42 Chua, K. B. *et al.* Nipah virus: a recently emergent deadly paramyxovirus. *Science* **288**, 1432-1435 (2000).

43 Chua, K. B. *et al.* Isolation of Nipah virus from Malaysian Island flying-foxes. *Microbes Infect* **4**, 145-151 (2002).

44 Parashar, U. D. *et al.* Case-control study of risk factors for human infection with a new zoonotic paramyxovirus, Nipah virus, during a 1998-1999 outbreak of severe encephalitis in Malaysia. *J Infect Dis* **181**, 1755-1759, doi:10.1086/315457 (2000).

45 Luby, S. P., Gurley, E. S. & Hossain, M. J. Transmission of human infection with Nipah virus. *Clin Infect Dis* **49**, 1743-1748, doi:10.1086/647951 (2009).

46 Hsu, V. P. *et al.* Nipah virus encephalitis reemergence, Bangladesh. *Emerg Infect Dis* **10**, 2082-2087, doi:10.3201/eid1012.040701 (2004).

47 Wong, K. T. *et al.* Nipah virus infection: pathology and pathogenesis of an emerging paramyxoviral zoonosis. *Am J Pathol* **161**, 2153-2167, doi:10.1016/s0002-9440(10)64493-8 (2002).

48 Bergemann, A. D. *et al.* Ephrin-B3, a ligand for the receptor EphB3, expressed at the midline of the developing neural tube. *Oncogene* **16**, 471-480, doi:10.1038/sj.onc.1201557 (1998).

49 Flenniken, A. M., Gale, N. W., Yancopoulos, G. D. & Wilkinson, D. G. Distinct and overlapping expression patterns of ligands for Eph-related receptor tyrosine kinases during mouse embryogenesis. *Dev Biol* **179**, 382-401, doi:10.1006/dbio.1996.0269 (1996).

50 Negrete, O. A. *et al.* EphrinB2 is the entry receptor for Nipah virus, an emergent deadly paramyxovirus. *Nature* **436**, 401-405, doi:10.1038/nature03838 (2005).

51 Bonaparte, M. I. *et al.* Ephrin-B2 ligand is a functional receptor for Hendra virus and Nipah virus. *Proc Natl Acad Sci U S A* **102**, 10652-10657, doi:10.1073/pnas.0504887102 (2005).

52 Negrete, O. A. *et al.* Two key residues in ephrinB3 are critical for its use as an alternative receptor for Nipah virus. *PLoS Pathog* **2**, e7, doi:10.1371/journal.ppat.0020007 (2006).

53 Lee, B. & Ataman, Z. A. Modes of paramyxovirus fusion: a Henipavirus perspective. *Trends Microbiol* **19**, 389-399, doi:10.1016/j.tim.2011.03.005 (2011).

CHAPTER 2

Nipah virus envelope pseudotyped lentiviruses efficiently target ephrinB2+ stem cell populations *in vitro* and bypass the liver sink when administered *in vivo*

Introduction

Lentiviruses are common vectors used in gene therapy because they can transduce non-dividing cells and offer stable integration into a target cell's genome. The host range can be altered by pseudotyping with glycoproteins derived from other enveloped viruses. The most commonly used is the glycoprotein (G) of vesicular stomatitis virus (VSV), which has great stability in the vector particle allowing concentration to high titers, and also has a ubiquitous host cell receptor allowing transduction of most cell types [1,2]. VSV-G pseudotyped particles (VSV-Gpp) have become the standard for evaluating the efficiency of transduction by other viral envelope pseudotypes. However, VSV-Gpp cannot be targeted to specific populations of cells, which is necessary for *in vivo* gene transfer applications.

More specific cell targeting can be achieved by pseudotyping with envelopes modified in various ways that allow for re-retargeting via some ligand specific domain [3,4]. Measles virus (MeV) glycoproteins (Edmonston strain) can also be efficiently pseudotyped onto a lentiviral vector, but only when the cytoplasmic tails of both envelope glycoproteins, the hemagglutinin (H) and fusion (F) proteins, were truncated. MeV_{Edm} uses CD46 and/or SLAM as entry receptors. In humans, CD46 is expressed on all nucleated cells [5], thus its natural tropism does not offer MeVpp any specific targeting advantage *in vivo*. However, *ex vivo*, MeVpp can transduce unstimulated primary human B and T cells that are relatively resistant to even VSV-Gpp transduction, suggesting that MeVpp are at least useful as an experimental tool [6,7].

More recently, the unique features of MeV entry have allowed for some innovations that have attracted considerable interest [8-10]. Measles virus is a member of the morbillivirus genus in the *Paramyxovirinae* subfamily of paramyxoviruses. Paramyxovirus entry requires the coordinated action of both the fusion (F) and attachment glycoproteins (designated HN, H, or G depending on its receptor binding properties); receptor binding to the viral attachment glycoprotein induces an allosteric change that triggers F to undergo a conformational cascade that results in virus-cell membrane fusion and entry [11-13]. Morbillivirus is one of only two genera

of paramyxoviruses that use protein-based receptors, the others use ubiquitous glycan-based receptors such as sialic acids. The aforementioned innovation takes advantage of the wealth of structure-function information that have not only mapped the receptor binding sites on MeV-H, but have also characterized key features of the ensuing receptor-binding triggerred fusion cascade [12,14]. Thus, by mutating the native receptor-binding sites on MeV-H, and appending to the C-terminus of the mutated MeV-H (a type II transmembrane protein), the single-chain variable fragment (scFv) from a monoclonal antibody recognizing specific cell-surface antigens, MeVpp can be successfully re-targeted, at least *in vitro*, to neurons, endothelial cells, and hematopoietic progenitors [15]. Nevertheless, the development as MeVpp as *in vivo* targeted human gene therapy vectors is limited by the wide-spread presence of pre-existing neutralizing antibodies in the vast majority of the human population that have received MeV vaccination.

Nipah (NiV) and Hendra (HeV) viruses belong to the only other genera (*Henipavirus*) of paramyxoviruses that use protein-based receptors. A recent study showed that the full-length Nipah virus envelope glycoproteins could be pseudotyped onto a lentiviral vector and mediate entry into various cell lines, although infectious titers were not determined [16]. For NiV, the attachment glycoprotein, NiV-G, functions in recognition of the receptor. As for MeV, binding of the receptor to NiV-G triggers a series of conformational changes that eventually lead to NiV-F triggering and virus-cell membrane fusion (reviewed in [13]). Henipaviruses use ephrinB2 as the primary receptor, and, somewhat less efficiently, ephrinB3 as an alternate receptor [17-19]. The remarkably high affinity of NiV-G for ephrinB2 (K_d = 0.06 nM) [19] suggests that NiV pseudotyped particles (NiVpp) can be efficiently and specifically targeted to ephrinB2+ cells. Thus, instead of re-targeting strategies, we sought to exploit the natural tropism of NiV for specific targeting of primary ephrinB2-expressing cell types that are of significant biological and clinical interest to the gene targeting community.

Eph-ephrin receptor-ligand pairs are membrane-associated receptor tyrosine kinases (RTKs) with well-established roles in many developmental processes; they regulate cell

boundaries during tissue and bone formation, as well as provide guidance cues during neurogenesis and angiogenesis [20]. EphrinB2-ephB4 interactions have been strongly implicated in tumor angiogenesis, migration, and invasion [21]. In addition, ephrinB2 has been proposed as a molecular marker of stemness, being expressed on murine embryonic stem cells, hematopoietic stem cells and neural stem cells [22]. Thus, the ability to target lentiviral vectors specifically to ephrinB2+ cells may be of utility for studying specific stem cell populations, or be of use for disrupting tumorigenesis where the ephrinB2-ephB4 axis plays a critical role [20].

Here, we systematically investigated what modifications to the cytoplasmic tails of the NiV glycoproteins could best enhance the efficiency of pseudotyping onto lentiviral particles. We found that efficient functional pseudotyping with NiV envelope requires only truncation of the F protein cytoplasmic tail, while full-length NiV-G can be used. Unlike MeVpp, full-length and truncated F were equally incorporated into NiVpp, indicating that the requirements for functional lentiviral pseudotyping differ between MeV and NiV. NiVpp can specifically target ephrinB2+ cells in a 1000-fold excess of ephrinB2-negative cells, and NiVpp transduced *human* embryonic, hematopoietic and neural stem cell populations in an ephrinB2-specific manner. Intravenous administration of the luciferase reporter NiVpp resulted in signals detected in the spleen and lung, but not the liver. Biodistribution studies quantifying genome integrated vector copy numbers in various tissues confirm these observations. Bypassing the liver sink is a critical barrier for targeted gene therapy [23,24], suggesting that the extraordinary specificity of NiV-G for ephrinB2 may allow for targeting of specific ephrinB2+ populations *in vivo*, or *in vitro* without the need for prior cell purification.

Materials and Methods

Plasmid construction. The codon-optimized NiV-F and NiV-G genes were tagged at their C termini with an AU1 (DTYRYI) or HA (YPYDVPDYA) tag, respectively, as previously described [25]. The β-lactamase (β-la) gene was fused to NiV-M as previously described [26]. NiV-G cytoplasmic truncation mutants were generated using the QuikChange site-directed mutagenesis kit (Stratagene, Cedar Creek, TX) with primers designed corresponding to the deletions. NiV T5F and T5FΔN3 mutants were previously made [27,28]. FUhLucW and FG12 were constructed from FUGW, as previously described [29,30]. pNL4-3.Luc.R^-.E^- was obtained through the NIH AIDS Research and Reference Reagent Program. VSV-ΔG-Luc has the G protein envelope replaced with *Renilla* Luc, as previously described [19].

Cells and culture conditions. 293T cells were cultured in IMDM with 10% FBS, 1% NEAA, 1% Glutamax, and antibiotics. CHO-pgsA745 is a mutant cell line derived from Chinese hamster ovary (CHO) cells that lack the endogenous expression of heparin sulfate proteoglycans [31], and was maintained in DMEM-F12 medium supplemented with 10% FBS. CHO cells expressing either ephrin-B2 (CHO-B2) or ephrin-B3 (CHO-B3) were made as previously described [19], and maintained in DMEM-F12 medium supplemented with 10% FBS and 1 mg/ml of G418 to drive plasmid expression through neomycin resistance. Vero (African green monkey kidney fibroblast) cells were maintained in α-MEM with 10% FBS. U87 cells were maintained in DMEM with 10% FBS. Human embryonic stem cells (hESCs) (H1, H9, and UCLA1 lines) were cultured on gelatin-coated plates on a feeder layer of mitotically-inactivated murine embryonic fibroblasts (MEFs). hESC medium is composed of DMEM/F:12 supplemented with 20% KnockOut Serum Replacement (KOSR, Life Technologies), 0.1 mM NEAA (Life Technologies), 1 mM L-Glutamine (Life Technologies), 0.1 mM 2-mercaptoethanol (Sigma-Aldrich), and 4 ng/ml basic fibroblast growth factor (bFGF, R&D Systems – obtained via National Cancer Institute Biological Resources Branch). hESCs were passaged in small clumps

every 5-7 days using collagenase (Life Technologies). For viral transductions, hESCs were transferred to feeder-free conditions. hESCs were dissociated to single cells using trypsin (Life Technologies) for counting and then plated on Matrigel- (BD Biosciences) coated plates in hESC medium that was conditioned overnight on MEFs and supplemented with 10 μM HA-1077 (ROCK inhibitor, Sigma-Aldrich) to promote hESC survival [32]. CD34+ cells were isolated from human fetal liver as previously described [33]. For viral transductions, the cells were seeded onto Retronectin (Takara)-coated plates with 2% bovine serum albumin in Yssel's medium (Gemini). As previously described [34], neuralization of undifferentiated HSF1 hESC colonies was induced *in situ* by switching to rosette media containing DMEM:F12, N-2 supplement (Gibco), B27 supplement (Gibco), 1uM retinoic acid (Sigma), 1uM Smoothened Agonist (Calbiochem), and 20 ng/mL FGF2. After 10-14 days, rosettes were mechanically isolated and passaged onto poly-ornithine- (Sigma) and laminin- (Sigma) coated plates. Once picked, rosettes were placed into neural progenitor cell (NPC) media containing DMEM:F12, N-2, B27, 50 ng/mL EGF (Peprotech), and 20 ng/mL FGF2 allowing for expansion and maintenance. 100,000 NPCs (passage #2) were plated onto 24-well plates using TrypLE (Gibco) for viral infection.

Virus production. Lentiviral vectors were produced by calcium phosphate-mediated transient transfection of 293T cells. 24 hours prior to transfection, 1.6 x 10^7 293T cells were seeded into a T175 flask. On the day of transfection, the medium was replaced with 25ml fresh medium containing 10mM chloroquine. 7 μg of NiV-F variant, 7 μg of NiV-G variant, 12.5 μg of the packaging plasmid pCMVΔR8.9, and 12.5 μg of the lentiviral transfer vector plasmid (FG12 or FUhLucW) were mixed with 133 μl of 2M $CaCl_2$ and brought up to a final volume of 980 μl with ddH_20. Next, 1,110 μl of 2X HEPES buffer saline buffer was added dropwise. Following a 20-minute incubation on ice, the precipitate was added to the cells. After 8 hours, the medium was replaced with 30 ml of AIM-V serum-free medium. 48 hours post-transfection, the cell supernatant containing the pseudotyped lentiviral vector particles was layered over a 20%

sucrose cushion and concentrated by centrifugation at 28,000 rpm at 4°C for 2 hours (Beckman SW-32 rotor). The viral pellet was resuspended in 300 µl of PBS and filtered (0.45µm filter). To determine viral titer, serial dilutions of unconcentrated and concentrated stocks were added to 2 x 10^5 293T cells and incubated for 2 hours at 37°C. The medium was replaced with fresh medium. 72 hours post-infection, the cells were collected and analyzed by flow cytometry for eGFP expression. The titers are expressed as infectious units per ml (IU/ml). Typical unconcentrated titers for NiVpp are 10^6 IU/ml, and can be concentrated to 10^8-10^9 IU/ml upon ultracentrifugation.

Western blot analysis. Concentrated viral stocks were normalized to HIV p24 (50 ng of p24 per lane). The samples were boiled in 6X sodium dodecyl sulfate (SDS) loading buffer containing 2-mercaptoethanol for 10 minutes, subjected to electrophoresis through a 10% SDS polyacrylamide gel, and transferred onto a PVDF (Millipore) membrane. Mouse anti-HA-tag (Covance), mouse anti-AU1-tag (Covance), and mouse anti-p24 (NIH AIDS Research and Reference Reagent Program) monoclonal antibodies were used to detect NiV-G, NiV-F, and p24 proteins, respectively. A goat anti-mouse IRDye 800CW (LI-COR Biosciences) was used as a secondary antibody. Signals were detected using the Odyssey infrared imaging system (LI-COR Biosciences).

β-lactamase-matrix entry assay. NiV and VSV-G β-lactamase-matrix virus-like particles (β-la-M VLPs) were produced as previously described [26]. 293T cells were seeded in a 24-well dish at 7.5 x 10^4 per well. 24 hours after seeding, concentrated NiV wt F/wt G, NiV T5F/wt G or VSV-G pseudotyped βla-M VLPs were added to the cells and spin-inoculated for 1 hour at 2,000 rpm at 4°C. After spin-inoculation, cells were gently washed and CCF2-AM (Invitrogen) was added according to manufacturer recommendations. Cells were then transferred to a pre-warmed 37°C micro-plate fluorometer (TECAN Infinite® M1000). Green (uncleaved CCF2-AM) and blue

(cleaved CCF2-AM) fluorescence was monitored at 530 nm and 460 nm, respectively. Kinetic readings were taken every 10 min for up to 5 hours.

***In vitro* infection of cells.** Increasing amounts of virus (based on MOI or p24) were added to 1 x 10^5 cells of each cell type and centrifuged at 2,000 rpm at 37°C for 2 hours. As a specificity control, 10 nM of soluble ephrinB2 (R&D Systems) was added to the infection medium. To exclude pseudotransduction, 5μM of nevirapine was added. For stem cell transductions, 4 ng/ml of polybrene (Sigma) was added. Following an overnight incubation with virus, the infection medium was removed and replaced with fresh medium. 72 hours post-infection, the cells were harvested and analyzed by flow cytometry for eGFP expression. For transduction of a mixed population of cells, ephrinB2+ human U87 cells were mixed with ephrinB2- non-human Chinese hamster ovary (CHO) cells at different ratios (U87:CHO ratios = 1:1, 1:10, 1:100, and 1:1000), and seeded at a density of 50,000 cells per well in 24-well plates. The next day, cells were infected with 1 or 10 ng of NiV T5F/wt G, T5FΔN3/wt G, and VSV-G pseudotypes. 72h post-infection, the cells were harvested, stained with the mouse W6/32 anti-human HLA-ABC monoclonal antibody (eBioscience), followed by Alexa 647-conjugated goat anti-mouse secondary antibodies. Samples were fixed and then analyzed by dual-color flow cytometry for human HLA and eGFP expression.

FACS-sorting of CD34+ fetal liver cells. CD34+ cells were isolated from human fetal liver as previously described [33]. The cell suspensions were stained with DAPI, CD34-APC, CD38-PE-Cy7, and CD90-FITC (BD-Biosciences) antibodies for 20 minutes on ice in the dark. Following washing, the cells were sorted on a BD FACS Aria into 4 populations: CD90+CD34+CD38-, CD90-CD34+CD38-, CD90-CD34+CD38+, and CD90-CD34-CD38+. Immediately following sorting, RNA was extracted from each population using a RNeasy Micro kit (Qiagen) and used for preparation of cDNA using a QuantiTect Reverse Transcription kit (Qiagen). Specific

primers for ephrinB2 (Forward- TCCCGATTGAGCCTTACGACACTT, Reverse- TTCACCTTGACACAGAGCACC) and GAPDH (Forward- ATCAAGAAGGTGGTGAAGCAGG, Reverse- TCAAAGGTGGAGGAGTGGGTGT) were used for real-time PCR analysis of gene expression.

Immunostaining. Coverslips were fixed in 4% PFA at room temperature for 15 minutes, permeabilized in 0.5% Triton-X-100 at room temperature for 10 minutes, and blocked in 5% bovine serum, 1% BSA, and 0.2% Triton-X-100 at room temperature for 30 minutes. They were then incubated overnight at 4°C with a mouse anti-Nestin antibody (Neuromics). Next, the coverslips were incubated with goat anti-mouse 594 (Molecular Probes) at room temperature for 1 hour and mounted in Prolong Gold with DAPI (Invitrogen). Imaging was performed using the Zeiss Axio Imager A1.

***In vivo* analysis of infection.** 5-week-old female C57/BL6 (The Jackson Laboratory) were maintained in the animal facilities at UCLA in accordance with the University of California Animal Research Committee guidelines. The FUhLucW vector was pseudotyped with VSV-G, T5F/wt G, or T5F ΔN3/wt G envelopes. 5 or 10 μg of p24 of each virus stock was injected into the tail vein. 5 days post-injection, the mice were anesthetized and injected intraperitoneally with 3 mg of D-luciferin (Xenogen). A cooled IVIS CCD camera (Xenogen) was used to obtain whole-body images. Organs (brain, lung, heart, spleen, liver) were excised from sacrificed mice for imaging. For biodistribution studies, which required the quantitation of integrated vector copy number in various tissues, the FG12 vector was pseudotyped with VSV-G or NiV envelopes. 5 ug of p24 of each virus stock was administered as above. 4 days post-injection, the mice were sacrificed and organs (liver, spleen, lung, brain, heart, kidney, bone marrow) were harvested. Organs were minced and cells dissociated as previously described [35]. We modified the protocol to extend the digestion time to one hour. Genomic DNA was harvested

using an Allprep kit (Qiagen). Quantitation of the vector copy number and cell number in the DNA isolate was performed with LightCycler 480 SYBR Green I Master (Roche) using the LightCycler 480 real-time PCR system (Roche). The FG12 plasmid was used as the standard for quantitation of vector copy number. The primers for the analysis of vector copy number were GFP-For (5' GCAGAAGAACGGCATCAAGGTG3') and GFP-Rev (5' TGGGTGCTCAGGTAGTGGT3'). The primers for the analysis of cell number were HPRT-For (5' GCAGCGTTTCTGAGCCATT3') and HPRT-Rev (5' AAAGCGGTCTGAGGAGGA3').

Gene Expression Analysis. The gene expression profiles of various pluripotent stem cell (PSC)-derived and primary (fetal and adult) tissues were determined by the human U133plus2.0 array (Affymetrix) at the UCLA Clinical Microarray Core. Multiple independent arrays (>3) were performed on each cell type shown in Table I.

Results

Efficient pseudotyping of a lentiviral vector with the Nipah virus envelope glycoproteins only requires truncations in the cytoplasmic tail of the F protein. Previous studies have shown that pseudotyping of lentiviral vectors with unmodified paramyxoviral glycoproteins is highly inefficient [36]. However, recent studies with the measles virus envelope showed that when the cytoplasmic tails of both the fusion (F) and attachment (H) glycoproteins are truncated, infectious particles are produced [6,7]. The highest titers were obtained when only 3 residues were left in the F protein cytoplasmic tail and 15 residues in the H protein cytoplasmic tail. In contrast, a study with the Nipah virus (NiV) envelope showed that the full-length glycoproteins (F and G) could be used to pseudotype a lentiviral luciferase reporter vector, although a truncated F mutant with only 4 residues left in its cytoplasmic tail did result in a ten-fold increase in luciferase expression compared to wild-type F [16]. However, no data regarding the infectious titers produced were given, and neither the transduction efficiency of their NiVpp on relevant primary cells, nor the potential of NiVpp for targeted transduction *in vivo* was examined.

To confirm and extend these findings, we took advantage of a previously characterized truncated variant of NiV-F, T5F [27], with 5 residues left in the cytoplasmic tail (Fig. 2-1A, top panel), but which was otherwise expressed and processed at wild-type levels [27]. When used in combination with wild-type (wt) NiV-G to pseudotype the FG12 lentiviral vector containing a GFP reporter gene, T5F/wtG NiVpp gave a titer of ~10^6 I.U./ml on 293T cells, a 100-fold increase in titer compared to wtF/wtG pseudotypes (Fig. 2-1B). Pseudotyping of NiV T5F/wtG onto the pNL4-3-Luc-E^-R^+ vector that was used in the above mentioned study [16] also resulted in a 100-fold increase in luciferase expression compared to wtF/wtG NiVpp across a three-log dilution of the virus stock (Fig. 2-1C). However, pNL4-3-Luc-E^-R^+ is obviously not suitable as a gene therapy vector as it expresses the entire set of HIV genes except for Env, and lacks the cardinal safety features of lentiviral-based gene therapy vectors. Thus, in our subsequent

studies, we will focus on using the FG12 vector, a HIV derived self-inactivating lentiviral vector designed for gene therapy purposes [30,33].

In an effort to further increase viral titers, we generated variants with stepwise truncations in the NiV-G cytoplasmic tail (Fig. 2-1A, bottom panel) and screened them in combination with T5F. Although the T5F/Δ10G and T5F/Δ25G variants demonstrated similar titers to T5F/wtG, none of the NiV-G variants produced greater titers than wtG (Fig. 2-1B). Moreover, all combinations of wt F with the different NiV-G truncation variants produced extremely low titers (data not shown). Collectively, these results indicate that only truncations in NiV-F are critical for producing high titer functional pseudotypes when combined with wt NiV-G. Thus, all subsequent experiments were performed with the T5F/wtG variant as a starting point. As for VSV-Gpp, NiVpp could be concentrated by ultracentrifugation without lost of infectivity to produce titers of ~10^8-10^9 IU/ml compared to 10^{10} for VSV-G (data not shown).

To determine whether the difference in titer between the T5F/wtG and wtF/wtG pseudotypes was due to the efficiency of envelope incorporation onto the lentiviral particle, we purified NiVpp by ultracentrifugation and determined the amount of F and G on an equivalent amount of virions (normalized by the amount of HIV capsid p24) by western blot. Unlike that for MeVpp, where full-length wtF/wtH were not detectably incorporated into pseudotyped particles, there was no difference in levels of NiV F and G incorporated between wtF/wtG and T5F/wtG pseudotypes (Fig. 2-1D). In addition, both wtF and T5F were equivalently processed (F_0/F_1). Thus, truncation of the NiV-F cytoplasmic tail did not necessarily enhance incorporation onto virus particles, as was demonstrated by studies with the measles virus envelope [6,7,37]. This suggests that there may be some incompatibility of the cytoplasmic tail of wild-type NiV-F with the matrix (gag) protein of HIV that compromises the fusogenicity of NiV-F, and hence the infectivity of NiVpp.

We hypothesized that if the incompatibility is specific to the HIV gag protein, then wtF/wtG “pseudotyped” onto NiV matrix (NiV-M), to make infectious virus-like particles (VLPs),

should not show a significant difference in infectivity compared to VLPs produced with T5F/wtG. To test this, we used an established β-lactamase-NiV matrix (βla-M) based assay to compare entry of wild-type NiV-F and T5F VLPs [26]. Entry of VLPs is detected by cytosolic delivery of βla-M to target 293T cells preloaded with the fluorescent CCF2-AM substrate. βla-mediated cleavage of CCF2-AM results in a shift of green to blue fluorescence. Thus, the blue to green fluorescence ratio can be monitored in real-time to compare the relative differences in entry efficiency due to virus-cell fusion. Fig. 2-1E shows that the rate and extent of virus-cell fusion between wt F and T5F VLPs were very similar, plateauing at 2.38 and 2.65, respectively. To further confirm this finding, we pseudotyped wild-type NiV-G with either NiV-F or T5F onto a VSVΔG-rLuc core, and infected 293T cells with 10-fold dilutions of each virus stock. T5F pseudotypes demonstrated only up to a 2-fold difference in R.L.U. compared to wt F pseudotypes (Fig. 2-1F). Thus, the 100-fold difference in titers of wt F and T5F lentiviral pseudotypes is most likely due to a specific incompatibility of the long cytoplasmic tail of NiV-F with HIV gag that compromises the fusogenic activity of NiV-F but not its ability to be incorporated into lentiviral particles.

A hypoglycosylated hyperfusogenic NiV-F mutant demonstrates increased infectivity *in vitro*. EphrinB2 is likely the primary entry receptor for NiV [17,18], while ephrinB3 may serve an alternate receptor on some cell types [19,38]. Chinese hamster ovary (CHO) cells do not express endogenous ephrinB2 and B3, and are therefore refractory to NiV envelope-mediated infection. However, stable CHO cell lines expressing ephrinB2 (CHO-B2) or ephrinB3 (CHO-B3) can readily support NiV infection [19]. To compare the relative entry efficiency of NiVpp via the ephrinB2 and ephrinB3 receptors, we first infected CHO-B2 or CHO-B3 cells with 0.01, 0.1, and 1 ng p24 equivalents of NiVpp bearing T5F/wtG (Fig. 2-2, A-C, grey bars), and normalized the infectivity observed with that obtained with 1 ng of VSV-Gpp (Fig. 2-2D). Since VSV-Gpp infection should *not* depend on the presence of ephrinB2 or B3, this normalization allows for

comparison across multiple independent experiments. Fig. 2-2, A-C shows that T5F/wtG pseudotypes infected a similar percentage of CHO-B2 and CHO-B3 cells in a dose-dependent manner such that at the maximal viral input (1 ng p24), 38% of CHO-B2 and 39% of CHO-B3 cells were infected relative to an equivalent amount of VSV-Gpp (compare Fig. 2-2C and 2-2D, grey bars at 1 ng).

Since we found that only modifications to NiV-F were critical for pseudotyping (Fig. 2-1), we sought to further improve transduction efficiency by pseudotyping lentiviral particles with a hyperfusogenic NiV-F variant in which an N-linked glycosylation site has been removed (T5FΔN3) [28]. The titer of T5FΔN3/wtG pseudotypes on highly permissive 293T cells was similar to that of T5F/wtG pseudotypes (data not shown). However, on CHO-B2 cells, the hyperfusogenic T5FΔN3/wtG pseudotypes consistently exhibited a two-fold increase in infectivity relative to the T5F/wtG pseudotypes (Fig. 2-2, A-C). This held true across a 100-fold difference in the amount of viral inoculum used. Although receptor specificity is determined by the attachment protein, there are examples of hyperfusogenic mutations in paramyxoviral F proteins that enable fusion triggering in the absence of their homotypic attachment proteins [39-42]. This does not appear to be true for the hyperfusogenic NiV-F as the increased infectivity of T5FΔN3/wtG pseudotypes was abrogated by soluble ephrinB2. Similar results were observed on CHO-B3 cells at moderate (0.1 ng) and high (1 ng) viral input levels (Fig. 2-2, B-C, compare black and grey bars); however, no specific infectivity was detected at the lowest viral inoculum level on CHO-B3 cells (Fig. 2-2A). At the highest viral inoculum used, T5FΔN3/wtG NiVpp infection approached the transduction efficiency of VSV-Gpp, infecting 80% and 97% of CHO-B2 and CHO-B3 cells, respectively (Fig. 2-2D).

Lastly, since ephrinB2 is endogenously expressed at high levels on endothelial cells and cells of the central nervous system, we compared the transduction efficiencies of T5F/wtG and T5FΔN3/wtG pseudotypes on human microvascular endothelial cells (HMVECs) and the U87 glioblastoma cell line (Fig. 2-2, E-F). The two-fold increase in infection efficiency of

T5FΔN3/wtG over T5F/wtG pseudotypes was observed for U87 (59.8% versus 32.3% at 1 ng) cells, but not for HMVECs (96.6% versus 87.6%), which were already highly permissive to NiVpp infection. In summary, although both pseudotypes had similar infectivity on highly permissive cells such as 293Ts and HMVECs, the hyperfusogenic T5FΔN3/wt G pseudotypes nevertheless exhibited increased infectivity on some cell lines.

NiV pseudotypes specifically target ephrinB2-positive cells in a vast excess of receptor-negative cells. Entry of T5F/wtG and T5FΔN3/wtG pseudotypes into multiple cell types was inhibited by soluble ephrinB2 (Fig. 2-2), confirming the specificity of receptor-mediated entry. Next, we investigated whether the NiV pseudotypes could specifically target ephrinB2-positive cells in a mixture of ephrinB2-positive and -negative cells. U87 (ephrinB2-positive) cells were mixed with CHO (ephrinB2-negative) cells in 1:1, 1:10, 1:100, and 1:1000 ratios, and transduced with 1 or 10 ng p24 equivalents of NiV or VSV-G pseudotypes (Fig. 2-3). To distinguish infection of the human U87 cells from non-human CHO cells, the infected cells were stained with an anti-HLA (anti-MHC class I) monoclonal antibody specific for human HLAs. At a 1:1 ratio and 1 ng of virus, the GFP+ cells transduced by both the T5F/wtG and T5FΔN3/wtG pseudotypes remained entirely within the HLA+ population (Fig. 2-3A, top panel). Increasing the amount of virus inoculum by 10-fold (10 ng) did not affect the specificity, since the NiVpp transduced GFP+ cells remained within the HLA+ population (Fig. 2-3A, bottom panel). Furthermore, across all cell ratios, the NiV pseudotypes selectively transduced the ephrinB2+ U87 cells even after accounting for the differential permissivity of CHO cells versus U87 cells for HIV-1 based lentiviral transduction (Fig. 2-3, B-C). VSV-G pseudotypes, on the other hand, transduced both HLA+ and HLA- cells, indicating its relative lack of specificity. In sum, our data suggest that NiV pseudotypes can selectively target ephrinB2-positive U87 cells even in a 1000-fold excess of ephrinB2-negative CHO cells (Fig. 2-3C). Our data also demonstrates that increasing the fusogenicity of NiVpp did not necessarily compromise its specificity.

NiV pseudotypes mediate entry into human embryonic, neural and hematopoietic stem cells. On the basis of microarray and bioinformatics analysis, ephrinB2 has been identified as a molecular stem cell signature common to mouse embryonic (ESCs), hematopoietic (HSCs) stem cells, and neural (NSCs) [22]. To determine if ephrinB2 also marks for their human stem cell counterparts, we determined if our NiVpp could mediate gene transfer into human ESCs, HSCs, and NSCs (Fig. 2-4). Indeed, adding increasing amounts of T5F/wtG pseudotypes to H9 hESCs resulted in a dose-dependent increase (14-36%) in the amount of cells positive for GFP and SSEA-4, a cell-surface human pluripotency marker (Fig. 2-4A). This infection was specific since it was blocked by soluble ephrinB2 (Fig. 2-4B). To ensure that this ephrinB2-mediated transduction was not specific to the H9 hESC line, we infected two other hESC lines (H1 and UCLA1) and obtained similar results (Fig. 2-4B). Since stem cells are more difficult to transduce than standard cell lines, we expected that the hyperfusogenic T5FΔN3/wt G variant would mediate entry more efficiently than T5F/wtG NiVpp. However, we did not see an increase in infection using the T5FΔN3/wt G pseudotypes (Fig. 2-4C).

Next, we infected purified CD34+ cells isolated from human fetal liver with NiV pseudotypes. CD34 is expressed on human hematopoietic stem and progenitor cells (HSPCs), although only a small fraction of CD34+ cells are true hematopoietic stem cells (HSCs) that have extensive self-renewal capacity *in vitro* and can engraft immunodeficient mice [30,43]. At a multiplicity of infection (MOI) of 1000, both T5F/wtG and T5FΔN3/wt G pseudotypes reproducibly transduced 3.6% and 3.5% of CD34+ cells, respectively. The specificity of this low-level infection was confirmed by blocking with soluble ephrinB2 (Fig. 2-4D). True human HSCs have two cardinal properties: multipotency, defined as the ability to differentiate into all blood cell lineages, and long-term self-renewal, defined by the inexhaustible ability to produce progeny functionally identical to the parent upon cell division [43]. Human HSCs with these properties are enriched in the Lin-CD90+CD34+CD38- fraction of cord blood [44]. To determine

whether ephrinB2 is expressed in this fraction, we FACS-sorted 4 populations from CD34+ cells isolated from human fetal liver: CD90+CD34+CD38-, CD90-CD34+CD38-, CD90-CD34+CD38+, and CD90-CD34-CD38+ (Fig. 2-4E). RNA was extracted from each sorted population and ephrinB2 expression quantified using real-time PCR analysis. Our results indicate that ephrinB2 is expressed the highest in the CD90+CD34+CD38- fraction (Fig. 2-4F). Thus, the NiV pseudotypes may be targeting the cognate population of CD34+ cells enriched for true HSC activity.

Lastly, we assessed the transduction efficiencies of the NiV pseudotypes on nestin+ NSCs derived from hESCs (Fig. 2-4G). Unlike hESCs and CD34+ HSPCs, increasing the MOI resulted in a dose-dependent increase in the percent of NSCs transduced such that the percent of GFP+ cells approached 100% at a MOI of 100 (Fig. 2-4H). However, similar to the hESC and hHSC transductions, the T5FΔN3/wt G pseudotypes did not demonstrate increased infectivity compared to the T5F/wtG pseudotypes. Nevertheless, we confirmed that ephrinB2 is functionally expressed on human ESCs, HSCs, and NSCs, at least at levels that can mediate NiVpp infection.

NiV pseudotypes bypass the liver sink *in vivo*. EphrinB2 is expressed on endothelial cells, smooth muscle cells, and neurons [45,46]. In contrast, ephrinB3 is not expressed in the endothelium, and demonstrates overlapping but also distinct expression patterns in the central nervous system [47]. This is consistent with our own microarray expression studies in a variety of human- and fetal tissue-derived as well as pluripotent stem cell (PSC) derived cell types (Table 2-1). The ephrinB2/ephrinB3 expression patterns are in concordance with NiV infection *in vivo*, since histopathological studies on human patients detected the highest levels of viral antigens in neurons and endothelial cells of small blood vessels in the brain, but some was also observed in the vasculature of the lung and spleen. [48,49]. Importantly, no viral antigens were detected in the

liver [49], also consistent with our data in Table 2-1, which shows the lack of ephrinB2 and B3 expression in adult tissue derived hepatocytes.

The inability to detect viral antigens in liver autopsy tissues from NiV infected patients, and the lack of viral receptor expression in the liver prompted us to examine whether intravenous administration of NiVpp might bypass the liver sink and target accessible ephrinB2+ cell types *in vivo*. We pseudotyped the FvcFlw lentiviral vector containing a firefly luciferase reporter gene with the NiV and VSV-G envelopes, and administered the viruses intravenously through the tail vein of C57/BL6 mice (Fig. 2-5). A CCD camera was used to quantify the level of luciferase expression in the mice after injection of the D-luciferin substrate. Consistent with previous studies, VSV-Gpp-mediated transgene expression was detected primarily in the liver and spleen (Fig. 2-5B, top panel). For the T5F/wtG pseudotypes, a slight signal was detected in the spleen in one case (Fig. 2-5B, middle panel). Strikingly, the T5FΔN3/wt G pseudotypes showed a substantially enhanced signal in the spleen in all cases and lung in one case (Fig. 2-5B, bottom panel). Thus, the T5FΔN3/wt G hyperfusogenic mutant demonstrates increased infectivity *in vitro* and *in vivo*. Significantly, neither the T5F/wtG or T5FΔN3/wtG pseudotypes exhibited any signal in the liver in all cases.

To complement and confirm these results, we also examined genomic vector integration in various tissues in an independent set of mice. The FG12 vector was pseudotyped with VSV-G and NiV envelopes, and viruses were administered as above. Four days post-injection, whole organs (liver, spleen, and lung) were harvested and cells dissociated. Genomic DNA was extracted and quantitation of vector integration was performed using real-time PCR analysis. This PCR based assay was more sensitive (limit of sensitivity ~0.01 vector integrants/10,000 cells) and confirmed key aspects of our luciferase imaging results: while VSV-Gpp and NiVpp transduced the spleen with high efficiencies, only the VSV-Gpp transduced the liver, confirming that the NiVpp clearly bypassed the liver sink (Fig. 2-5C). Interestingly, using the FG12 vector,

VSV-G also transduced the lung as well as the NiVpp, although it is unclear whether the same cell types were transduced. The significance of these findings will be discussed.

Discussion

Measles virus and Nipah virus belong to the only two paramyxovirus genera that use protein-based receptors for entry. Studies with the measles virus envelope have shown that complex modifications to its attachment protein, including disruption of its binding site to its natural receptors and appending scFv or other targeting domains, result in specific re-targeting to desired cell populations *in vitro* and *in vivo* [9,50]. Some of these modifications have been successfully adapted to make scFV-directed targeting lentiviral MeVpp [7,51]. However, pre-existing neutralizing antibodies due to wide-spread MeV vaccination may compromise the transduction efficiency of MeVpp when administered in vivo, although deletion of immunodominant epitopes on MeV-H and other modifications have reduced the sensitivity of MeVpp to serum neutralization in vitro [52]. In contrast, NiV is an emerging and lethal pathogen thus far confined to Southeast Asia [53]. Thus, it is unlikely that pre-existing antibodies will pose a barrier to the development of NiVpp as a vehicle for targeted gene therapy. However, in the case of NiV, we sought to take advantage of the physiologically restricted and pathologically relevant expression patterns of ephrinB2, the primary high affinity receptor for NiV. Thus, instead of mimicking the re-targeting strategies used for MeV, we investigated the prospects of generating high-titer NiV pseudotypes that allow for specific targeting of biologically significant ephrinB2+ populations *in vitro* and *in vivo.*

The picomolar affinity of NiV-G for ephrinB2 is amongst the strongest viral envelope-receptor interactions known [13]. This likely accounts for the extraordinary specificity of NiVpp for ephrinB2-expressing cells. We examined whether further increasing the *efficiency* of transduction on a per virion basis without compromising the specificity of NiV-G-mediated infection may facilitate the development of NiVpp for targeted gene therapy to ephrinB2 expressing cells. To that end, we generated NiVpp with a hyperfusogenic F and wt G. Our hyper-fusogenic T5FΔN3/wt G NiVpp appeared to infect some cell types (CHO-B2, CHO-B3, and U87 cells) twice as well as T5F/wt G pseudotypes, but not in other highly permissive cells

such as 293T cells and HMVECs, where transduction efficiencies of the normo-fusogenic T5F/wt G NiVpp already approached that of VSV-Gpp.

Unexpectedly, in hard-to-transduce stem cell populations such as human ESCs and HSCs, the hyper-fusogenic T5FΔN3/wt G pseudotypes also did not show an increase in transduction efficiency over T5F/wt G NiVpp. In addition, both demonstrated similar dose-dependent transduction efficiencies that plateaued at a relatively low percentage of the putative stem cell population. Thus, even at a saturating MOI of 1,000, both T5F- and T5FΔN3-based NiVpp transduced only ~36% and ~3.5% of SSEA4+ hESCs and CD34+ hHSCs, respectively. The limited transduction efficiency seen in human ESCs and CD34+ HSCs may be due to ephrinB2 expression only on a subset of these stem cell populations.

In hESCs, which are optimally passaged as colonies of cells, each colony contains heterogeneous subpopulations of cells that interact as an "ecosystem" to maintain the cardinal properties of hESCs: self-renewal and pluripotency [54,55]. For example, Stella and Nanog expressing subpopulations are biased towards self-renewal, whereas GATA-6 expressing subpopulations are more poised towards differentiation, and in between is a continuum of cells that contributes to the unique phenotypic properties of each hESC line [56]. The ephrinB2+ subpopulation, or rather the fraction of ephrinB2+ cells that is maintained in hESC colonies, may be regulated to provide the optimal milieu for maintaining the cardinal properties of "stemness". This speculation is consistent with the known properties of ephrin-eph ligand-receptor interactions (both are receptor tyrosine kinases) for maintaining or enforcing tissue and cell type boundaries [57,58]. Thus, the ability to mark a subpopulation of hESCs with NiVpp-mediated transduction provides an experimentally tractable tool to examine the role of these ephrinB2+ subsets in hESC fate: survival, self-renew and pluripotency.

On the other hand, only a small subpopulation of CD34+ cells harbors true multipotent HSCs capable of long-term (LT) self-renewal, operationally defined by multi-lineage reconstitution in immunodeficient NOD-SCID mice. These LT-SCID repopulating cells can be

found at least within the CD34+/CD38-/CD90+ subset [44,59,60]. Intriguingly, we found that ephrinB2 is expressed highest in this subset (Fig. 2-4F). This is also consistent with the finding that ephrinB2 is found in the functional murine equivalent of LT-HSC [22]. Moreover, data from Fig. 2-4, E-F indicate that the CD38-/CD90+ subset comprises less than 8% of total CD34+ cells from human fetal liver, which is close to but more than the ~3.5% of CD34+ cells infected by NiVpp at maximal MOI. Since LT-SCID repopulating cells are highly enriched in, but do not comprise the totality of CD34+/CD38-/CD90+ cells, this raises the possibility that NiVpp may indeed be targeting the elusive "true" HSC population within the CD34+/CD38-/CD90+ subset. Functional confirmation will require limiting dilution in LT-SCID repopulating assays, which is a focus for future studies.

We are cognizant that cell-type dependent post-entry restriction factors may limit the efficiency of NiVpp transduction no matter how fusogenic we make the F protein to be. However, the extraordinary specificity of NiVpp exhibited by its ability to selectively target ephrinB2+ cells even in a 1000-fold excess of ephrinB2-negative cells (Fig. 2-3), prompted us to examine the transduction efficiency of NiVpp *in vivo*, especially when the NiV pseudotypes are administered intravenously, and therefore subjected not only to dilution into the blood and tissue volume, but also to the problem of hepatic clearance, a critical barrier for *in vivo* virus-based gene therapy [23,24,61]. Interestingly, when VSVpp and NiVpp carrying a luciferase reporter gene were injected into mice intravenously, and subsequently subjected to whole animal and organ imaging for D-luciferin-induced bioluminescent signals, T5FΔN3/wt G pseudotypes demonstrated an enhanced signal in the spleen and lungs compared to T5F/wt G (Fig. 2-5B). Significantly, we did *not* detect a signal in the liver with either NiVpp as was observed with the VSV-G pseudotypes, suggesting that NiVpp could bypass the liver sink. However, in vivo bioluminescent imaging has limited sensitivity as signals are generally detected only when high local concentrations of cells are transduced (typically $>10^3$ to 10^4) [62,63]. Thus, we performed a sensitive PCR based biodistribution study to quantify the copy number of genomic vector

integrants in these tissues (Fig. 2-5C). This PCR assay confirmed that NiVpp did not transduce the liver to any significant level above background, while VSV-Gpp clearly could.

Rapid clearance and degradation of intravenously administered viral vectors by the liver has long been noted as an important obstacle in virus-based gene therapy [23,24,61]. Our data suggests that the NiVpp can effectively bypass the liver sink and target ephrinB2+ cells in selected organs *in vivo* without the need for modifying the intrinsic specificity of the receptor binding attachment protein (NiV-G). Interestingly, our PCR based biodistribution studies (Fig. 2-5C) showed that both normo- (T5F/wt G) and hyper- fusogenic (T5FD3)/wt G) NiVpp could transduce the spleen and lung with equivalent efficiencies, which is in contrast to the bioluminescent results (Fig. 2-5B). Additionally, our biodistribution assay also showed that VSV-Gpp (FG12 vector based) could transduce the lung at the same levels as NiVpp, but bioluminescent signals was clearly lacking in the lung of VSV-Gpp (FvcF1w vector based) transduced animals. VSV-Gpp can transduce a wide array of tissues, and thus the lack of detectable bioluminescent signals in the lung is likely a reflection of the limits of the detection methodology as discussed above. However, identification of the specific cell populations infected in the spleen and lungs is necessary for future optimization of the NiVpp platform for targeted gene therapy. EphrinB2 is expressed *highly* on endothelial cells, smooth muscle cells surrounding some arterioles, and neurons [45,46]. Unlike ephrinB2, ephrinB3 is mostly expressed in the CNS [47]. Our own expression studies on multiple cell types and tissues confirm and extend these findings (Table 2-1). As mentioned, these expression patterns are in concordance with the tissues that are targeted in the context of a natural human Nipah virus infection [64]. Importantly, Table I also shows that endoderm tissues do not express ephrinB2 or B3. Indeed, of the major organs examined in a large autopsy series, the liver is one of the few organs that exhibited no pathology or presence of any detectable viral antigens [49]. The latter observations are consistent with the lack of liver transduction seen with our NiVpp. In spleen, viral antigen staining can be seen in macrophages and multinucleated giant cells. In the lung, viral antigen is

most commonly seen in small blood vessels, and less often, in bronchial epithelial cells and alveolar macrophages. Since intravenous administration of NiVpp does not reflect the natural mode of NiV infection, determining the cell types transduced by NiVpp in the spleen and lung will be an important focus of future studies.

Altogether, our data demonstrates that we can generate high-titer, concentrated stocks (10^8-10^9 IU/ml) of NiVpp that can specifically target ephrinB2- and ephrinB3-positive cells *in vitro* and *in vivo*. Although NiV uses ephrinB3 as an alternate receptor, the affinity of NiV-G for ephrinB3 is less than that for ephrinB2 [19]. Nevertheless, ephrinB3 is expressed in regions in the CNS where ephrinB2 is lacking, including the corpus callosum and spinal cord [65]. Thus, NiV pseudotypes can potentially be used to also target these ephrinB3-positive regions. EphrinB2 has been shown to be upregulated in many types of cancer, including ovarian [66], uterine [67], and colon [68]. In the appropriate context, inhibition of ephrinB2-ephB4 interactions has resulted in inhibition of tumor growth and angiogenesis [69]. In some cases, breast cancer stromal cells over express ephB4 to attract tumor angiogenic vessels that overexpress ephrinB2 [70]. Thus, NiV pseudotypes can be potentially used to either target appropriate tumors where overexpression of ephrinB2 has been linked to poorer prognosis, or antagonize ephrinB2 interactions with ephB4 to inhibit tumor angiogenesis (reviewed in [20,21]).

Many other viral envelopes have been modified for targeted gene therapy. For many of them, the receptor-binding domain and the fusion domain of the envelope are produced from a single viral *env* gene. Thus, manipulation to enhance receptor-targeting specificity is more likely to adversely affect the fusion domain of the envelope protein, resulting in low viral titers. For paramyxoviruses, the receptor-binding attachment protein and the fusion protein are produced from two independent viral genes. Mechanistic studies as to how receptor binding to the attachment protein leads to allosteric triggering of the fusion protein is an area of intense study by many labs (reviewed in [9,13,50,51,71,72]). For the henipaviruses, a large body of work has accumulated regarding the independent determinants of fusogenicity in F and G. Thus, F can

be made even more fusogenic by incorporating other mutations that are already well characterized in the literature [4,27,28,73-75]. Indeed, even the specificity and fusogenicity of G itself can be optimized based on published structural and functional data [5,13,39,40,52,53,76]. Altogether, this confluence of properties makes NiV pseudotypes highly attractive for further development as a targeted gene therapy vector for *in vitro* and *in vivo* applications.

Figure 2-1

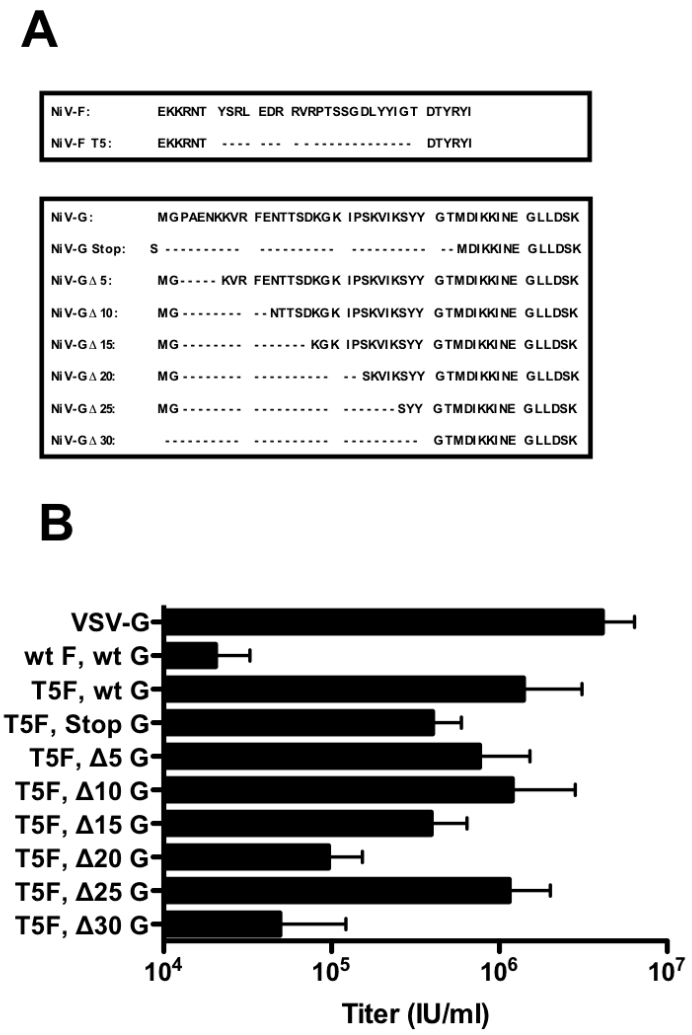

Figure 2-1. Characterization of NiV-F and -G protein variants used for pseudotyping of an HIV-1-derived lentiviral vector. (A) A schematic of the amino acid sequences of the cytoplasmic tails of the NiV F (top) and G (bottom) protein variants is shown. T5F is a cytoplasmic tail truncation of NiV-F previously described [27]. The 6 amino acids to the right is the AU1 tag at the cytoplasmic C-terminus of the F protein. Stepwise truncations in the cytoplasmic tail of NiV-G were generated and screened in combination with T5F for the ability to form functional lentivirus pseudotypes. **(B)** Pseudotyped lentiviruses were made with the FG12 vector where the UbiC promoter drives eGFP expression. Codon-optimized NiV-F and NiV-G genes were transfected at a 1:1 ratio and supernatants harvested at 48h after transfection. Serial dilutions of unconcentrated viral supernatants were titered on 293T cells. Cells were examined for GFP expression 72h post-transduction by FACS analysis. Titers are expressed as IU/ml. Data shown are averages ± standard deviations from three independent experiments.

Figure 2-1 (continued)

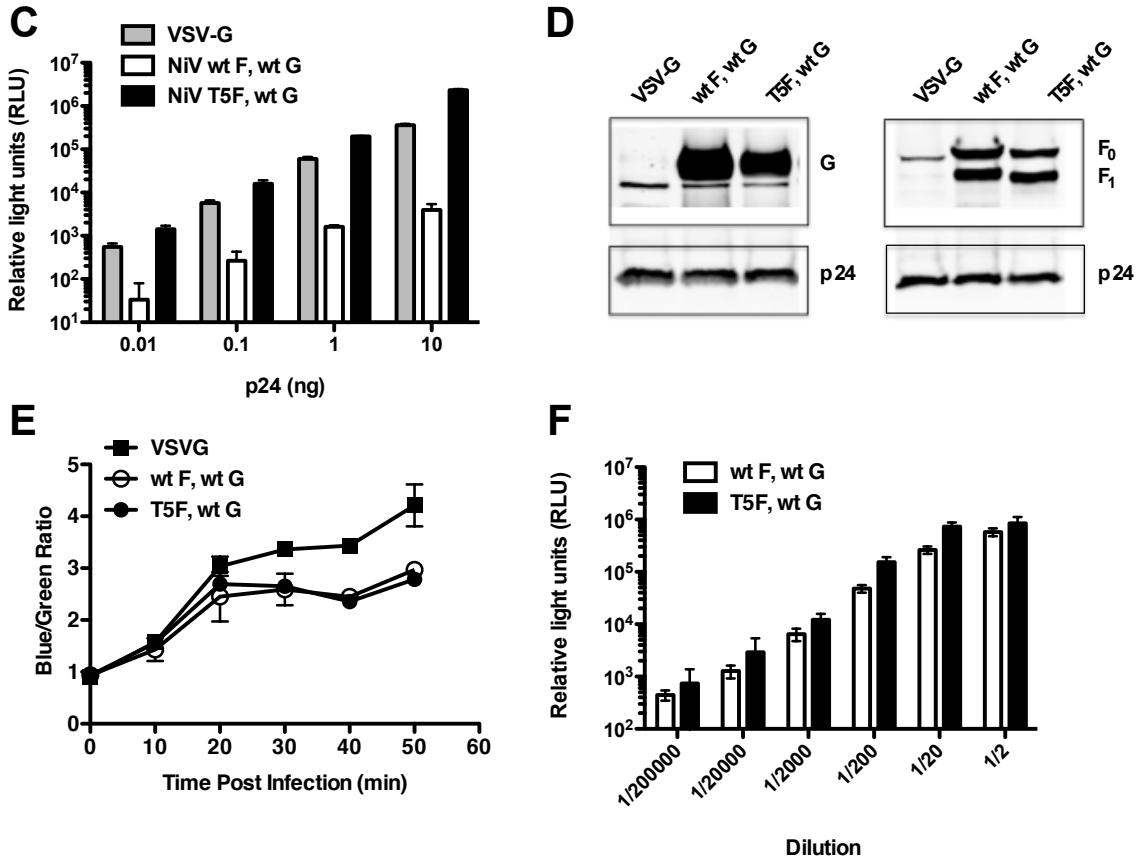

Figure 2-1 (cont.) Characterization of NiV-F and -G protein variants used for pseudotyping of an HIV-1-derived lentiviral vector. (C) pNL4-3.Luc.R$^-$.E$^-$ was pseudotyped with VSV-G or NiV envelopes. 293T cells were infected with 0.01 ng, 0.1 ng, 1 ng, and 10 ng (p24 equivalents) of VSV-G or NiV pseudotypes. 72h post-infection, the cells were lysed and analyzed for luciferase activity. Data shown are averages of three replicates ± standard deviations. **(D)** Western blot analysis of HIV-1 pseudotyped particles, pseudotyped with VSV-G and NiV wild-type or variant proteins. NiV-F was detected using an anti-AU1 antibody and NiV-G with an anti-HA antibody. One out of three representative experiments is shown. **(E)** Virus-like particles (VLPs) were produced with NiV β-lactamase-matrix (β-lac-M) and VSV-G, NiV wt F/wt G or NiV T5F/wt G envelopes. Based on densitometry of βla-M blots, equivalent amounts of concentrated VLPs were added to 293T cells for 1 hour at 4°C and then incubated with CCF2-AM substrate at 37°C. The blue and green fluorescence ratios were monitored as a measure of virus-cell fusion as described in the text and Methods. Data is presented as blue:green ratios every 10 minutes. Kinetic readings up to the 50 minutes time point are shown. Duplicate readings are taken at each time point. Data shown are averages ± standard deviations from three independent experiments. **(F)** A VSV-ΔG-Luc core was pseudotyped with NiV wt F/wt G or NiV T5F/wt G envelopes as previously described [19]. Serial dilutions of unconcentrated viral supernatants were titered on Vero cells. 24 hours post-infection, the infected cells were lysed and analyzed for luciferase activity. Data shown are averages of four replicates ± standard deviations.

Figure 2-2

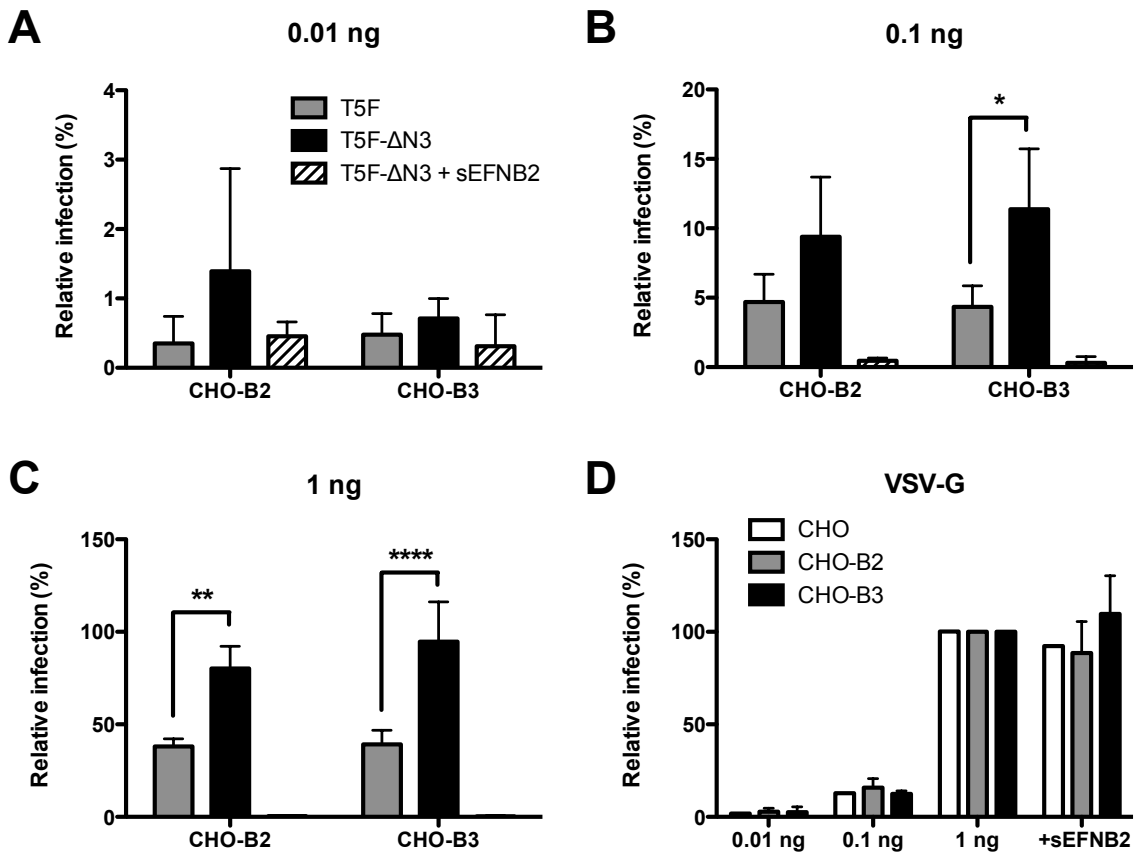

Figure 2-2. NiV T5FΔN3/ wt G hyperfusogenic mutant demonstrates increased infectivity *in vitro*. (A-C) CHO, CHO-B2, and CHO-B3 cells were infected with 0.01 ng, 0.1 ng, and 1 ng (p24 equivalents) of NiV envelope or **(D)** VSV-G lentiviral pseudotypes carrying the GFP reporter gene (CHO cells not shown for NiVpp infection). Infectivity was determined by the percent of GFP+ cells at 48h post-infection via FACS analysis. The % GFP+ cells in each of the CHO cell lines infected by VSV-Gpp at maximal viral input (1 ng) was set at 100%, and all other infections in that cell line were normalized to this value. For reference, at 1 ng, VSV-G infected 20.2% of CHO, 22.7% of CHO-B2, and 21.6% of CHO-B3 cells. For clarity of comparisons, the relative infectivity of T5F/wtG NiVpp versus the hyperfusogenic T5FΔN3/wtG variant on CHO-B2 and CHO-B3 cells using low (0.01 ng), medium (0.1 ng), or high (1 ng) amounts of viral inoculum are shown separately in **(A), (B),** and **(C),** respectively.

Figure 2-2 (continued)

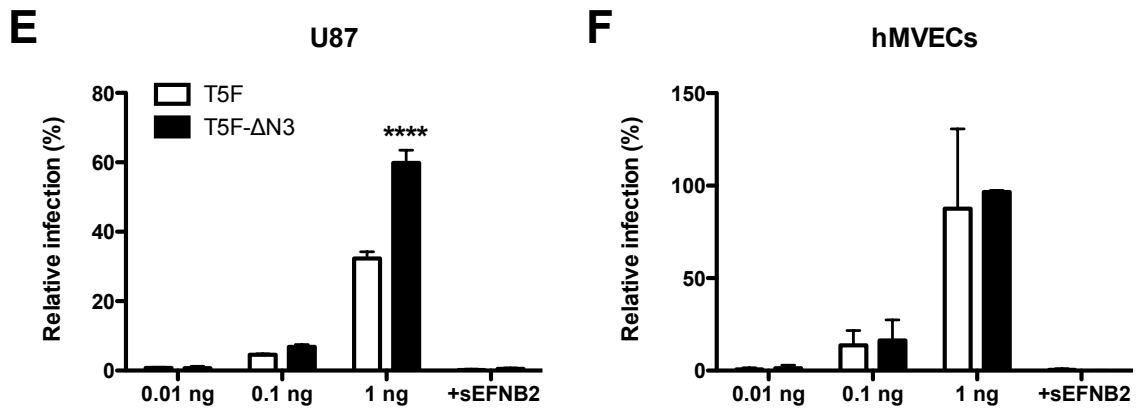

Figure 2-2 (cont.) NiV T5FΔN3/ wt G hyperfusogenic mutant demonstrates increased infectivity *in vitro*. (E) U87 cells and **(F)** HMVECs were infected with T5F/wt G and T5FΔN3/wt G pseudotypes as described for (A-C) but normalized to VSV-Gpp infection of the same cell line (U87 or HMVECs) at maximal viral input (1 ng). For reference, at 1 ng, VSV-G infected 36.5% of U87 cells and 14.4% of HMVECs. Inhibition by 10 nM of soluble ephrinB2 (sEFNB2) was used to demonstrate specificity of NiV receptor-mediated entry. All pseudotyped particle infections, regardless of envelope used, were also abrogated by 5 μM niverapine (NVP), a reverse transcriptase inhibitor (data not shown). Data shown in **(A**-**F)** are averages ± standard deviations for three independent experiments. Statistical analyses were performed using a two-way ANOVA with Bonferroni post-test comparison using GraphPad PRISM™. *: $p < 0.05$, **: $p < 0.01$, ****: $p < 0.0001$.

Figure 2-3

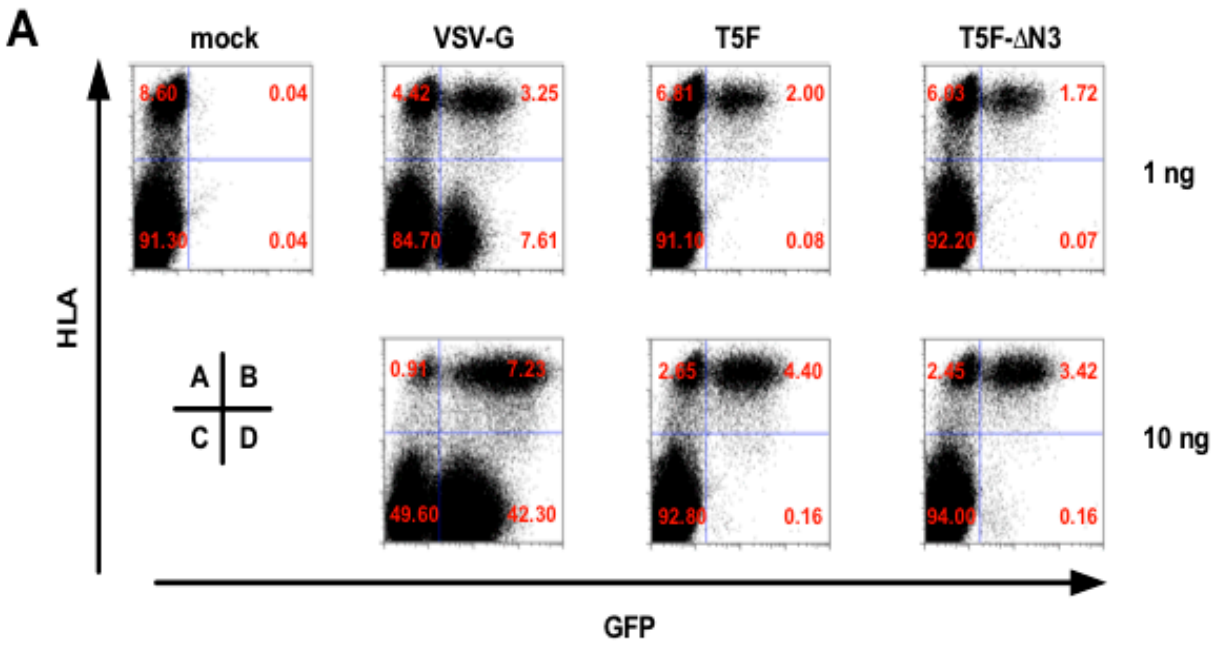

Figure 2-3. NiV pseudotypes can specifically target ephrinB2-positive cells in up to a 1000-fold excess of ephrinB2-negative cells. (A) U87 (ephrinB2+) cells were mixed with CHO (ephrinB2-) cells at different ratios (U87:CHO ratios = 1:1, 1:10, 1:100, and 1:1000) and seeded at a density of 50,000 cells per well in 24-well plates. The next day, cells were infected with 1 or 10 ng of NiV T5F/wt G, T5FΔN3/wt G, and VSV-G pseudotypes. 72h post-infection, the cells were harvested and stained with the W6/32 anti-human HLA-ABC monoclonal antibody and the infection rate (GFP-positive cells) was determined by FACS analysis. Representative FACS plots are shown for data acquired on infection of the 1:1 mixture of U87:CHO cells. Although the cells were seeded and infected at the indicated ratio, the CHO cells divided faster and outgrew the U87 cells by about ten-fold in each sample. Each FACS plot is representative of one of the triplicates at 1 ng and one of the duplicates at 10 ng. Data from 300,000 cells were acquired for every condition used for analysis in part B of this figure.

Figure 2-3

B

Cell-specific Selectivity Index

$$\text{U87 SI} = \frac{B/(A+B)}{D/(C+D)}$$

NiV receptor-specific Selectivity Index

$$\text{EphrinB2 SI} = \frac{\text{(VSV or NiV Env) U87 SI}}{\text{VSV-G U87 SI}}$$

U87:CHO = 1:1		VSV-G	T5F	T5F-ΔN3
U87 SI	1 ng	5.14	258.7	292.5
U87 SI	10 ng	1.93	362.8	342.9
EphrinB2 SI	1 ng	1.00	50.3	56.9
EphrinB2 SI	10 ng	1.00	188.0	177.7

C

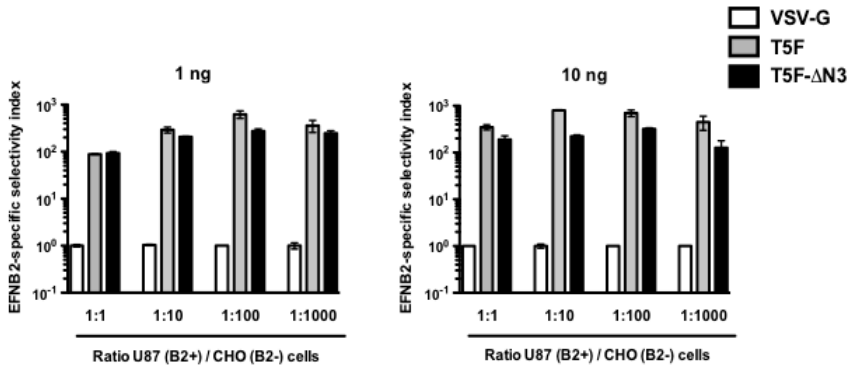

Figure 2-3 (cont.) NiV pseudotypes can specifically target ephrinB2-positive cells in up to a 1000-fold excess of ephrinB2-negative cells. (B) To take into account the differential permissivity of U87 and CHO cells to lentiviral transduction, we first calculated the "cell-specific selectivity index" for U87 cells, the U87 SI as {B/(A+B)}/{D/(C+D)} where B and D represents the % of infected (GFP+) U87 and CHO cells, respectively, and A and C represents their uninfected counterparts, such that the total fraction of U87 (A+B) and CHO (C+D) cells in any given mixture upon analysis must equal 100%. A U87 SI of >1 indicates a selective preference for infecting U87 over CHO cells. For VSV-Gpp, the U87 SI at 1 and 10 ng is 5.14 and 1.93, respectively. This likely reflects the receptor-independent preference for U87 over CHO cells due to the HIV-1 based vector backbone alone. The reduction in U87 SI at a higher inoculum of VSV-Gpp is also consistent with the known ability of VSV-G-delivered gag to saturate non-human post-entry restriction factors such TRIM5a. Since VSV-G is not known to have a cell-type specific receptor, we calculated the "NiV receptor-specific selectivity index", or the "EphrinB2 SI" as the VSV-G or NiV Env specific U87 SI divided by the U87 SI for VSV-G. This normalizes for differences in the intrinsic permissiveness of U87 over CHO cells for lentiviral transduction. This formulation now allows one to evaluate the selectivity of NiVpp for infecting ephrinB2-expressing cells relative to VSV-Gpp under all conditions analyzed. The values of the U87 SI and EphrinB2 SI for the data shown in (A) are indicated here as an example of our analysis. **(C)** The EphrinB2 Selectivity Index for VSV-Gpp, and NiVpp bearing T5F or T5F-DN3 was calculated for all the indicated conditions. Data shown are averages ± standard deviations for triplicates done at 1 ng, and average ± range for duplicates done at 10 ng.

Figure 2-4

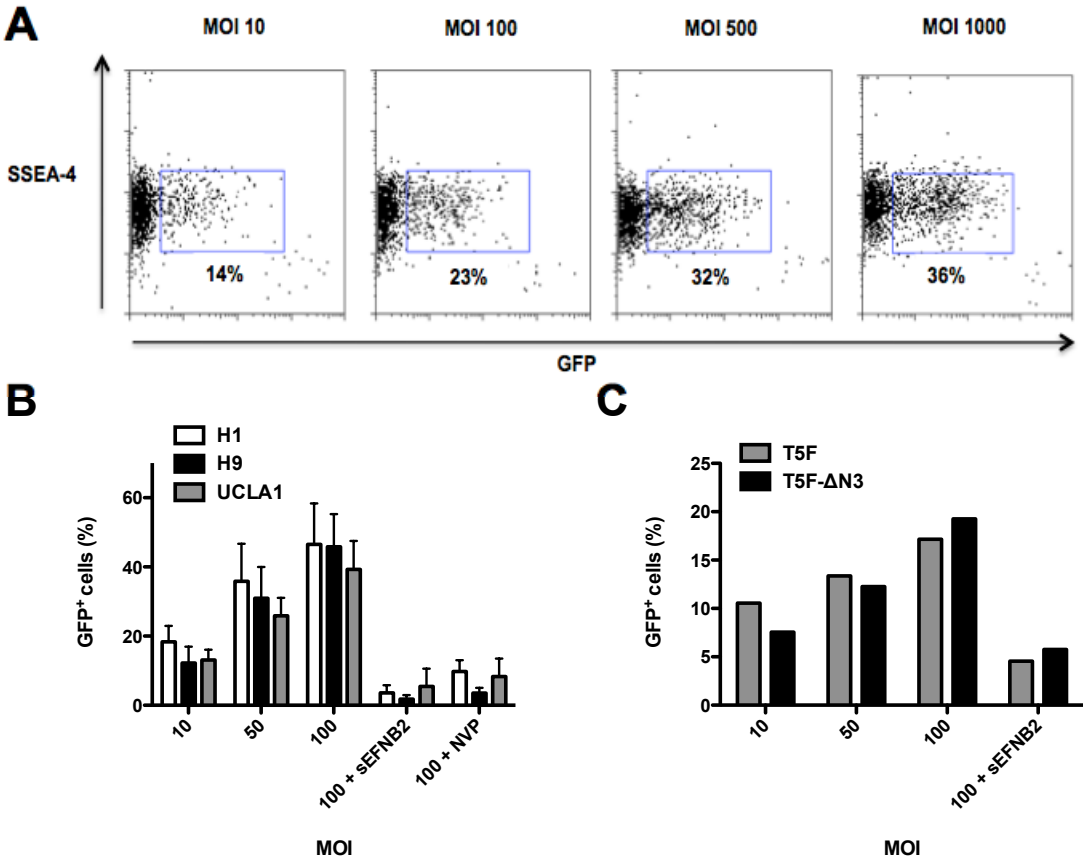

Figure 2-4. NiV pseudotyped lentiviruses infect human embryonic, neural and hematopoietic stem cells. (A) Increasing amounts of NiV T5F/wt G pseudotypes were added to H9 hESCs. Cells were stained for the cell-surface pluripotency marker, SSEA-4, and examined for GFP expression 72h post-transduction by FACS analysis. **(B)** H1 and UCLA1 hESC lines were infected with NiV T5F/wt G pseudotypes as in part (A). Infection was blocked with 10 nM soluble ephrinB2 or 5 μM nevirapine. Data shown are averages ± standard deviations from three independent experiments. **(C)** H9 hESCs were infected with NiV T5F/wt G and T5FΔN3/wt G pseudotypes as in part (A). One out of two representative experiments is shown.

Figure 2-4 (continued)

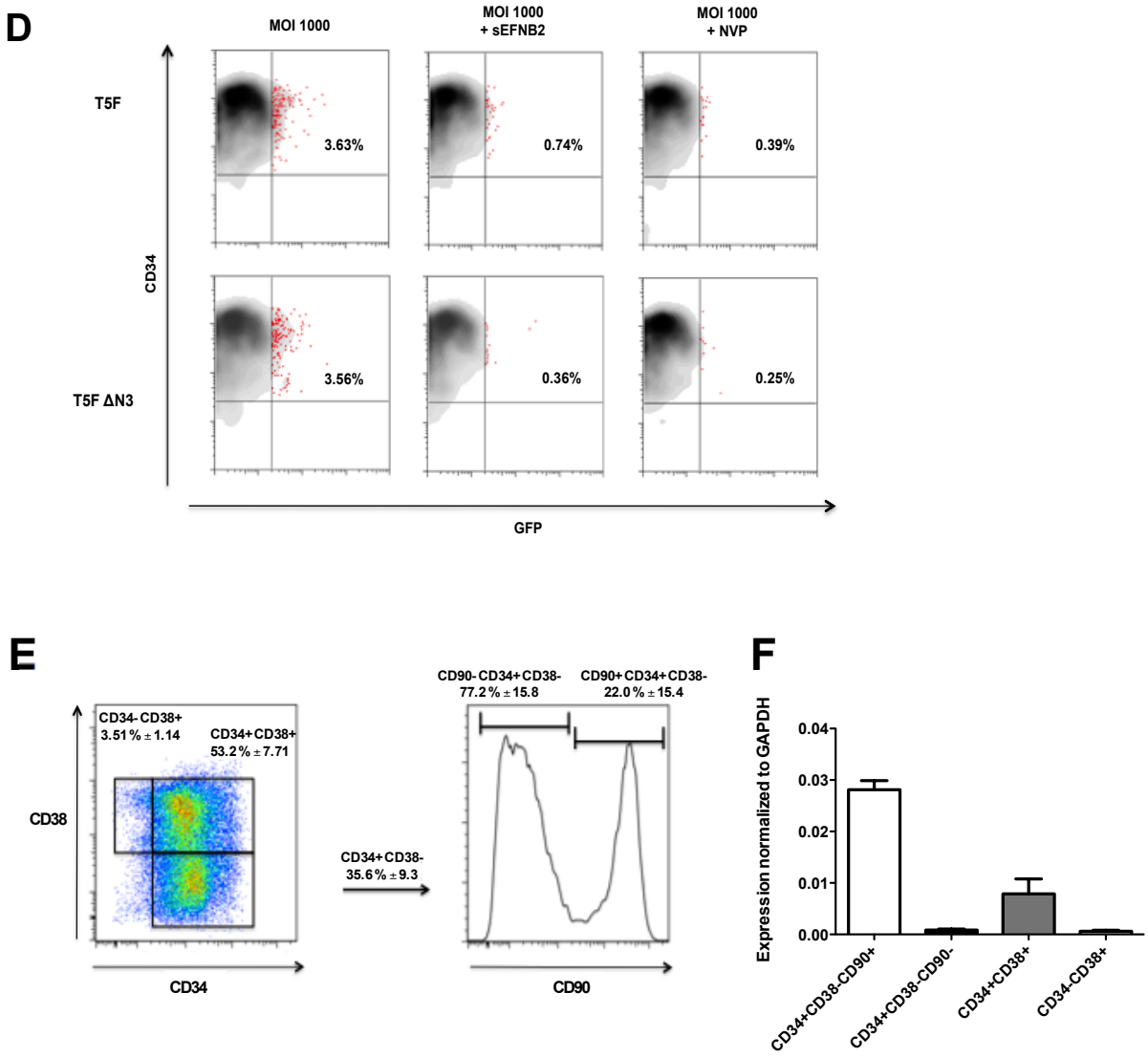

Figure 2-4 (cont.) NiV pseudotyped lentiviruses infect human embryonic, neural and hematopoietic stem cells. (D) Purified $CD34^+$ cells from human fetal liver were infected with the indicated NiVpp in the presence or absence of 10 nM sEFNB2 and 5 μM NVP. 72h post-transduction, cells were stained for the cell-surface marker, CD34, and analyzed for GFP expression by FACS analysis. One representative donor out of three is shown. **(E)** CD34+ cells isolated from human fetal liver were stained with CD90-FITC, CD34-APC, CD38-PE-Cy7 antibodies and DAPI, and FACS-sorted into the 4 populations as indicated. Data shown are averages ± standard deviations from 3 donors. **(F)** RNA was extracted from each cell population indicated in (**E**) and ephrinB2 expression was examined by real-time PCR analysis and normalized against GAPDH as indicted in methods. Data shown are averages ± standard deviations from 3 donors.

Figure 2-4 (continued)

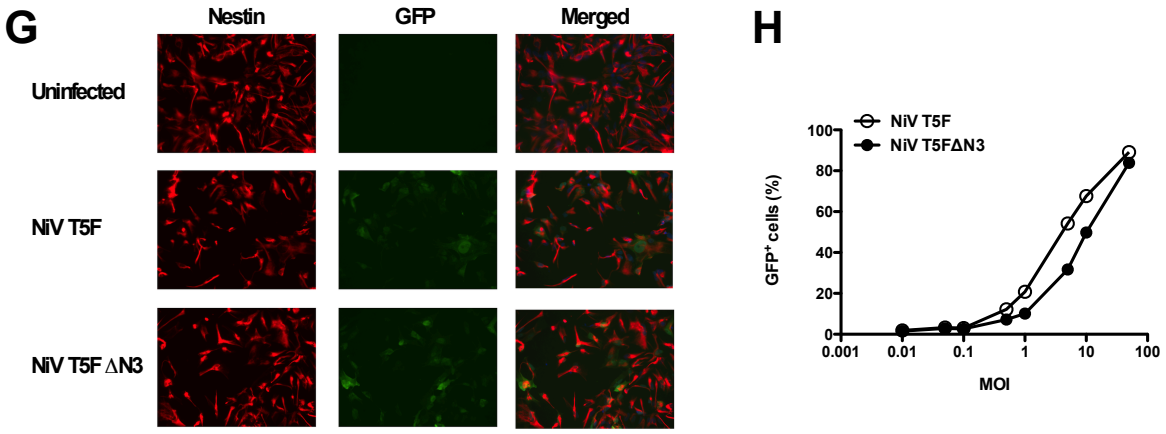

Figure 2-4 (cont.) NiV pseudotyped lentiviruses infect human embryonic, neural and hematopoietic stem cells. (G) Neural progenitors were derived from HSF1 hESCs and infected with NiVpp. 72h post-transduction, cells were stained for nestin and examined by microscopy. **(H)** hNSC GFP expression at each M.O.I. (0.01, 0.05, 0.1, 0.5, 1, 5, 10, and 50) was quantified by FACS analysis. Data shown in **(G)** and **(H)** are from one representative experiment out of four.

Figure 2-5

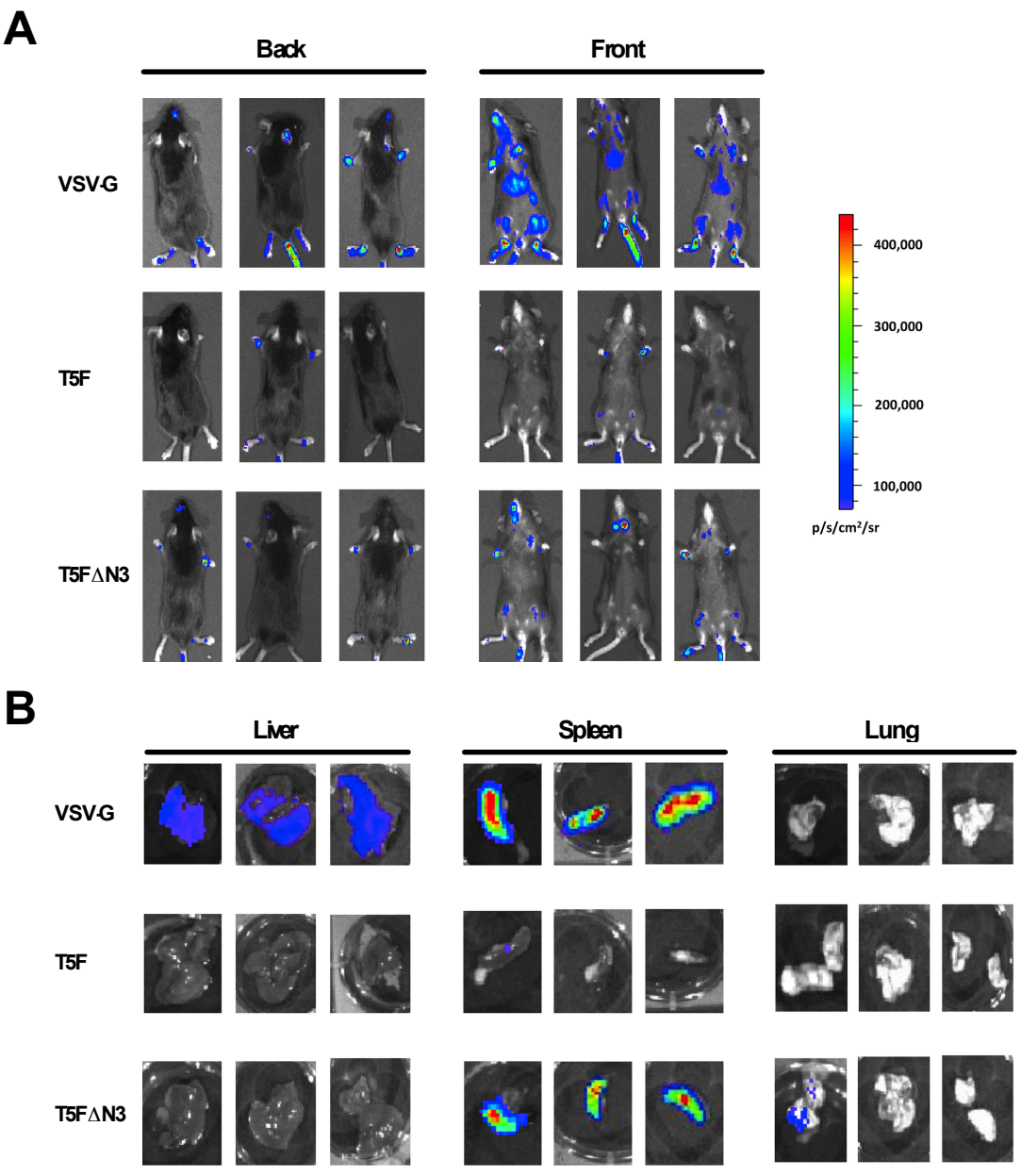

Figure 2-5. NiV pseudotypes bypass the liver sink *in vivo*. **(A)** The FvcFlw (firefly luciferase) vector was pseudotyped with VSV-G and the indicated NiV envelopes. 5-10 ng of p24 equivalent of each pseudotyped lentivirus was injected into C57/BL6 mice through the tail vein. 5 days post-injection, luciferase expression was monitored by CCD imaging of the whole animal after injection of the D-luciferin substrate as described in methods. Three mice from three independent experiments are shown per virus. **(B)** Following whole-body imaging, each organ was isolated and luciferase activity was imaged and quantified as in (**A**). Three organs from three different mice are shown per virus.

Figure 2-5 (continued)

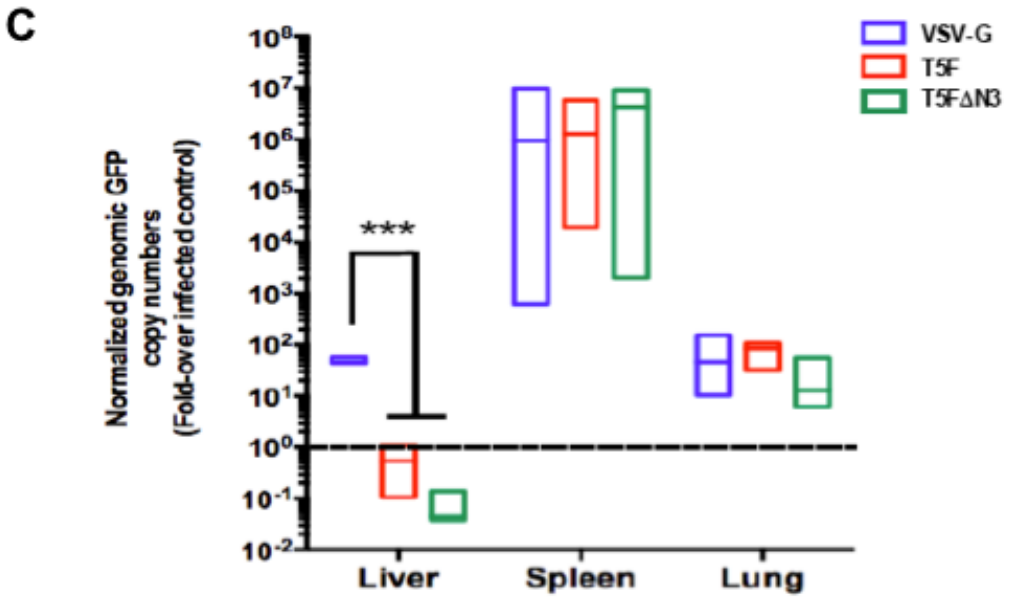

Figure 2-5 (cont.) NiV pseudotypes bypass the liver sink *in vivo*. (C) The FG12 (GFP) vector was pseudotyped with VSV-G and the NiV envelopes. 5 µg of p24 equivalent of each pseudotyped lentivirus was administered to mice as above. 4 days post-injection, the mice were sacrificed and the indicated organs harvested. Genomic DNA was extracted and quantitation of the vector copy number was determined using real-time PCR analysis for GFP vector sequences. GFP copy numbers were normalized to HPRT copy numbers. Normalized GFP copy numbers are presented as fold-increase over background numbers obtained from matched organs in an uninfected mouse. 3 mice were used for each indicated pseudotyped vector (VSV-G, NiV-T5F, and NiV-T5FD3). The median and range are shown as box plots, using the average of quadruplicates for each PCR reaction. Statistical significance was accessed by *t* tests corrected for multiple comparisons by the Holm-Sidak method in GraphPad PRISM™ 6. ***, $p<0.001$.

Table 2-1

Gene	Specificity marker	Source: Cell type:	PSC	PSC DE	Adult tissue Hepatocytes	PSC Neural progenitor	PSC Neurons	Fetal tissue Neural progenitor	Adult tissue Keratinocyte	Adult tissue Mesothelial	Adult tissue Kidney epithelial	Adult tissue Blood vessels
EFNB2			1186	716	85	2131	1794	3961	2244	1935	3008	5415
EFNB3			349	525	53	1622	7789	2275	273	190	219	184
GAPDH	Housekeeping genes		19143	17814	13047	17359	17637	17303	19032	22349	21258	19544
ACTB			18106	18917	17098	18191	17065	19266	17449	10505	19893	18052
FABP7	NPCs		281	64	22	4351	4640	15172	31	17	30	25
ALB	Hepatocyte		13	11	22065	11	10	10	10	9	8	10
VWF	Endothelium		65	105	67	63	49	40	37	46	31	12953
KRT14	Keratinocyte		13	11	13	12	12	11	19365	16	11	12
POU5F1	PSCs		8332	13192	229	508	135	123	188	144	369	146
			Pluripotent	Endoderm		Ectoderm				Mesoderm		

Table 2-1. Tissue and cell type expression of ephrinB2 and ephrinB3. A human U133plus2.0 array (Affymetrix) was performed on various pluripotent stem cell (PSC)-derived and primary (fetal and adult) tissues to examine whole genome expression. Shown here are the normalized mean expression values from multiple biological repeats ($\geq$ 3). EphrinB2/B3 (yellow for significant positives), housekeeping genes (grey), and cell-specific genes (red) are color coded as indicated.

PSC, Pluripotent Stem Cell
DE, Definitive Endoderm derived from PSC cultured in chemically defined medium (CDM-ABFLY) supplemented with Activin, BMP4, FGF2, and the PI3K inhibitor LY294002. DE gives rise to other endoderm progenitors (pancreatic, endocrine etc.), and can retain expression of the POU5F1 pluripotency marker (also called Oct4) during early stages of PSC→DE differentiation [77].

References

1 Mochizuki, H., Schwartz, J. P., Tanaka, K., Brady, R. O. & Reiser, J. High-titer human immunodeficiency virus type 1-based vector systems for gene delivery into nondividing cells. *J Virol* **72**, 8873-8883 (1998).

2 Reiser, J. *et al.* Transduction of nondividing cells using pseudotyped defective high-titer HIV type 1 particles. *Proc Natl Acad Sci U S A* **93**, 15266-15271 (1996).

3 Morizono, K. *et al.* Lentiviral vector retargeting to P-glycoprotein on metastatic melanoma through intravenous injection. *Nat Med* **11**, 346-352, doi:10.1038/nm1192 (2005).

4 Morizono, K. *et al.* Redirecting lentiviral vectors pseudotyped with Sindbis virus-derived envelope proteins to DC-SIGN by modification of N-linked glycans of envelope proteins. *J Virol* **84**, 6923-6934, doi:10.1128/jvi.00435-10 (2010).

5 Ni Choileain, S. & Astier, A. L. CD46 processing: a means of expression. *Immunobiology* **217**, 169-175, doi:10.1016/j.imbio.2011.06.003 (2012).

6 Frecha, C. *et al.* Stable transduction of quiescent T cells without induction of cycle progression by a novel lentiviral vector pseudotyped with measles virus glycoproteins. *Blood* **112**, 4843-4852, doi:10.1182/blood-2008-05-155945 (2008).

7 Funke, S. *et al.* Targeted cell entry of lentiviral vectors. *Mol Ther* **16**, 1427-1436, doi:10.1038/mt.2008.128 (2008).

8 Frecha, C., Levy, C., Cosset, F. L. & Verhoeyen, E. Advances in the field of lentivector-based transduction of T and B lymphocytes for gene therapy. *Mol Ther* **18**, 1748-1757, doi:10.1038/mt.2010.178 (2010).

9 Buchholz, C. J., Muhlebach, M. D. & Cichutek, K. Lentiviral vectors with measles virus glycoproteins - dream team for gene transfer? *Trends Biotechnol* **27**, 259-265, doi:10.1016/j.tibtech.2009.02.002 (2009).

10 Arce, F., Breckpot, K., Collins, M. & Escors, D. Targeting lentiviral vectors for cancer immunotherapy. *Curr Cancer Ther Rev* **7**, 248-260, doi:10.2174/157339411797642605 (2011).

11 Chang, A. & Dutch, R. E. Paramyxovirus fusion and entry: multiple paths to a common end. *Viruses* **4**, 613-636, doi:10.3390/v4040613 (2012).

12 Plemper, R. K., Brindley, M. A. & Iorio, R. M. Structural and mechanistic studies of measles virus illuminate paramyxovirus entry. *PLoS Pathog* **7**, e1002058, doi:10.1371/journal.ppat.1002058 (2011).

13 Lee, B. & Ataman, Z. A. Modes of paramyxovirus fusion: a Henipavirus perspective. *Trends Microbiol* **19**, 389-399, doi:10.1016/j.tim.2011.03.005 (2011).

14 Navaratnarajah, C. K., Leonard, V. H. & Cattaneo, R. Measles virus glycoprotein complex assembly, receptor attachment, and cell entry. *Curr Top Microbiol Immunol* **329**, 59-76 (2009).

15 Anliker, B. *et al.* Specific gene transfer to neurons, endothelial cells and hematopoietic progenitors with lentiviral vectors. *Nat Methods* **7**, 929-935, doi:10.1038/nmeth.1514 (2010).

16 Khetawat, D. & Broder, C. C. A functional henipavirus envelope glycoprotein pseudotyped lentivirus assay system. *Virol J* **7**, 312, doi:10.1186/1743-422x-7-312 (2010).

17 Negrete, O. A. *et al.* EphrinB2 is the entry receptor for Nipah virus, an emergent deadly paramyxovirus. *Nature* **436**, 401-405, doi:10.1038/nature03838 (2005).

18 Bonaparte, M. I. *et al.* Ephrin-B2 ligand is a functional receptor for Hendra virus and Nipah virus. *Proc Natl Acad Sci U S A* **102**, 10652-10657, doi:10.1073/pnas.0504887102 (2005).

19 Negrete, O. A. *et al.* Two key residues in ephrinB3 are critical for its use as an alternative receptor for Nipah virus. *PLoS Pathog* **2**, e7, doi:10.1371/journal.ppat.0020007 (2006).

20 Pasquale, E. B. Eph-ephrin bidirectional signaling in physiology and disease. *Cell* **133**, 38-52, doi:10.1016/j.cell.2008.03.011 (2008).

21 Pasquale, E. B. Eph receptors and ephrins in cancer: bidirectional signalling and beyond. *Nat Rev Cancer* **10**, 165-180, doi:10.1038/nrc2806 (2010).

22 Ivanova, N. B. *et al.* A stem cell molecular signature. *Science* **298**, 601-604, doi:10.1126/science.1073823 (2002).

23 Elvevold, K., Smedsrod, B. & Martinez, I. The liver sinusoidal endothelial cell: a cell type of controversial and confusing identity. *Am J Physiol Gastrointest Liver Physiol* **294**, G391-400, doi:10.1152/ajpgi.00167.2007 (2008).

24 Ganesan, L. P. *et al.* Rapid and efficient clearance of blood-borne virus by liver sinusoidal endothelium. *PLoS Pathog* **7**, e1002281, doi:10.1371/journal.ppat.1002281 (2011).

25 Levroney, E. L. *et al.* Novel innate immune functions for galectin-1: galectin-1 inhibits cell fusion by Nipah virus envelope glycoproteins and augments dendritic cell secretion of proinflammatory cytokines. *J Immunol* **175**, 413-420 (2005).

26 Wolf, M. C. *et al.* A catalytically and genetically optimized beta-lactamase-matrix based assay for sensitive, specific, and higher throughput analysis of native henipavirus entry characteristics. *Virol J* **6**, 119, doi:10.1186/1743-422x-6-119 (2009).

27 Aguilar, H. C. *et al.* Polybasic KKR motif in the cytoplasmic tail of Nipah virus fusion protein modulates membrane fusion by inside-out signaling. *J Virol* **81**, 4520-4532, doi:10.1128/jvi.02205-06 (2007).

28 Aguilar, H. C. *et al.* N-glycans on Nipah virus fusion protein protect against neutralization but reduce membrane fusion and viral entry. *J Virol* **80**, 4878-4889, doi:10.1128/jvi.80.10.4878-4889.2006 (2006).

29 Lois, C., Hong, E. J., Pease, S., Brown, E. J. & Baltimore, D. Germline transmission and tissue-specific expression of transgenes delivered by lentiviral vectors. *Science* **295**, 868-872, doi:10.1126/science.1067081 (2002).

30 Qin, X. F., An, D. S., Chen, I. S. & Baltimore, D. Inhibiting HIV-1 infection in human T cells by lentiviral-mediated delivery of small interfering RNA against CCR5. *Proc Natl Acad Sci U S A* **100**, 183-188, doi:10.1073/pnas.232688199 (2003).

31 Esko, J. D., Stewart, T. E. & Taylor, W. H. Animal cell mutants defective in glycosaminoglycan biosynthesis. *Proc Natl Acad Sci U S A* **82**, 3197-3201 (1985).

32 Damoiseaux, R., Sherman, S. P., Alva, J. A., Peterson, C. & Pyle, A. D. Integrated chemical genomics reveals modifiers of survival in human embryonic stem cells. *Stem Cells* **27**, 533-542, doi:10.1634/stemcells.2008-0596 (2009).

33 Shimizu, S. *et al.* A highly efficient short hairpin RNA potently down-regulates CCR5 expression in systemic lymphoid organs in the hu-BLT mouse model. *Blood* **115**, 1534-1544, doi:10.1182/blood-2009-04-215855 (2010).

34 Karumbayaram, S. *et al.* Directed differentiation of human-induced pluripotent stem cells generates active motor neurons. *Stem Cells* **27**, 806-811, doi:10.1002/stem.31 (2009).

35 Van Handel, B. *et al.* Scl represses cardiomyogenesis in prospective hemogenic endothelium and endocardium. *Cell* **150**, 590-605, doi:10.1016/j.cell.2012.06.026 (2012).

36 Kobayashi, M., Iida, A., Ueda, Y. & Hasegawa, M. Pseudotyped lentivirus vectors derived from simian immunodeficiency virus SIVagm with envelope glycoproteins from paramyxovirus. *J Virol* **77**, 2607-2614 (2003).

37 Frecha, C. *et al.* Measles virus glycoprotein-pseudotyped lentiviral vector-mediated gene transfer into quiescent lymphocytes requires binding to both SLAM and CD46 entry receptors. *J Virol* **85**, 5975-5985, doi:10.1128/jvi.00324-11 (2011).

38 Pernet, O., Wang, Y. E. & Lee, B. Henipavirus receptor usage and tropism. *Curr Top Microbiol Immunol* **359**, 59-78, doi:10.1007/82_2012_222 (2012).

39 Ayllon, J., Villar, E. & Munoz-Barroso, I. Mutations in the ectodomain of newcastle disease virus fusion protein confer a hemagglutinin-neuraminidase-independent phenotype. *J Virol* **84**, 1066-1075, doi:10.1128/jvi.01473-09 (2010).

40 Rawling, J., Garcia-Barreno, B. & Melero, J. A. Insertion of the two cleavage sites of the respiratory syncytial virus fusion protein in Sendai virus fusion protein leads to enhanced cell-cell fusion and a decreased dependency on the HN attachment protein for activity. *J Virol* **82**, 5986-5998, doi:10.1128/jvi.00078-08 (2008).

41 Sergel, T. A., McGinnes, L. W. & Morrison, T. G. A single amino acid change in the Newcastle disease virus fusion protein alters the requirement for HN protein in fusion. *J Virol* **74**, 5101-5107 (2000).

42 Seth, S., Vincent, A. & Compans, R. W. Mutations in the cytoplasmic domain of a paramyxovirus fusion glycoprotein rescue syncytium formation and eliminate the hemagglutinin-neuraminidase protein requirement for membrane fusion. *J Virol* **77**, 167-178 (2003).

43 Geisbert, T. W., Feldmann, H. & Broder, C. C. Animal Challenge Models of Henipavirus Infection and Pathogenesis. *Curr Top Microbiol Immunol*, doi:10.1007/82_2012_208 (2012).

44 Majeti, R., Park, C. Y. & Weissman, I. L. Identification of a hierarchy of multipotent hematopoietic progenitors in human cord blood. *Cell Stem Cell* **1**, 635-645, doi:10.1016/j.stem.2007.10.001 (2007).

45 Gale, N. W. *et al.* Ephrin-B2 selectively marks arterial vessels and neovascularization sites in the adult, with expression in both endothelial and smooth-muscle cells. *Dev Biol* **230**, 151-160, doi:10.1006/dbio.2000.0112 (2001).

46 Shin, D. *et al.* Expression of ephrinB2 identifies a stable genetic difference between arterial and venous vascular smooth muscle as well as endothelial cells, and marks subsets of microvessels at sites of adult neovascularization. *Dev Biol* **230**, 139-150, doi:10.1006/dbio.2000.9957 (2001).

47 Flenniken, A. M., Gale, N. W., Yancopoulos, G. D. & Wilkinson, D. G. Distinct and overlapping expression patterns of ligands for Eph-related receptor tyrosine kinases during mouse embryogenesis. *Dev Biol* **179**, 382-401, doi:10.1006/dbio.1996.0269 (1996).

48 Maisner, A., Neufeld, J. & Weingartl, H. Organ- and endotheliotropism of Nipah virus infections in vivo and in vitro. *Thromb Haemost* **102**, 1014-1023, doi:10.1160/th09-05-0310 (2009).

49 Wong, K. T. *et al.* Nipah virus infection: pathology and pathogenesis of an emerging paramyxoviral zoonosis. *Am J Pathol* **161**, 2153-2167, doi:10.1016/s0002-9440(10)64493-8 (2002).

50 Galanis, E. Therapeutic potential of oncolytic measles virus: promises and challenges. *Clin Pharmacol Ther* **88**, 620-625, doi:10.1038/clpt.2010.211 (2010).

51 Munch, R. C. *et al.* DARPins: an efficient targeting domain for lentiviral vectors. *Mol Ther* **19**, 686-693, doi:10.1038/mt.2010.298 (2011).

52 Levy, C. *et al.* Lentiviral Vectors Displaying Modified Measles Virus gp Overcome Pre-existing Immunity in In Vivo-like Transduction of Human T and B Cells. *Mol Ther*, doi:10.1038/mt.2012.96 (2012).

53 Luby, S. P. & Gurley, E. S. Epidemiology of Henipavirus Disease in Humans. *Curr Top Microbiol Immunol*, doi:10.1007/82_2012_207 (2012).

54 Graf, T. & Stadtfeld, M. Heterogeneity of embryonic and adult stem cells. *Cell Stem Cell* **3**, 480-483, doi:10.1016/j.stem.2008.10.007 (2008).

55 Hough, S. R., Laslett, A. L., Grimmond, S. B., Kolle, G. & Pera, M. F. A continuum of cell states spans pluripotency and lineage commitment in human embryonic stem cells. *PLoS One* **4**, e7708, doi:10.1371/journal.pone.0007708 (2009).

56 Hayashi, K., Lopes, S. M., Tang, F. & Surani, M. A. Dynamic equilibrium and heterogeneity of mouse pluripotent stem cells with distinct functional and epigenetic states. *Cell Stem Cell* **3**, 391-401, doi:10.1016/j.stem.2008.07.027 (2008).

57 Poliakov, A., Cotrina, M. & Wilkinson, D. G. Diverse roles of eph receptors and ephrins in the regulation of cell migration and tissue assembly. *Dev Cell* **7**, 465-480, doi:10.1016/j.devcel.2004.09.006 (2004).

58 Sela-Donenfeld, D. & Wilkinson, D. G. Eph receptors: two ways to sharpen boundaries. *Curr Biol* **15**, R210-212, doi:10.1016/j.cub.2005.03.013 (2005).

59 Baum, C. M., Weissman, I. L., Tsukamoto, A. S., Buckle, A. M. & Peault, B. Isolation of a candidate human hematopoietic stem-cell population. *Proc Natl Acad Sci U S A* **89**, 2804-2808 (1992).

60 Craig, W., Kay, R., Cutler, R. L. & Lansdorp, P. M. Expression of Thy-1 on human hematopoietic progenitor cells. *J Exp Med* **177**, 1331-1342 (1993).

61 Zhang, L., Dailey, P. J., Gettie, A., Blanchard, J. & Ho, D. D. The liver is a major organ for clearing simian immunodeficiency virus in rhesus monkeys. *J Virol* **76**, 5271-5273 (2002).

62 Contag, C. H. & Ross, B. D. It's not just about anatomy: in vivo bioluminescence imaging as an eyepiece into biology. *J Magn Reson Imaging* **16**, 378-387, doi:10.1002/jmri.10178 (2002).

63 Shah, K., Jacobs, A., Breakefield, X. O. & Weissleder, R. Molecular imaging of gene therapy for cancer. *Gene Ther* **11**, 1175-1187, doi:10.1038/sj.gt.3302278 (2004).

64 Wong, K. T. & Tan, C. T. Clinical and pathological manifestations of human henipavirus infection. *Curr Top Microbiol Immunol* **359**, 95-104, doi:10.1007/82_2012_205 (2012).

65 Liebl, D. J., Morris, C. J., Henkemeyer, M. & Parada, L. F. mRNA expression of ephrins and Eph receptor tyrosine kinases in the neonatal and adult mouse central nervous system. *J Neurosci Res* **71**, 7-22, doi:10.1002/jnr.10457 (2003).

66 Alam, S. M., Fujimoto, J., Jahan, I., Sato, E. & Tamaya, T. Coexpression of EphB4 and ephrinB2 in tumour advancement of ovarian cancers. *Br J Cancer* **98**, 845-851, doi:10.1038/sj.bjc.6604216 (2008).

67 Alam, S. M., Fujimoto, J., Jahan, I., Sato, E. & Tamaya, T. Overexpression of ephrinB2 and EphB4 in tumor advancement of uterine endometrial cancers. *Ann Oncol* **18**, 485-490, doi:10.1093/annonc/mdl414 (2007).

68 Liu, W. *et al.* Coexpression of ephrin-Bs and their receptors in colon carcinoma. *Cancer* **94**, 934-939 (2002).

69 Kertesz, N. *et al.* The soluble extracellular domain of EphB4 (sEphB4) antagonizes EphB4-EphrinB2 interaction, modulates angiogenesis, and inhibits tumor growth. *Blood* **107**, 2330-2338, doi:10.1182/blood-2005-04-1655 (2006).

70 Noren, N. K., Lu, M., Freeman, A. L., Koolpe, M. & Pasquale, E. B. Interplay between EphB4 on tumor cells and vascular ephrin-B2 regulates tumor growth. *Proc Natl Acad Sci U S A* **101**, 5583-5588, doi:10.1073/pnas.0401381101 (2004).

71 Russell, S. J. & Peng, K. W. Measles virus for cancer therapy. *Curr Top Microbiol Immunol* **330**, 213-241 (2009).

72 Blechacz, B. & Russell, S. J. Measles virus as an oncolytic vector platform. *Curr Gene Ther* **8**, 162-175 (2008).

73 Aguilar, H. C., Aspericueta, V., Robinson, L. R., Aanensen, K. E. & Lee, B. A quantitative and kinetic fusion protein-triggering assay can discern distinct steps in the nipah virus membrane fusion cascade. *J Virol* **84**, 8033-8041, doi:10.1128/jvi.00469-10 (2010).

74 Morizono, K. *et al.* A versatile targeting system with lentiviral vectors bearing the biotin-adaptor peptide. *J Gene Med* **11**, 655-663, doi:10.1002/jgm.1345 (2009).

75 Wong, L. F. *et al.* Lentivirus-mediated gene transfer to the central nervous system: therapeutic and research applications. *Hum Gene Ther* **17**, 1-9, doi:10.1089/hum.2006.17.1 (2006).

76 Xu, K. *et al.* Host cell recognition by the henipaviruses: crystal structures of the Nipah G attachment glycoprotein and its complex with ephrin-B3. *Proc Natl Acad Sci U S A* **105**, 9953-9958, doi:0804797105 [pii]10.1073/pnas.0804797105 (2008).

77 Teo, A. K. *et al.* Pluripotency factors regulate definitive endoderm specification through eomesodermin. *Genes Dev* **25**, 238-250, doi:10.1101/gad.607311 (2011).

CHAPTER 2

Supplementary Information

Supplementary Introduction

EphrinB2 is expressed on mouse long-term hematopoietic stem cells (LT-HSCs) [1]. In the manuscript entitled "Nipah virus envelope pseudotyped lentiviruses efficiently target ephrinB2+ stem cell populations *in vitro* and bypass the liver sink when administered *in vivo*," we showed that NiVpp transduce ~3% of human fetal liver CD34+ cells (Fig. 2-4D), and infection is completely abrogated with soluble ephrinB2. Thus, ephrinB2 is also functionally expressed on human HSCs (hHSCs). Furthermore, we found that ephrinB2 is expressed the highest in the CD90+CD34+CD38- subset of human fetal liver (Fig. 2-4 F). This finding suggested that NiVpp could potentially target the most primitive HSC. To further explore this, we performed a self-renewal assay on NiV-transduced cells on supportive OP9 stroma. The results of these experiments confirmed that NiV-transduced cells are enriched in the CD90+CD34+CD38- subset of human fetal liver.

Supplementary Material and Methods

Cells and culture conditions. CD34+ cells were isolated from human fetal liver as previously described [2]. For viral transductions, 1 x 10^5 cells were seeded onto OP9 stroma in MEM α (Invitrogen) supplemented with 20% FBS, 10 μg/ml TPO, 50 μg/ml SCF, and 10 μg/ml Flt3-ligand.

***In vitro* infection of cells.** NiV pseudotyped lentiviruses at MOI 1000 and 4ng/ml of polybrene (Sigma) were added to the cells, and centrifuged at 2,000 rpm at 37°C for 2 hours. 10 nM of soluble ephrinB2 (R&D Systems) was added to the infection medium as a specificity control. To exclude pseudotransduction, 5μM of nevirapine was added. Following an overnight incubation with virus, the infection medium was removed and replaced with fresh medium.

Self-renewal assay. 72 hours post-infection, the cells were harvested and passed through a 40 μm strainer. Half of the cell suspension was seeded on OP9 stroma ("unsorted"). The remaining cell suspension was stained with DAPI, CD34-APC, CD38-PE-Cy7, and CD90-PE (BD-Biosciences) antibodies for 20 minutes on ice in the dark. Following washing, GFP+ and GFP- cells were sorted on a BD FACS Aria, and also seeded on OP9 stroma. The cells were cultured for 7 days. At each passage, a maximum of 1 x 10^5 cells were re-seeded for the next passage the percentage of CD90+CD34+CD38- cells was determined using FACS analysis. This was repeated for 3 passages.

Supplementary Results

NiV-transduced cells are enriched in the CD90+CD34+CD38- subset of human fetal liver. Although we showed that NiVpp transduced 3% of CD34+ cells (Fig. 2-4D), we did not examine expression of other markers used to fractionate the various subpopulations present in fetal liver. Here, we examined CD90, CD34, and CD38 expression of NiV-transduced cells in culture. First, we modified our previous transduction conditions to promote survival of the most primitive HSCs. The cells were seeded on OP9 stroma in media supplemented with TPO, SCF, and Flt3 ligand growth factors. 72h post-transduction, we used FACS analysis to examine infection efficiency. NiV transduced 1.3% of CD34+ cells (Fig. 2-6A). We sorted the GFP+ and GFP- cell populations for a self-renewal assay. Every 7 days for three consecutive weeks, we examined CD90, CD34, and CD38 expression of three populations: sorted GFP+, sorted GFP-, and un-sorted cells. At week 1, the sorted GFP+ cells still showed a small population of GFP- cells, so we included that in our analyses (Fig. 2-6 B-D). For both the GFP+ and GFP- cells, only 5% of the cells were CD34+CD38- at week 1 (Fig. 2-6B). These numbers increased to 17% for the GFP+ cells and 12% for the GFP- cells at week 2 (Fig. 2-6C). Interestingly, 51% of the CD34+CD38- population was also CD90+ for the GFP+ cells, and only 13% were CD90+ for the GFP- cells, indicating a four-fold enrichment for the GFP+ cells. By week 3, 20% of the cells were CD90+CD34+CD38- for the GFP+ cells, and 2% for the GFP- cells, indicating a ten-fold enrichment for the GFP+ cells. For the sorted GFP- cells, 27% of the cells were CD90+CD34+CD38- at week 2 and 13% at week 3 (Fig. 2-6 F-G), still indicating a 2-fold enrichment for the sorted GFP+ cells. Surprisingly, we did not see enrichment for the GFP+ cells in the unsorted population at any of the weeks (Fig. 2-6, H-J). Lastly, we also counted the number of cells per population to determine fold expansion in culture. For all three populations, we observed the highest fold expansion at week 1 (Fig. 2-7). The sorted GFP+ cells demonstrated a higher fold expansion than the sorted GFP- cells, but it was lower than the

unsorted cells. A few modifications to the assay might be necessary and will be discussed below.

Supplementary Discussion

Here, we sought to determine what specific subset of CD34+ cells is transduced by NiV pseudotyped lentiviruses. If NiVpp are truly targeting the most primitive HSC, then those cells should have the capacity to proliferate in culture. Following transduction, we characterized the self-renewal capacity of sorted GFP+, sorted GFP-, and un-sorted cells. Indeed, the sorted GFP+ cells demonstrated a 2-fold enrichment in the CD90+CD34+CD38- population compared to sorted GFP- cells at week 2 (Fig. 2-6 C, F). However, this trend was not maintained for the unsorted cells. One possibility that may account for this is an inconsistency in the amount of cells we seeded for each population at each passage. Since NiVpp only transduced 1.3% of cells (Fig. 2-6A), we only sorted ~1,500 GFP+ cells and >400,000 GFP- cells. We seeded 200-fold less GFP+ cells than GFP- cells and unsorted cells. For future experiments, the same amount of sorted GFP+, sorted GFP-, and unsorted cells should be seeded for an equal comparison between the 3 populations. Equal densities might result in a more striking difference between the sorted GFP+ and sorted GFP- cells.

Overall, our preliminary findings suggest that NiVpp are targeting a subset of cells enriched in the CD90+CD34+CD38- population of fetal liver. Future experiments should address whether progeny derived from NiV-transduced cells have both lymphoid and myeloid potential. In addition, transplantation into immunodeficient NOD-SCID mice is necessary to confirm multi-lineage reconstitution.

Figure 2-6

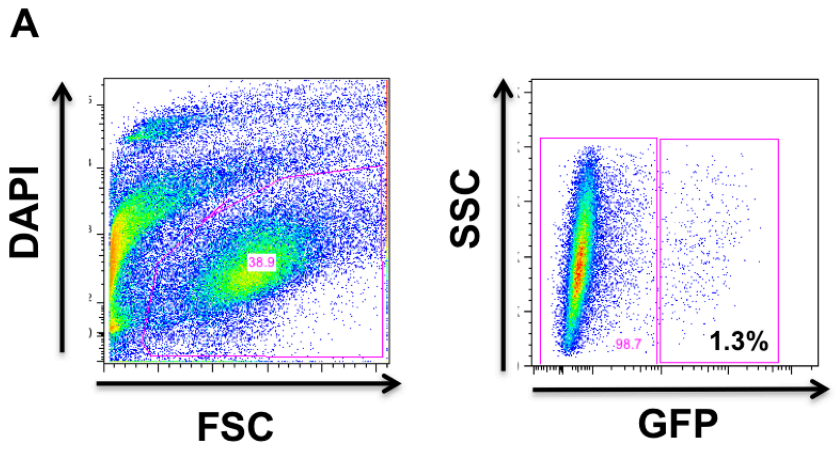

Figure 2-6. NiV-transduced GFP+ cells are enriched in the CD90+CD34+CD38- subset of human fetal liver. **(A)** Purified $CD34^{+}$ cells from human fetal liver were infected with NiVpp. 72h post-transduction, cells were stained for the cell-surface marker, CD34, and analyzed for GFP expression by FACS analysis. GFP+ and GFP- cells were FACS-sorted. Sorted GFP+ **(B-D)**, sorted GFP- **(E-G)**, and unsorted cells **(H-J)** were cultured for 7 days. CD90, CD34, and CD38 expression was examined at each passage.

Figure 2-6 (continued)

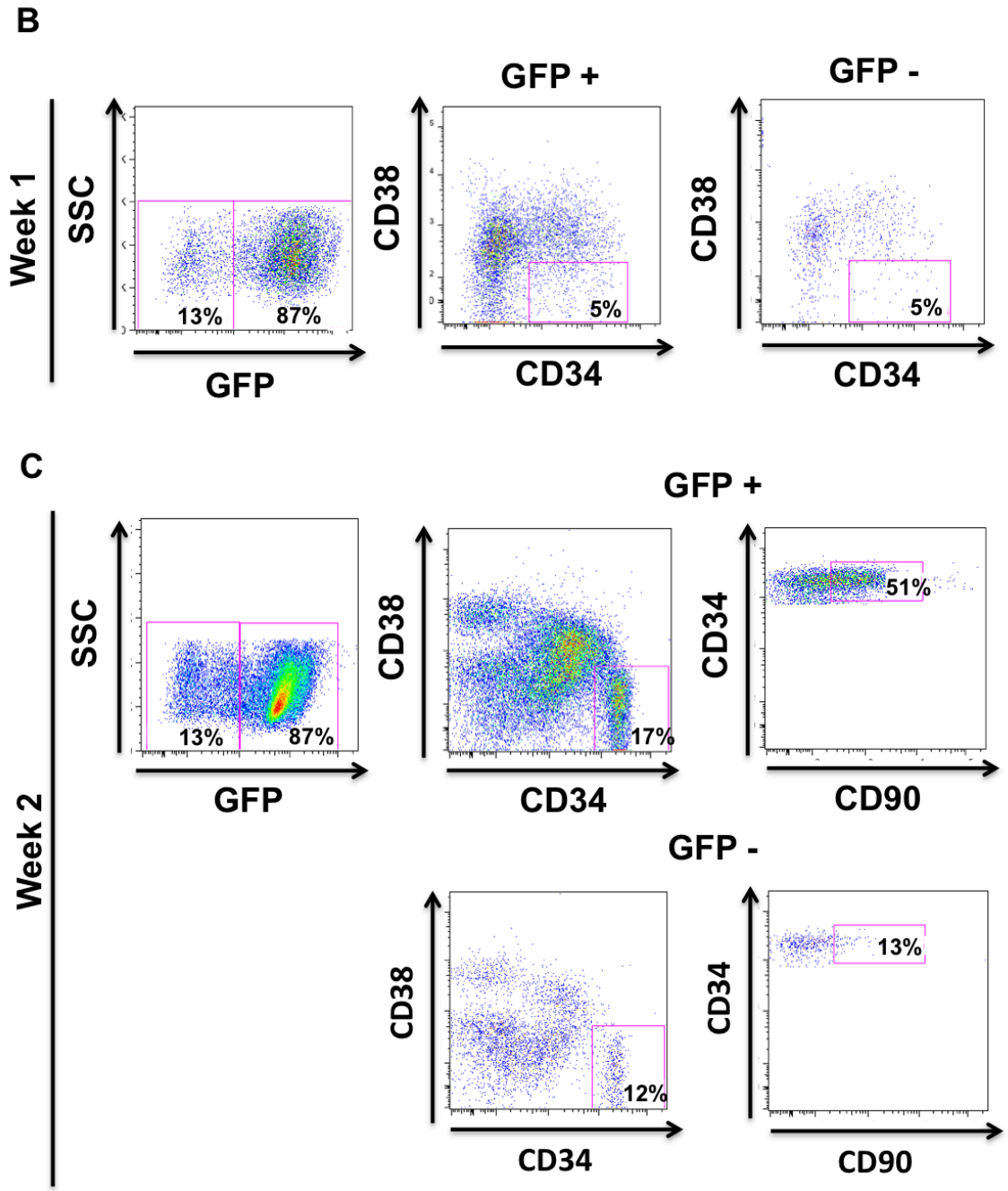

Figure 2-6. (cont.) NiV-transduced GFP+ cells are enriched in the CD90+CD34+CD38- subset of human fetal liver. (A) Purified $CD34^+$ cells from human fetal liver were infected with NiVpp. 72h post-transduction, cells were stained for the cell-surface marker, CD34, and analyzed for GFP expression by FACS analysis. GFP+ and GFP- cells were FACS-sorted. Sorted GFP+ **(B-D)**, sorted GFP- **(E-G)**, and unsorted cells **(H-J)** were cultured for 7 days. CD90, CD34, and CD38 expression was examined at each passage.

Figure 2-6 (continued)

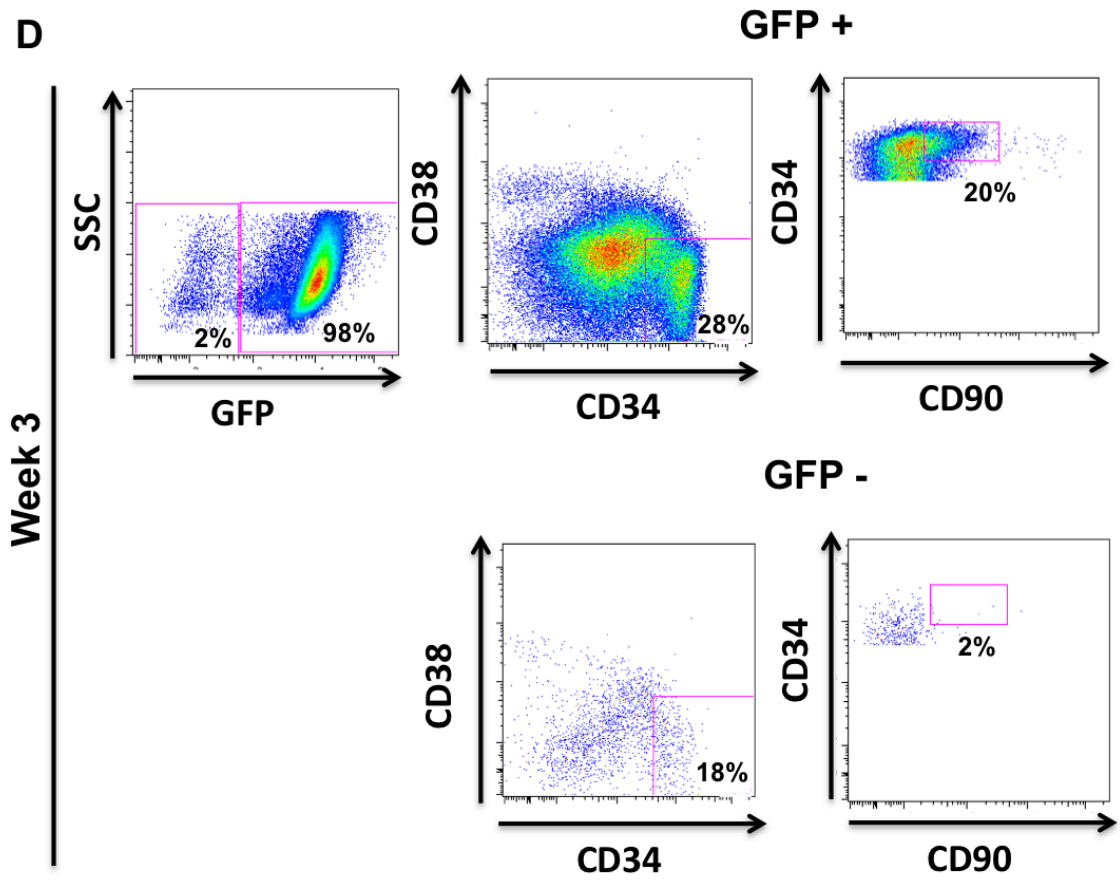

Figure 2-6. (cont.) NiV-transduced GFP+ cells are enriched in the CD90+CD34+CD38- subset of human fetal liver. (A) Purified $CD34^{+}$ cells from human fetal liver were infected with NiVpp. 72h post-transduction, cells were stained for the cell-surface marker, CD34, and analyzed for GFP expression by FACS analysis. GFP+ and GFP- cells were FACS-sorted. Sorted GFP+ **(B-D)**, sorted GFP- **(E-G)**, and unsorted cells **(H-J)** were cultured for 7 days. CD90, CD34, and CD38 expression was examined at each passage.

Figure 2-6 (continued)

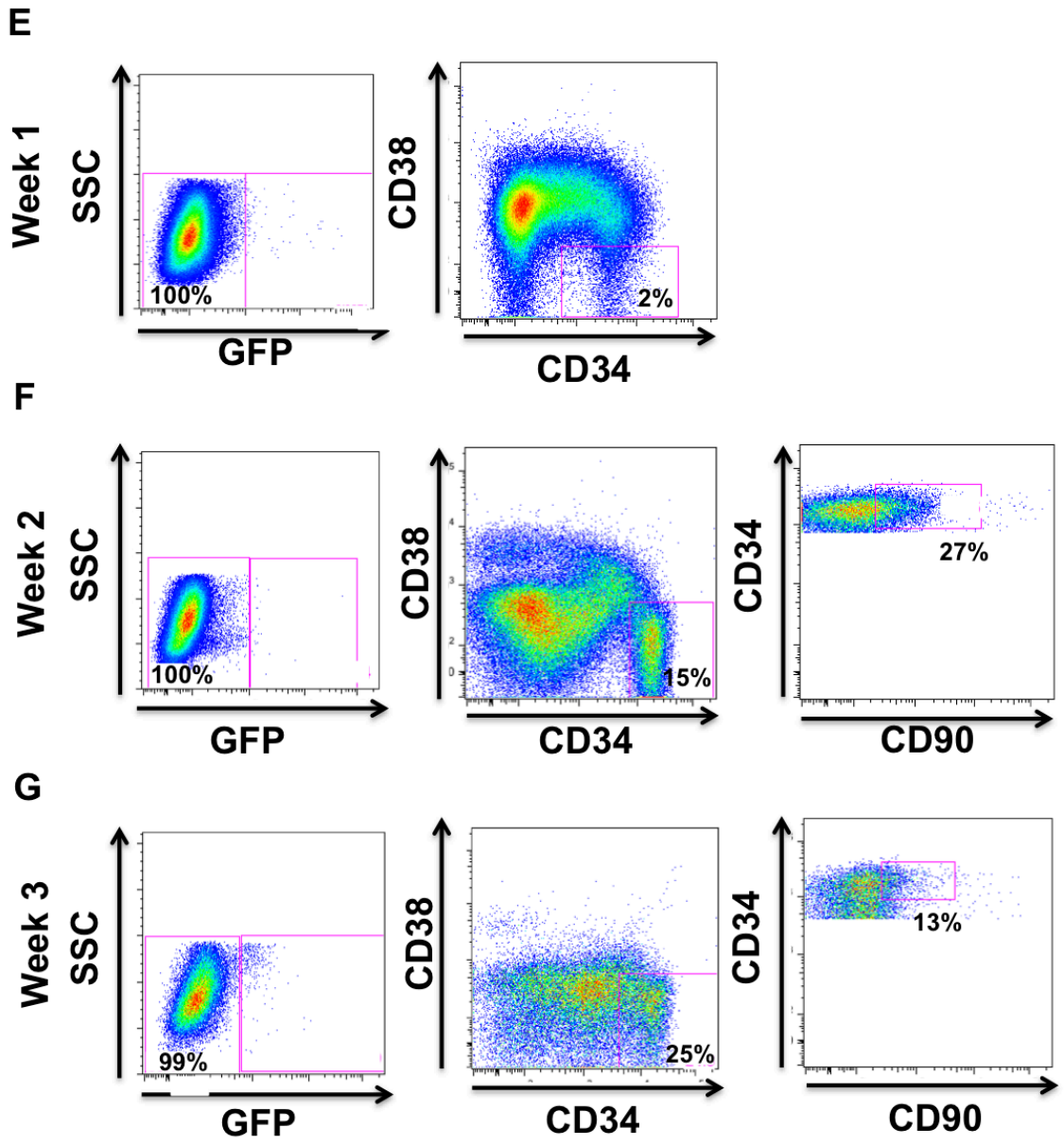

Figure 2-6. (cont.) NiV-transduced GFP+ cells are enriched in the CD90+CD34+CD38- subset of human fetal liver. (A) Purified $CD34^+$ cells from human fetal liver were infected with NiVpp. 72h post-transduction, cells were stained for the cell-surface marker, CD34, and analyzed for GFP expression by FACS analysis. GFP+ and GFP- cells were FACS-sorted. Sorted GFP+ **(B-D)**, sorted GFP- **(E-G)**, and unsorted cells **(H-J)** were cultured for 7 days. CD90, CD34, and CD38 expression was examined at each passage.

Figure 2-6 (continued)

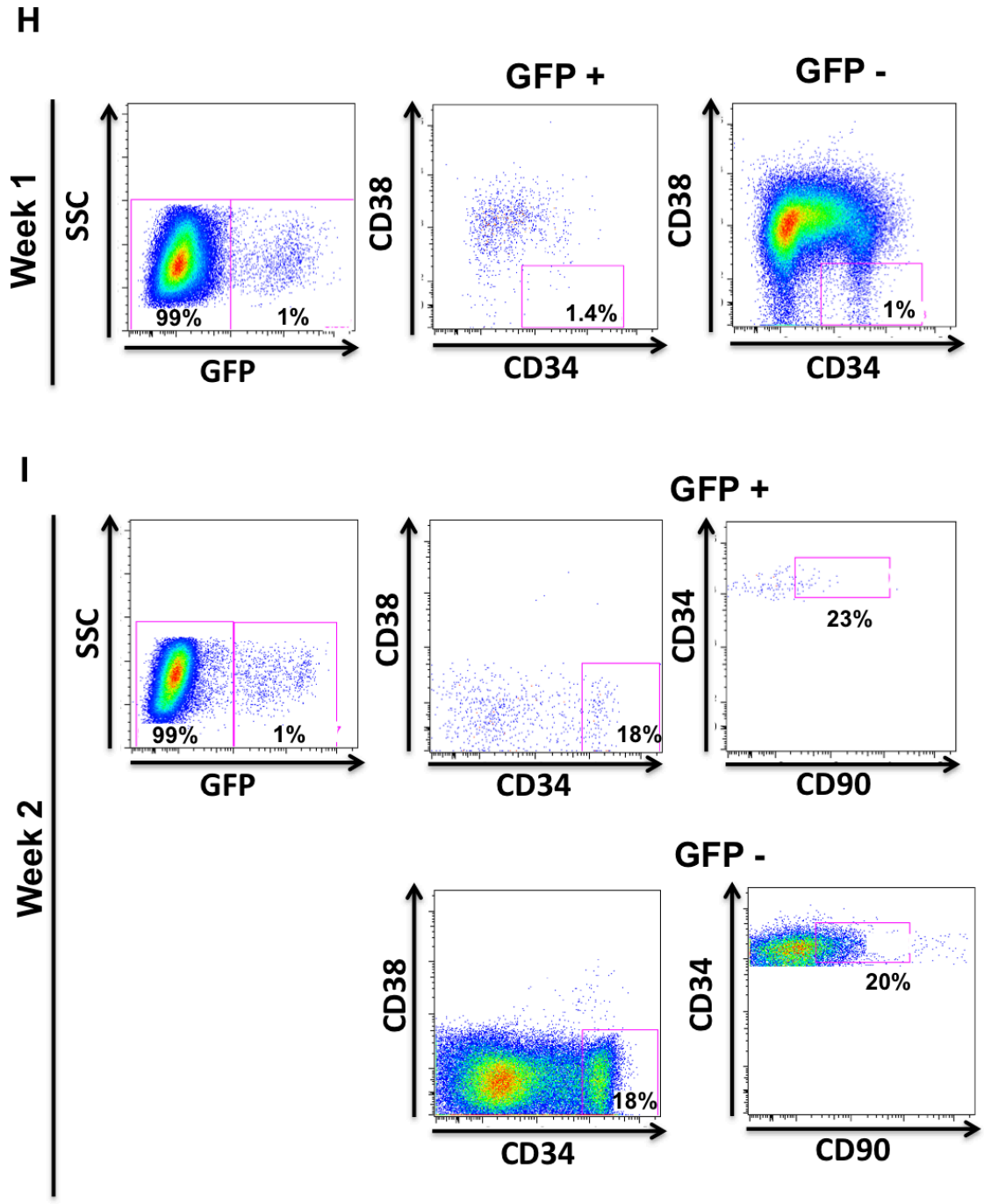

Figure 2-6. (cont.) NiV-transduced GFP+ cells are enriched in the CD90+CD34+CD38- subset of human fetal liver. (A) Purified $CD34^{+}$ cells from human fetal liver were infected with NiVpp. 72h post-transduction, cells were stained for the cell-surface marker, CD34, and analyzed for GFP expression by FACS analysis. GFP+ and GFP- cells were FACS-sorted. Sorted GFP+ **(B-D)**, sorted GFP- **(E-G)**, and unsorted cells **(H-J)** were cultured for 7 days. CD90, CD34, and CD38 expression was examined at each passage.

Figure 2-6 (continued)

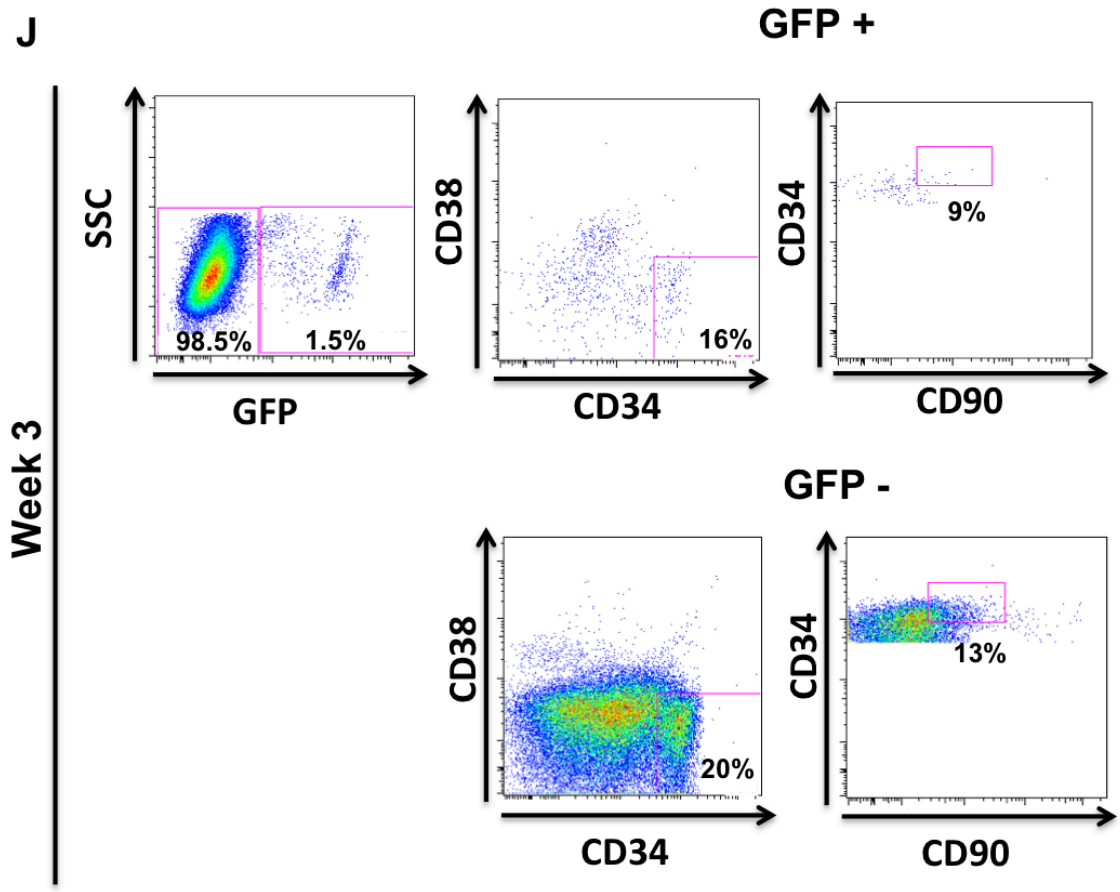

Figure 2-6. (cont.) NiV-transduced GFP+ cells are enriched in the CD90+CD34+CD38- subset of human fetal liver. (A) Purified $CD34^{+}$ cells from human fetal liver were infected with NiVpp. 72h post-transduction, cells were stained for the cell-surface marker, CD34, and analyzed for GFP expression by FACS analysis. GFP+ and GFP- cells were FACS-sorted. Sorted GFP+ **(B-D)**, sorted GFP- **(E-G)**, and unsorted cells **(H-J)** were cultured for 7 days. CD90, CD34, and CD38 expression was examined at each passage.

Figure 2-7

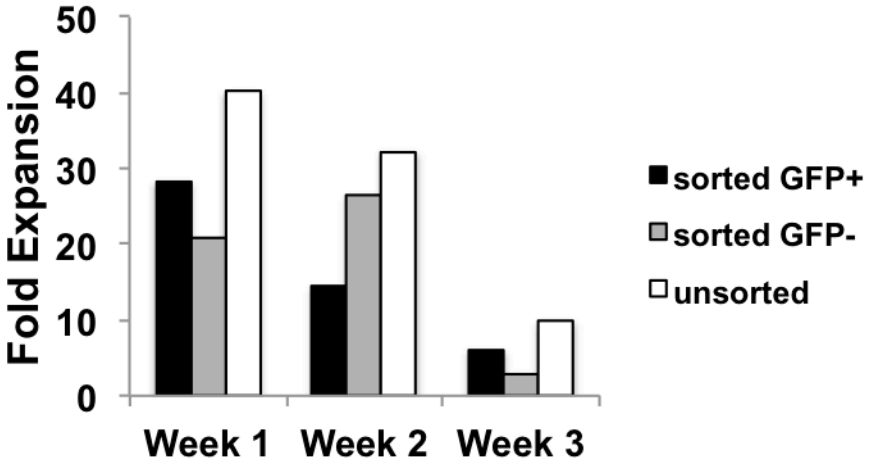

Figure 2-7. NiV-transduced, sorted GFP+ cells demonstrate higher fold expansion in culture compared to sorted GFP- cells. Sorted GFP+, sorted GFP-, and unsorted cells were cultured for 7 days. At each passage, cells were counted to calculate fold expansion.

References

1 Ivanova, N. B. *et al.* A stem cell molecular signature. *Science* **298**, 601-604, doi:10.1126/science.1073823 (2002).

2 Shimizu, S. *et al.* A highly efficient short hairpin RNA potently down-regulates CCR5 expression in systemic lymphoid organs in the hu-BLT mouse model. *Blood* **115**, 1534-1544, doi:10.1182/blood-2009-04-215855 (2010).

CHAPTER 3

EphrinB2 marks a subset of human embryonic stem cells and regulates differentiation into the three germ layers

Introduction

Human embryonic stem cells (hESCs) are derived from a developing blastocyst and have the capacity to self-renew indefinitely and to differentiate into all cell types derived from ectoderm, mesoderm and endoderm lineages [1]. Thus, differentiation of hESCs may provide insight into the biological processes involved in the earliest stages of human embryo development. In addition, cells derived from hESCs have great potential for therapeutic applications, contingent upon the development of methods to control their differentiation and expansion *in vitro*. Identifying the pathways regulating differentiation will contribute to the generation of specific cell types for use in regenerative medicine.

Eph-ephrin receptor-ligand pairs are membrane-associated receptor tyrosine kinases (RTKs) with well-established roles in many developmental processes, including vascular development, tissue-border formation, cell migration, and neurogenesis [2]. Fourteen eph receptors and eight ephrin ligands are divided into A and B subclasses based on their affinity for ligands. Since both ephs and ephrins are membrane-bound, signaling is restricted to sites of direct cell-cell contact and induces bi-directional signaling in the interacting cells. Depending on the cell type, ephrin-eph activation can lead to repulsion of neighboring cells or increased adhesion/attraction. The repulsive response is particularly important for sorting of ephrin-expressing cells from eph-expressing cells in boundary formation during development.

Ephrin-eph signaling also regulates the balance between self-renewal and differentiation of stem cells in the intestinal crypt [3] and the subventricular zone (SVZ) of the brain [4]. In addition, two studies found that ephB4 potentially modulates mesoderm induction [5,6]. *EphB4*$^{-/-}$ mouse ESCs (mESCs) were impaired in mesoderm differentiation. Conversely, overexpression of ephB4 in umbilical cord blood CD34+ cells resulted in a loss of the most primitive stem cells and differentiation into more lineage-committed progenitors. EphB4 and its ligand, ephrinB2, are both expressed in hESCs and likely regulate many aspects of stem cell fate. However, while ephrinB2 is involved in ectoderm and endoderm differentiation [7], ephB4 is not expressed in the

central nervous system. Thus, ephrinB2 “reverse” signaling and ephB4 “forward” signaling likely play overlapping but distinct roles in germ layer commitment and differentiation. Understanding the contribution of each signaling pathway may result in more optimal conditions for directing the differentiation of specific cell types for use in regenerative medicine. Thus, the overall goal of this chapter is to characterize the role of ephrinB2 in hESC fate.

We previously showed that we could efficiently pseudotype a lentiviral vector with the Nipah virus (NiV) envelope that could efficiently target ephrinB2+ cells *in vitro* (**Chapter 2**, manuscript in press). These NiV pseudotyped particles specifically transduced a sub-population of hESCs. Here, we sought to further characterize these ephrinB2+ hESCs by FACS-sorting the NiV-transduced GFP+ cells and examining their properties in culture. Passaging of the sorted cells revealed that ephrinB2 does not mark for a stable population of cells, but may be an intrinsic marker of heterogeneity. The ephrinB2+ hESCs demonstrated the abilities to self-renew *in vitro*, to differentiate into the three germ layers *in vitro*, and to form teratomas *in vivo*. To further examine the role of ephrinB2 in hESC fate, we generated a H9 cell line stably expressing an shRNA against ephrinB2 (shEFNB2). Real-time PCR analysis of embryoid bodies (EBs) derived from shEFNB2 cells demonstrated a severe deficiency in neuro-ectoderm gene expression and an up-regulation of mesoderm genes during differentiation. Microarray analysis of shEFNB2 EBs further confirmed that genes involved in mesendoderm specification were up-regulated, while genes that play roles in neuro-ectoderm formation were down-regulated. Lastly, functional mesoderm-directed differentiation assays revealed that shEFNB2 hESCs have an increased propensity to differentiate into one specific sub-type of mesenchymal cells. These exciting results suggest that manipulation of the ephrinB2 signaling axis may improve the directed differentiation of hESCs into mesoderm subtypes, which are very difficult to obtain robustly from standard hESC lines.

Materials and Methods

Plasmid construction. The codon-optimized NiV-F and NiV-G genes were tagged at their C termini with an AU1 (DTYRYI) or HA (YPYDVPDYA) tag, respectively, as previously described [8,9]. The lentiviral FG12 and FG11F vectors were provided by Dr. Dong Sung An at UCLA [10,11]. Open Biosystems pGIPZ lentiviral non-target shRNAmir (shNT) and ephrinB2 shRNAmir (shEFNB2) vectors were purchased (Thermo Scientific).

Cells and culture conditions. hESCs (H1, H9, UCLA1) were cultured on gelatin-coated plates on a feeder layer of mitotically-inactivated murine embryonic fibroblasts (MEFs). hESC medium is composed of DMEM/F:12 supplemented with 20% KnockOut Serum Replacement (KOSR, Invitrogen), 0.1 mM NEAA (Invitrogen), 1 mM L-Glutamine (Invitrogen), 0.1 mM 2-mercaptoethanol (Sigma-Aldrich), 1mM penicillin/streptomycin (Hyclone), and 4 ng/ml basic fibroblast growth factor (bFGF, R&D Systems – obtained via National Cancer Institute Biological Resources Branch). hESCs were passaged in small clumps every 5-7 days using 1mg/ml of collagenase type IV (Invitrogen). NiV ("ephrinB2+") and VSV-G (control) GFP+ H9 stable hESC lines were generated by transduction with NiV and VSV-G envelope pseudotyped lentiviruses, respectively. 3 days post-transduction, SSEA4+GFP+ hESCs were FACS-sorted. shNT and shEFNB2 stable hESC lines were generated by lentiviral-mediated transduction of pGIPZ shRNAmir vectors. 3 days post-transduction, 2 μg/ml of puromycin (Sigma) was added to the media. The lines were maintained in selection media for all subsequent experiments. 293T cells were cultured in IMDM with 10% FBS, 1% NEAA, 1% Glutamax, and antibiotics.

Lentivirus production. Lentivirus was produced as previously described (manuscript in press). To determine viral titer, serial dilutions of concentrated stocks were added to 2 x 10^5 293T cells and incubated for 2 hours at 37°C. The medium was replaced with fresh medium. 72 hours

post-infection, the cells were collected and analyzed by flow cytometry for eGFP expression. Titers were expressed as infectious units per ml (IU/ml).

***In vitro* infection of cells.** For viral transductions, hESCs were transferred to feeder-free conditions. hESCs were dissociated to single cells using 0.05% trypsin (Invitrogen) for counting and then plated on Matrigel- (BD Biosciences) coated plates in hESC medium that was conditioned overnight on MEFs and supplemented with 10 μM HA-1077 (ROCK inhibitor, Sigma-Aldrich) to promote hESC survival [12]. Increasing amounts of virus (based on MOI) and 4ng/ml of polybrene (Sigma) were added to the cells, and centrifuged at 2,000 rpm at 37°C for 2 hours. For transductions with NiV pseudotyped lentiviruses, 10 nM of soluble ephrinB2 (R&D Systems) was added to the infection medium as a specificity control. To exclude pseudotransduction, 5μM of nevirapine was added. Following an overnight incubation with virus, the infection medium was removed and replaced with fresh medium. 72 hours post-infection, the cells were harvested, stained with anti-SSEA4 PE (BD Biosciences), and analyzed by flow cytometry for eGFP expression.

Self-renewal assay. hESCs were rinsed with phosphate-buffered saline solution (PBS), dissociated to single cells using 0.05% trypsin, and passed through a 40 μm cell strainer. MEFs were depleted with feeder removal microbeads (Miltenyi) prior to cell counting. 5×10^5 cells were seeded per well of a 6-well plate and cultured for 1 week. This experiment was repeated for five passages. At each passage, the cells were stained with SSEA4-PE (BD Biosciences) and TRA-1-81 antibodies, and FACS analysis was performed to determine the percentage of hESCs.

Teratoma assay. Two confluent wells of hESCs (6-well plate) were dissociated with collagenase and passed through a 100 μm cell strainer. Following centrifugation, the cell pellet

was resuspended in 30 µl of PBS and injected into the testis of 4-week-old SCID BEIGE mice, as previously described [13]. 8 weeks later, the teratomas were harvested and fixed in 4% PFA overnight. The fixed teratomas were embedded and processed by the Translational Pathology Core Laboratory (TPCL) at UCLA.

Standard and spin embryoid body differentiation assays. For "standard embyroid bodies (EBs)," confluent wells of hESCs were detached by collagenase treatment for 1 hour at 37°C. The cell clumps were re-plated onto low-attachment 6-well plates (Fisher) in EB medium consisting of DMEM-F12 supplemented with 20% KOSR, 0.1 mM NEAA, 1 mM L-Glutamine, 0.1 mM 2-mercaptoethanol, and 1mM penicillin/streptomycin. For "spin EBs," hESCs were dissociated to single cells using 0.05% trypsin. The cell pellet was resuspended in "serum-free media (SFM)," consisting of Stemline II medium (Sigma) supplemented with 1X CD lipid concentrates (Invitrogen), 2mM GlutaMAX (Invitrogen), 1X insulin transferrin selenium (Invitrogen), 400 µM monothioglycerol (Sigma), and 1mM penicillin/streptomycin. 100 µg/ml of Matrigel and 10 µM HA-1077 were also added to the cell suspension. 100 µl containing the proper cell density (3,000, 5,000, 7,000, or 10,000) was transferred to each well of a low attachment round-bottom 96-well plate (Fisher), and centrifuged at 1400 rpm for 7 min. The plates were incubated at at 37°C overnight. 48 hours later, the proper differentiation medium was added to the spin EBs. For "spontaneous differentiation," EB medium was added. For mesoderm-directed differentiation, SFM containing 5 ng/ml of bFGF, 10 ng/ml of BMP-4 (Peprotech), and 20 ng/ml of VEGF (Peprotech) was added. Individual EBs were harvested at the corresponding time points during the differentiation for each analysis.

Real-time PCR analysis. For hESCs, RNA was extracted using a RNeasy kit (Qiagen). For spin EBs, a RNeasy Micro kit (Qiagen) was used. cDNA was prepared using a QuantiTect

Reverse Transcription kit (Qiagen). Real-time PCR was performed using iQ SYBR Green supermix (Bio-rad) and an iQ iCycler (Bio-rad). Primer sequences are shown in Table 3-1.

Differential gene expression analysis. RNA was extracted from shNT hESCs (day 0), shNT spin EBs (days 6 and 13), shEFNB2 hESCs (day 0), and shEFNB2 spin EBs (days 6 and 13) using the RNeasy kit (Qiagen). Gene expression was examined using the human U133plus2.0 array (Affymetrix) at the UCLA Clinical Microarray Core. Two biological replicates were analyzed for each sample. Data was analyzed as previously described [14]. Briefly, to assess differential expression, the R package *Limma* [15] provided through Bioconductor [16] was used. The RMA (Robust Multiarray Averaging) method was used to calculate absolute mRNA expression levels. To calculate PMA detection calls, the mas5calls algorithm [17] was used. The algorithm employs a signed rank test to consider the significance of the difference between the PM (Perfect Match) and MM (MisMatch) values for each probeset and returns a detection p-value that is used to flag a transcript as 'Present', 'Marginal' or 'Absent' (P/M/A). Probes that were “absent” for all samples analyzed were excluded. Heat maps of differentially expressed genes were generated using Cluster 3.0 and Java Treeview.

Mesoderm-directed differentiation assay. hESCs were detached using collagenase and seeded onto matrigel-coated plates in mTESR medium (Stem Cell Technologies). When the cells reached 50-60% confluency, differentiation was induced by adding SFM medium supplemented with 10 ng/ml of activin A (Peprotech), VEGF, BMP4, and bFGF. The next day, the medium was replaced with fresh SFM containing only VEGF, BMP4, and bFGF. At day 3.5, the cells were dissociated into a single cell suspension using Accutase (Invitrogen), and stained with CD326-PerCP/Cy5.5 (BioLegend) and CD56-PE (BioLegend) antibodies for 20 min at 4°C. CD56+CD326- cells were FACS-sorted on a BD FACS Aria, and seeded onto mouse OP9 stroma in EGM-2 complete medium (Lonza) supplemented with ALK 4/5/7 blocker SB-431542

(Sigma). The cells were cultured for 7 days, with medium changes every 2 days. Following the incubation, the cells were stained with CD29-APC/Cy7, CD43-APC, CD73-PE/Cy7, CD31-Pacific Blue, and CD146-PE antibodies to examine hematopoietic, endothelial, and mesenchymal cell differentiation using FACS analysis.

Results

EphrinB2 is an intrinsic marker of hESC heterogeneity. Microarray profiles of mouse embryonic (ESC), hematopoietic (HSC), and neural (NSC) stem cells identified ephrinB2 as a marker expressed in all three populations [18]. We recently extended this finding to their human counterparts and found that ephrinB2 is functionally expressed in human ESCs, HSCs, and NSCs (**Chapter 2**, manuscript in press). Our lab previously identified ephrinB2 as the entry receptor for Nipah virus (NiV) [19], and established that the viral envelope attachment glycoprotein (NiV-G) has picomolar affinity for ephrinB2 [20]. We engineered the NiV fusion (F) and attachment (G) envelope glycoproteins to be efficiently pseudotyped onto a lentiviral vector carrying an eGFP reporter, and infected H9 hESCs with the NiV pseudotyped particles (NiVpp) (Fig. 3-1A). At a MOI 100, NiVpp transduced up to 15% of SSEA-4+ H9 cells, and infection was abrogated by soluble ephrinB2 (Fig. 3-1B). At lower MOIs of 10 and 50, NiVpp transduced 9% and 12% of cells, respectively (Fig. 3-1C). VSV-Gpp, on the other hand, transduced up to 37% of cells, and infection was not blocked with soluble ephrinB2. Thus, NiVpp transduction can be used to specifically mark for ephrinB2+ cells.

To further characterize the ephrinB2+ subpopulation in hESC cultures, NiVpp-transduced H9s were FACS-sorted to achieve a homogenous population of GFP+ cells. The sorted GFP+ hESCs were expanded and then re-infected with NiVpp or VSV-Gpp carrying a different fluorescent reporter (mCherry) (Fig. 3-2A). Although we FACS-sorted only the GFP+ cells from the initial transduction, only 53% of the cells were GFP+ after passaging in culture, prior to the secondary transduction (Fig. 3-2B). Nevertheless, this population should contain only ephrinB2+ hESCs, and we expected an increase in infection efficiency. However, in the secondary round of infection, NiVpp transduced a similar percentage (~13-17%) of Tra181+GFP+ hESCs (Fig. 3-2C), recapitulating the original transduction patterns. This indicates that ephrinB2 does not mark for an independent, phenotypically stable population of

cells. Instead, ephrinB2 may be an intrinsic marker of stem cell heterogeneity specifying a subset of cells poised for self-renewal or differentiation.

EphrinB2+ hESCs self-renew *in vitro,* differentiate into the three germ layers *in vitro*, and form teratomas *in vivo*. hESCs are defined by two properties. First, they have the ability to survive and proliferate *in vitro* indefinitely in an undifferentiated state ("self-renewal"). Second, they have the ability to differentiate into many specialized cell types *in vitro* and *in vivo*. Here, we sought to confirm that ephrinB2+ hESCs have these two basic properties. To assess self-renewal capacity, 500,000 cells of the NiV and VSV-G GFP+ lines were seeded per well and the percentage of SSEA-4+GFP+ cells was determined after 7 days in culture. This was repeated for 5 consecutive passages. For both the NiVpp- and VSV-Gpp- transduced cells, the SSEA-4+GFP+ population was maintained across the 5 passages (Fig. 3-3A, B). Thus, ephrinB2+ hESCs demonstrated similar self-renewal capacity to control cells.

Next, we sought to examine the differentiation potential of ephrinB2+ hESCs *in vivo*. When transplanted into immune-deficient mice, hESCs form teratomas containing differentiated progeny representing the three germ layers. Hence, teratoma formation is considered to be the ultimate test to measure pluripotency of a hESC line. To confirm that ephrinB2+ hESCs maintain pluripotency, equivalent numbers of NiV and VSV-G GFP+ H9 cells were injected in the testes of SCID-biege mice and teratomas assessed after 8 weeks. Both the NiV and VSV-G GFP+ cells gave rise to teratomas of comparable sizes (Fig. 3-3C). Also, H&E staining demonstrated the presence of endoderm and mesoderm lineages (Fig. 3-3D). Formation of ectoderm lineages has yet to be determined, but will be confirmed with immunofluorescence in subsequent experiments.

Lastly, to examine the differentiation potential of ephrinB2+ hESCs *in vitro*, we performed the standard embryoid body (EB) assay. H9, NiV, and VSV-G GFP+ H9 colonies were dissociated with collagenase and cultured in spontaneous differentiation conditions for 30

days. EBs were harvested at various time points to examine lineage marker expression using real-time PCR (Fig. 3-4). Both the NiV and VSV-G GFP+ cells demonstrated similar trends in Oct4 and ephrinB2 expression. Also, for both lines, ectoderm (Pax6 and NeuroD1) expression peaked at day 20. However, for NiV GFP+ cells, mesoderm (Pecam and Brachyury) and endoderm (Gata4 and Sox17) expression was delayed compared to VSV-G GFP+ cells. This variability could be due to the inherent variability of the standard EB formation assay. Collagenase dissociation of hESC colonies results in a wide range of EB sizes, which may affect germ layer differentiation potential and kinetics [21].

We then developed a modified version of the spin EB method where forced aggregation of defined cell numbers controls EB size [22,23] (Fig. 3-5A). H9 hESCs were dissociated with trypsin and various cell densities (3,000, 5,000, 7,000, and 10,000) were seeded per well of a low-attachment 96-well plate. Spin EBs were cultured individually for 20 days. At each time point, we examined gene expression of individual EBs (Fig. 3-5B). Unlike the heterogeneous standard EB assay, the spin EB method resulted in a pattern of germ layer marker expression that was temporally and quantitatively reproducible. Moreover, the differentiation patterns were very similar for all cell densities. Ectoderm markers (Pax6 and NeuroD1) were consistently upregulated by day 10, while mesoderm (CD34 and Brachyury) and endoderm (Sox17 and Gata4) markers were initially downregulated and did not emerge until day 15. Interestingly, ephrinB2 increased throughout the 20-day time course, suggesting that antagonizing this axis could potentially also skew differentiation.

Using the spin EB method, we then re-examined the differentiation potential of the ephrinB2+ hESCs (Fig. 3-6). 3,000 or 10,000 cells from the NiV and VSV-G GFP+ lines were used to prepare spin EBs. Unlike with the standard EB method (Fig. 3-4), the NiV and VSV-G lines demonstrated similar differentiation patterns for all germ layer markers. The only variability between the two lines was Pecam expression, but the fold-change values were low since mesoderm genes are not induced under spontaneous differentiation conditions. Thus far, we

have demonstrated that ephrinB2+ hESCs have the ability to differentiate into all three germ layers *in vitro* and two germ layers *in vivo*.

EphrinB2-knockdown hESCs exhibit altered differentiation potential. EBs derived from *ephB4*$^{-/-}$ mESCs demonstrated a downregulation of mesoderm genes and an upregulation of neuro-ectoderm genes, suggesting that ephB4 may play a role in modulating mesoderm induction [5]. To determine the role of ephrinB2 in hESC fate, we generated ephrinB2-knockdown (shEFNB2) and control (shNT) H9 hESC lines using lentiviral-mediated transduction of pGIPZ shRNAmir vectors. The CMV promoter in the pGIPZ vector drives expression of the shRNAmir, a TurboGFP reporter, and a puromycin selection marker. 3 days post-transduction, puromycin was added to the culture media. Real-time PCR analysis of the stable hESC lines showed a 70% reduction of ephrinB2 expression in shEFNB2 cells compared to shNT cells (Fig. 3-7). Due to potential silencing of the CMV promoter during hESC differentiation [24], we maintained our shNT and shEFNB2 H9 lines in puromycin selection media throughout all experiments to achieve consistent knockdown.

As with the ephrinB2+ hESCs, we first sought to confirm that the basic properties of hESCs were maintained in the shEFNB2 line. We performed a self-renewal assay on shNT and shEFNB2 cells (Fig. 3-8). At passage 1, the shNT line had 72% SSEA-4+GFP+ cells and the shEFNB2 line had 56% SSEA-4+GFP+ cells. By passage 3, the SSEA-4+GFP+ population decreased for both lines, but more drastically for the shNT cells. At passage 5, the SSEA-4+GFP+ population increased to values near that of passage 1, with 77% and 53% cells for shNT and shEFNB2 lines, respectively. Overall, the self-renewal capacity of ephrinB2-knockdown hESCs does not seem to be affected, but further repetitions of this assay will be necessary to support this conclusion.

Next, we examined the ability of the ephrinB2-knockdown hESCs to differentiate *in vitro*. Our results demonstrated that ephrinB2 expression increased during a 20-day time course,

suggesting that downregulation may alter differentiation patterns (Fig. 3-5). 3,000 or 10,000 cells from the shNT and shEFNB2 lines were used to prepare spin EBs. To examine differentiation into all 3 germ layers, the spin EBs were cultured in both spontaneous (Fig. 3-9A, B) and mesoderm-directed differentiation media (Fig. 3-9C, D). Interestingly, under spontaneous differentiation conditions, shEFNB2 EBs demonstrated a 10-fold decrease in Pax6 expression compared to shNT EBs at all time points (Fig. 3-9B). NeuroD1 expression also demonstrated a 10-fold decrease at days 10 and 15. Under mesoderm-directed differentiation conditions, shEFNB2 EBs exhibited a 2-fold increase in CD34 expression and a 4-fold increase in Pecam expression compared to shNT EBs (Fig. 3-9D). Taken together, ephrinB2-knockdown hESCs demonstrated a severe deficiency in neuro-ectoderm gene expression and an up-regulation of mesendoderm genes during differentiation.

To compare global gene expression profiles, we performed microarrays on H9, shNT, and shB2 hESCs, and on their derived EBs (days 6 and 13) under spontaneous differentiation conditions (Fig. 3-10). Venn diagrams revealed that 93, 170, and 735 genes were specifically up-regulated in shEFNB2 cells compared to H9 and shNT cells on days 0, 6, and 13, respectively (Fig. 3-10A). To identify the genes that were most differentially expressed, we calculated log ratios of averaged replicate values divided by the mean of all samples. A heat map of the top fifty up-regulated genes at day 13 identified major components of signaling pathways involved in regulating tissue differentiation, body patterning, and organogenesis, including TGF-β, WNT5A, and GREM1 (Fig. 3-10B, Table 3-2). Snail-2, a key transcriptional regulator of epithelial-to-mesenchymal transition (EMT), as well as another gene involved in specifying mesoderm commitment, PDGFR-α [25], were also significantly up-regulated. Genes involved in controlling the onset of endoderm specification were up-regulated, including EOMES [26] and Sox17 [27]. Interestingly, although we detected a 10-fold decrease in NeuroD1 expression by real-time PCR (Fig. 3-9A), microarray analysis revealed a significant increase in

expression in shEFNB2 cells. Our results thus far suggest that ephrinB2 knockdown may enhance the generation of mesendoderm progenitors.

Venn diagrams showed that 15, 95, and 267 genes were specifically down-regulated in shEFNB2 cells on days 0, 6, and 13, respectively (Fig. 3-10A). A heat map of the top fifty down-regulated genes at day 13 identified genes that play roles in the development of mutiple organ systems (Figure 3-10C, Table 3-3). SPINK5 functions in skin and hair morphogenesis [28]. RAX is involved in eye development [29]. NRG1 is a signaling protein that mediates cell-to-cell interactions and enhances the proliferation of neural progenitors and formation of neurons [30]. Transcription factors that regulate the morphogenesis, development, and differentiation of neurons were significantly down-regulated, including OTX2 [31] and PAX6 [32]. Since PAX6 is a major determinant of neuro-ectoderm formation, ephrinB2 knockdown may inhibit specification of ectoderm lineages.

Since the eph receptors and ephrin ligands constitute the largest family of RTKs, we also examined the effect of ephrinB2 knockdown on expression of the other family members (Fig. 3-11). Surprisingly, although ephB4 is the receptor for ephrinB2, the knockdown did not affect its expression. However, at day 13, shEFNB2 cells demonstrated down-regulation of ephA4 and up-regulation of ephrinA1 genes. EphA4 is the only receptor that can bind to both ephrinA and ephrinB ligands [33], and has been identified as an important regulator of neurogenesis [34].

Lastly, we compared our gene expression analysis of ephrinB2-knockdown hESCs to that of *ephb4*$^{-/-}$ mESCs [5]. EBs derived from *ephb4*$^{-/-}$ mESCs exhibited decreased expression of mesoderm genes and increased expression of neuro-ectoderm genes during mesoderm-directed differentiation. A heat map of selected mesoderm genes indicated that most of the genes were undetected or expressed at very low levels even in the H9 line (Fig. 3-12), which is expected since we did not use mesoderm induction conditions. Nevertheless, at day 13, we did see up-regulation of some genes in shEFNB2 cells. BMP4 is a marker specifiying mesendoderm commitment [26,35], PAX3 is a marker of myogenesis induction [36], and GATA3 is

transcription factor involved in hematopoiesis [37]. Changes in this gene expression pattern may become more obvious under the proper differentiation conditions. Thus, to further evaluate whether shEFNB2 cells have increased mesoderm potential, we will be performing microarrays with H9, shNT and shEFNB2 EBs under mesoderm induction. This may facilitate future efforts to generate mesoderm progenitor cells for use in regenerative therapies.

EphrinB2 knockdown enhances mesoderm-directed differentiation into mesenchymal cells. Our real-time PCR (Fig. 3-9) and microarray (Fig. 3-10) data analyses both indicated that ephrinB2 knockdown may enhance the formation of mesendoderm progenitors. To functionally confirm this, we performed a mesoderm-directed differentiation assay on the H9, shNT, and shEFNB2 H9 lines (Fig. 3-13). A recent study found that mesoderm commitment from hESCs is represented by an up-regulation of NCAM (CD56) and a down-regulation of EpCAM (CD326), and that CD56+CD326- progenitors generate all mesodermal lineages (Fig. 3-13A) [38]. The cells were treated with a combination of BMP4, VEGF, bFGF, and a 1-day exposure to activin A. On day 3.5, the resulting CD56+CD326- populations from each line were FACS-sorted. 9%, 24%, and 12% of the total cells were CD56+CD326- for the H9, shNT, and shEFNB2 lines, respectively (Fig. 3-13B). The sorted cells were then cultured on mouse OP9 stroma for 10 days to examine tri-lineage differentiation. The shEFNB2 line demonstrated reduced survival and proliferation, with a final count of 20,000 cells compared to 60,000 cells for the shNT line (Fig. 3-13C). Since puromycin selection was continued during differentiation, the OP9 stroma was lost for the shNT and shEFNB2 cultures. Consequently, hematopoietic (CD43+) and endothelial (CD31+) cell lineages were not detected for either of these lines (Fig. 3-13D). However, the mesenchymal (CD73+) lineage was detected for both. Mesenchymal cell populations can be further fractionated into 2 populations based on intensity of CD146 expression. Interestingly, while the shNT cells exhibited a fairly equal distribution of $CD146^{bright}$ versus $CD146^{dim}$ cells, the shEFNB2 cells demonstrated a skewed ratio in favor of $CD146^{bright}$

cells (Fig. 3-13E). 80% of the cells were CD146^{bright}, while only 9% were CD146^{dim}. Thus, ephrinB2 knockdown may potentially enhance mesoderm-directed differentiation towards one sub-population of mesenchymal cells.

Discussion

Ephrins and ephs have well-established roles in providing cues for cell migration and organized patterning of tissues. Previous studies have also implicated that a gradient of ephrin-eph expression may regulate the abundance of primitive stem cells and their differentiated derivatives [5,6]. While ephB4 deficiency resulted in decreased mesoderm differentiation of mESCs, ephB4 overexpression in human cord blood CD34+ cells accelerated differentiation into lineage-committed progenitors. Taken together, these findings suggested that eph expression might also have a function in regulating differentiation kinetics of stem cells. In this chapter, we investigated the role of ephrinB2, the ligand for ephB4, in hESC fate.

Since ephrin-eph interactions are very promiscuous, highly specific tools are necessary to interrogate the role of ephrinB2 signaling. **Chapter 2** demonstrated that lentiviruses pseudotyped with the NiV envelope glycoproteins specifically transduced a population of hESCs, and infection was completely abrogated with soluble ephrinB2. Our group previously identified ephrinB2 as the primary receptor for NiV [19], and ephrinB3 as an alternate receptor [20]. Thus, our findings provided the first functional confirmation that ephrinB2 is expressed on hESCs. Microarray analysis revealed that ephrinB3 is not expressed on day 0 H9 cells (Fig. 3-11), further demonstrating that NiV pseudotyped lentiviruses could specifically "tag" ephrinB2+ hESCs.

In order to examine the basic stem cell properties of the ephrinB2+ sub-population of hESCs, we FACS-sorted NiV-infected GFP+ cells to generate a homogenous population of ephrinB2-expressing cells. However, expansion of the sorted cells in culture and subsequent re-infection with a NiV pseudotyped lentivirus revealed that the population no longer consisted of *only* ephrinB2-expressing cells. Although ~50% of the cells were GFP+, only 17% were re-infected (Fig. 3-2, B-C), recapitulating the original transduction patterns (Fig. 3-1, B-C). This suggests that the percentage of ephrinB2+ that can exist in hESC cultures is restricted. Based on our previous transduction data (**Chapter 2**), at any given time, 5-30% of hESCs express

ephrinB2. EphrinB2 expression also varied from passage to passage, as demonstrated by the variability in transduction efficiency with NiV pseudotyped lentiviruses (data not shown). This heterogeneity in ephrinB2 expression might be necessary for maintaining "stemness."

Studies have shown that hESC cultures consist of heterogeneous populations of cells with distinct gene expression profiles [39,40]. Although SSEA-3 is a standard cell-surface pluripotency marker, these studies showed that its expression could be used to identify two subpopulations of hESCs with distinct expression of Oct4 and Nanog, as well as distinct clonogenic capacity. Nevertheless, sorted SSEA-3- cells generated cultures with SSEA-3+ and SSEA-3- cells, indicating that they still maintained their stem cell properties. Other studies identified pluripotency cell-surface markers that were expressed in a continuous gradient [40,41]. A detailed examination of the various subpopulations revealed that the amount of cell-surface marker expression reflected the pluripotency gene expression and self-renewal capacity. Interesting, cells at the middle of the spectrum co-expressed both pluripotency and lineage-specific markers. Thus, populations of cells with heterogeneous expression of cell-surface markers may demonstrate unique differentiation potentials.

Although the FACS-sorted, NiV-infected GFP+ cells did not represent a homogenous population of "ephrinB2-expressing cells," we nevertheless confirmed that the cell line exhibited basic stem cell properties. Indeed, the ephrinB2+ cells demonstrated the ability to self-renew *in vitro*, to differentiate into EBs containing markers from the three germ layers, and to form teratomas *in vivo* (Fig. 3-3, 3-6). Future studies should focus on determining whether ephrinB2+ hESCs are poised for self-renewal or differentiation. The methods presented in this chapter did not allow us to propagate a homogenous population of ephrinB2-expressing cells in culture for detailed analyses, but gene expression analysis of the cells immediately after sorting might reveal differences in pluripotency and lineage-specific marker expression. If ephrinB2+ hESCs do demonstrate differences in differentiation potential, then ephrinB2 heterogeneity may be potentially manipulated to direct differentiation towards a specific lineage.

Next, we used a more direct approach to determine whether ephrinB2 functions in regulating differentiation kinetics of hESCs. We generated stable lines of H9 cells expressing either a non-target shRNA (shNT) or a potent shRNA against ephrinB2 (shEFNB2) (Fig. 3-7). Compared to shNT cells, shEFNB2 cells demonstrated a 70% reduction in ephrinB2 expression. Although ephrinB2 expression appeared to also be down-regulated in shNT cells compared to control H9 cells, the shNT and shEFNB2 cells demonstrated drastic differences in phenotype. Real-time PCR analysis of EBs derived from shEFNB2 cells detected significantly decreased expression of neuro-ectoderm markers, Pax6 and NeuroD1, and increased expression of mesoderm markers, Pecam and CD34 (Fig. 3-9). Microarray analysis further supported this down-regulation of neuro-ectoderm formation genes and up-regulation of mesoderm induction genes (Fig. 3-10, Table 3-2, Table 3-3). In addition, shEFNB2 cells demonstrated increased expression of genes involved in EMT and in specification of endoderm. Thus, ephrinB2 knockdown potentially enhances the formation of mesendoderm progenitors.

Taken together, both ephrinB2 and ephB4 have significant roles in regulating differentiation kinetics of ESCs. *EphB4*$^{-/-}$ mESCs were associated with a severe deficiency in mesoderm induction genes and an overexpression of neuro-ectoderm genes [5]. EphrinB2 knockdown hESCs demonstrated the exact opposite phenotype- overexpression of genes involved in formation of mesendoderm progenitors and a severe deficiency in genes specifying neuro-ectoderm formation. It has yet to be functionally determined whether this latter phenotype is due to lack of ephrinB2 “reverse” signaling, lack of ephB “forward” signaling, or lack of both. EphB4 is unique amongst ephB receptors for not being expressed in the central nervous system, but ephrinB2 could potentially activate the signaling of another ephB receptor. To address this, soluble ephrinB2-Fc could be added to the medium to see if the phenotype is rescued. Nevertheless, since ephB4 is not expressed in the central nervous system, our data suggests that ephrinB2 reverse signaling and ephB4 forward signaling most likely play *distinct* roles in germ layer commitment and differentiation.

Our data supports a model in which a gradient of ephrin-eph expression may regulate boundary formation between primitive stem cells and differentiated cells [5]. It would be interesting to determine how ephrinB2 knockdown affects germ layer separation in hESCs during gastrulation. Studies with Xenopus embryos showed that ephrin-eph signaling at the ectoderm-mesoderm boundary is necessary to locally regulate cell detachment and eventually tissue separation [42]. Although multiple ephrinB ligands and ephB receptors are expressed on each side of the boundary, overexpression of ephrinB2 in the ectoderm was sufficient to trigger separation, suggesting that expression of this subtype in each of the two tissues may be the main determinant for tissue separation. Thus, our ephrinB2 knockdown hESC lines may serve as a good model to further examine separation of the germ layers during gastrulation.

In sum, the findings of this chapter suggest that the heterogeneity of ephrinB2 expression and perturbation of ephrinB2 signaling may both be manipulated to enhance directed differentiation of hESCs *in vitro*. Derivatives from mesoderm and endoderm lineages are very difficult to obtain robustly from standard hESC lines, and requires the addition of multiple growth factors for efficient differentiation [43]. Our results indicate that ephrinB2 knockdown under spontaneous differentiation conditions alone is enough to enhance the formation of mesendoderm progenitors. Hence, manipulation of this signaling axis may potentially lead to more robust culture conditions that give rise to more homogenous population of cells for use in regenerative medicine.

Figure 3-1

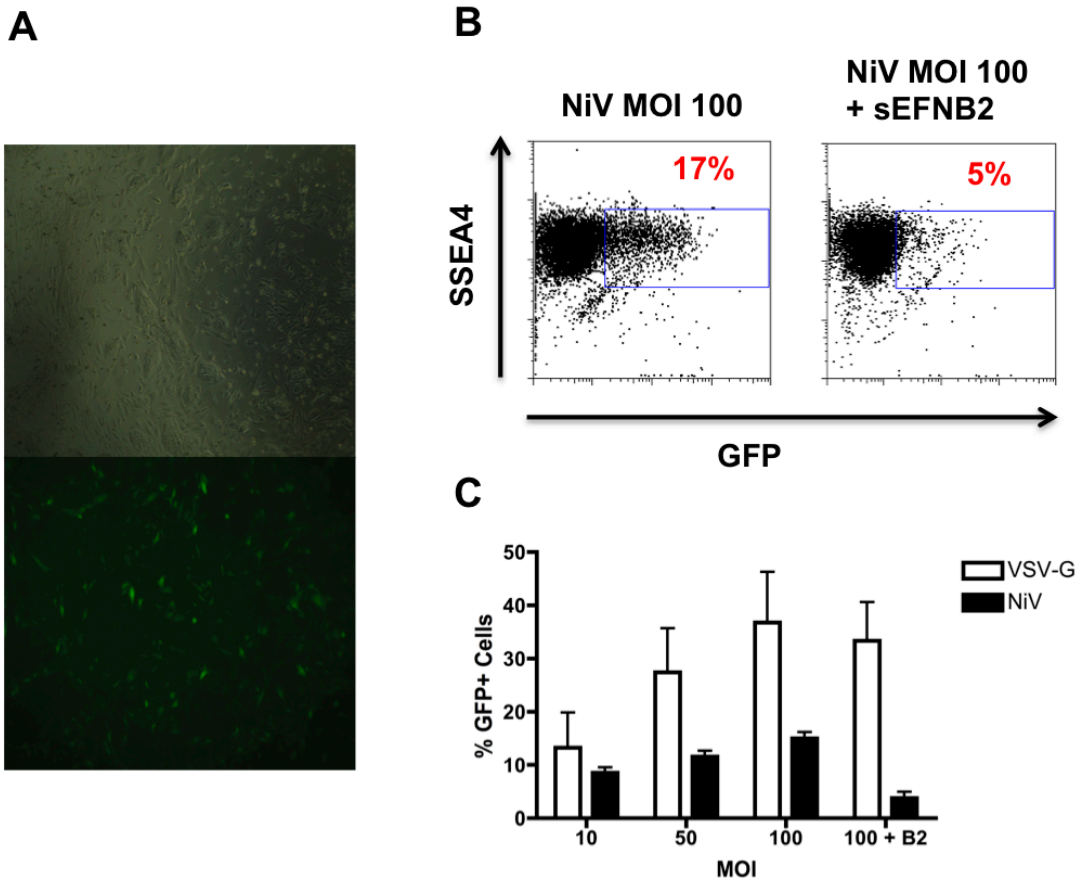

Figure 3-1. NiV pseudotyped lentiviruses mark ephrinB2+ hESCs. **(A)** NiV and VSV-G envelopes were pseudotyped onto a FG12 lentiviral vector in which the ubiquitin C promoter drives eGFP gene expression. H9 hESCs were transduced with the NiV pseudotyped lentiviruses. 72h post-infection, the cells were examined by microscopy. Shown here are brightfield and fluorescent images of NiV-transduced cells. **(B)** The transduced cells were also stained with cell-surface pluripotency marker, SSEA-4, and examined by FACs analysis. Shown here are two representative FACS plots at MOI 100. NiV infection is blocked with 10nM soluble ephrinB2. **(C)** Adding increasing amounts of lentivirus to H9 hESCs results in a dose-dependent increase in the amount of SSEA4+GFP+ cells. Data shown are averages ± standard deviations from three independent experiments.

Figure 3-2

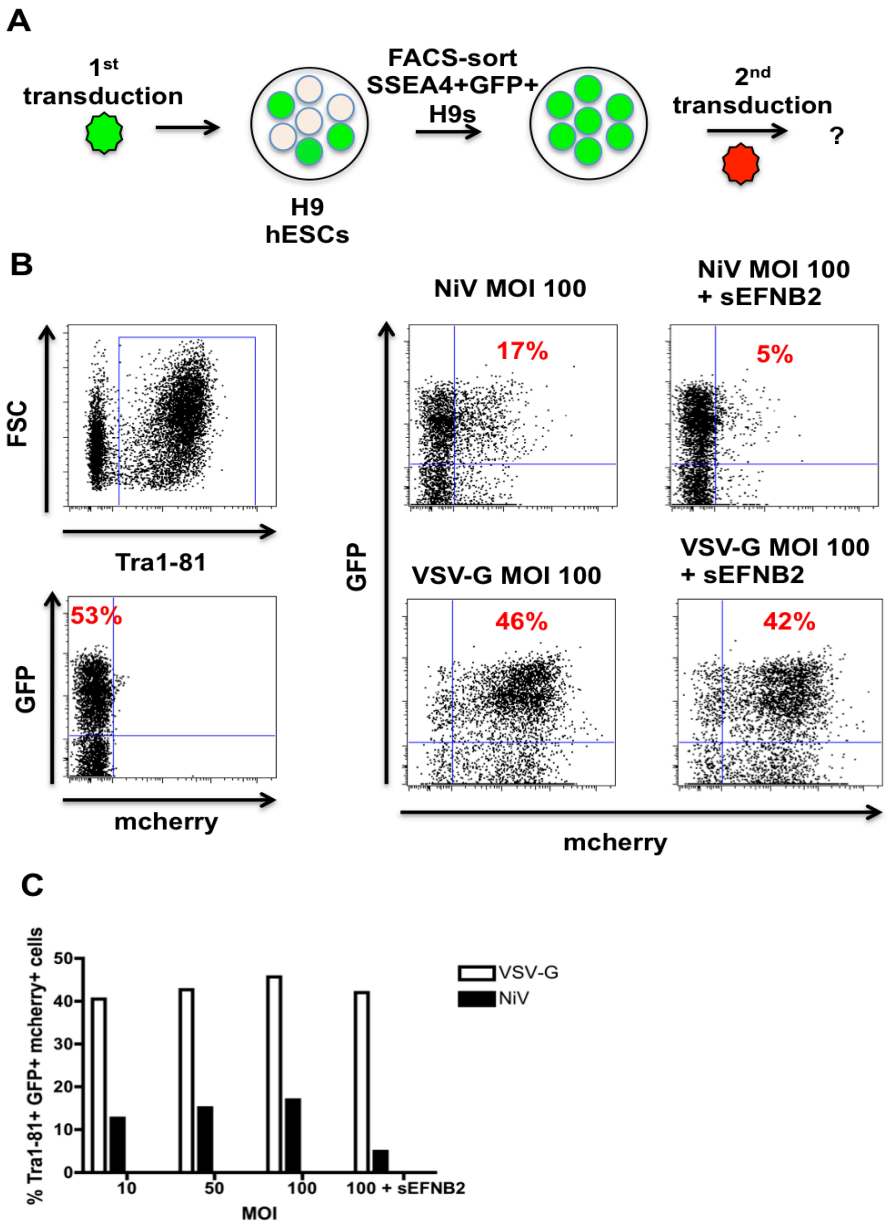

Figure 3-2. EphrinB2 does not mark for a stable population of hESCs. (A) A schematic of the experimental design. NiV GFP+ ("ephrinB2+") H9s were FACS-sorted and re-infected with NiV and VSV-G pseudotyped lentiviral vectors in which the ubiquitin C promoter drives mCherry expression. **(B)** 72h post-infection, the transduced cells were stained with cell-surface Tra-1-81 pluripotency marker and the infection rate determined by FACS analysis. We first gated on Tra-1-81+ cells (top left), then looked at the percentage of GFP+mCherry+ cells. Representative FACS plots of uninfected (bottom left), NiV-infected (top middle and right), and VSV-G infected (bottom middle and right) cells are shown. **(C)** The percentage of Tra181+GFP+mcherry+ cells was quantified at all MOIs. Data shown is representative of one experiment.

Figure 3-3

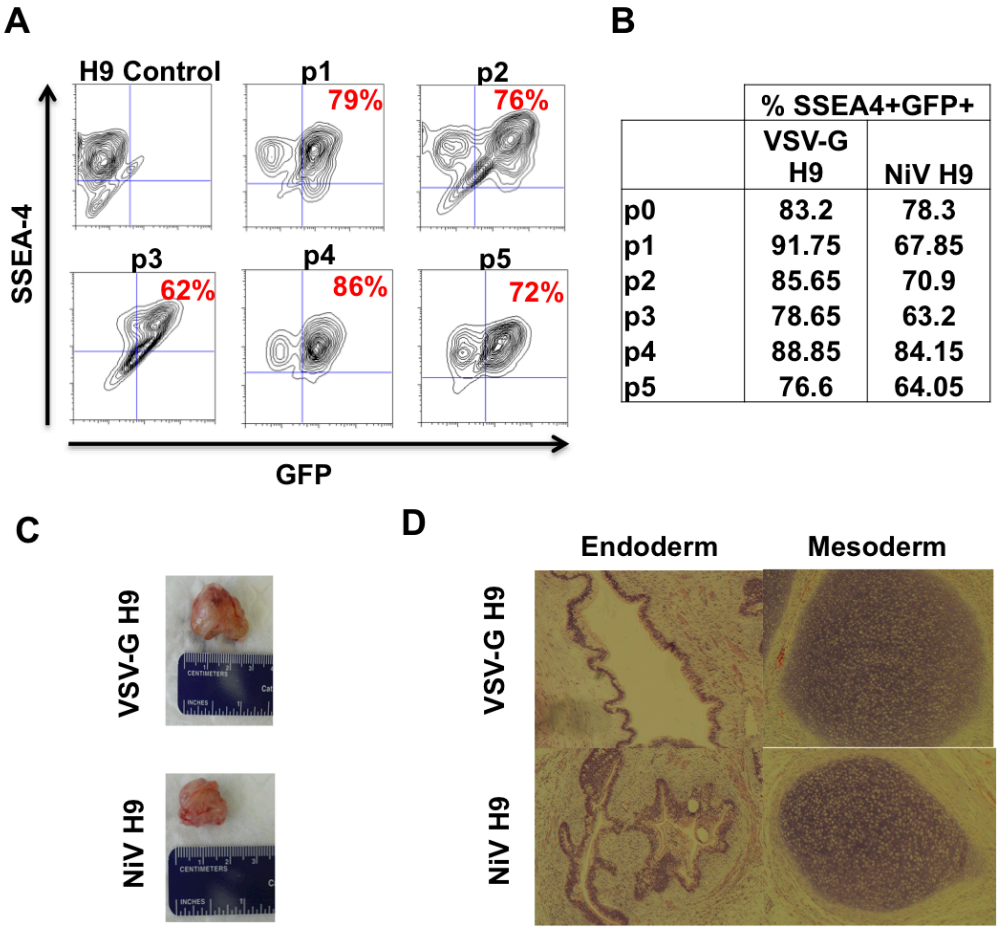

Figure 3-3. EphrinB2+ hESCs self-renew *in vitro* and give rise to teratomas *in vivo*. (A) To evaluate self-renewal of the NiV and VSV-G GFP+ stable hESC lines, 500,000 cells were seeded per well of a 6-well plate and cultured for 7 days. The cells were stained with SSEA-4 and the percentage of GFP+ stem cells determined by FACS analysis. Self-renewal was examined over 5 consecutive passages. Shown here is one representative FACS plot of the NiV GFP+ cells at each passage. **(B)** The percentage of SSEA-4+GFP+ cells was quantified for both NiV and VSV-G GFP+ lines. Data shown are averages from two independent experiments. **(C)** Two confluent wells from the NiV and VSV-G GFP+ lines were injected into the testes of immunodeficient mice. Resulting teratomas were harvested 8 weeks later. One representative image from each line is shown. **(D)** Teratomas were examined by histology. Bright-field images of endoderm and mesoderm lineages are shown for each line.

Figure 3-4

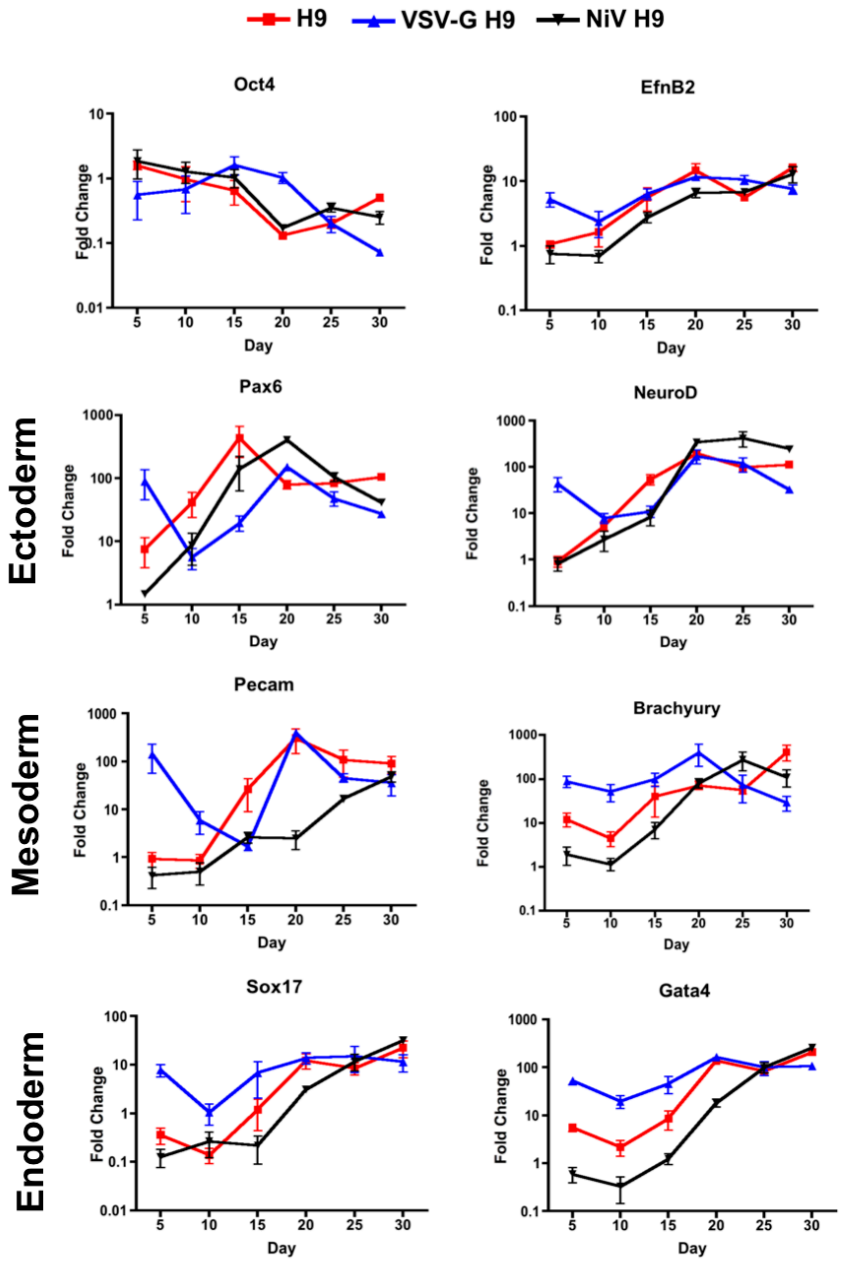

Figure 3-4. EphrinB2+ hESCs exhibit altered differentiation patterns using standard EB method. H9, NiV, and VSV-G GFP+ H9 colonies were dissociated with collagenase and cultured in bulk in 6-well low-attachment plates. Ectoderm (Pax6 and NeuroD1), mesoderm (Pecam and Brachyury), and endoderm (Gata4, Sox17) marker expression was examined using real-time PCR across a 30-day time course. Data shown are averages ± standard deviations from three independent experiments.

Figure 3-5

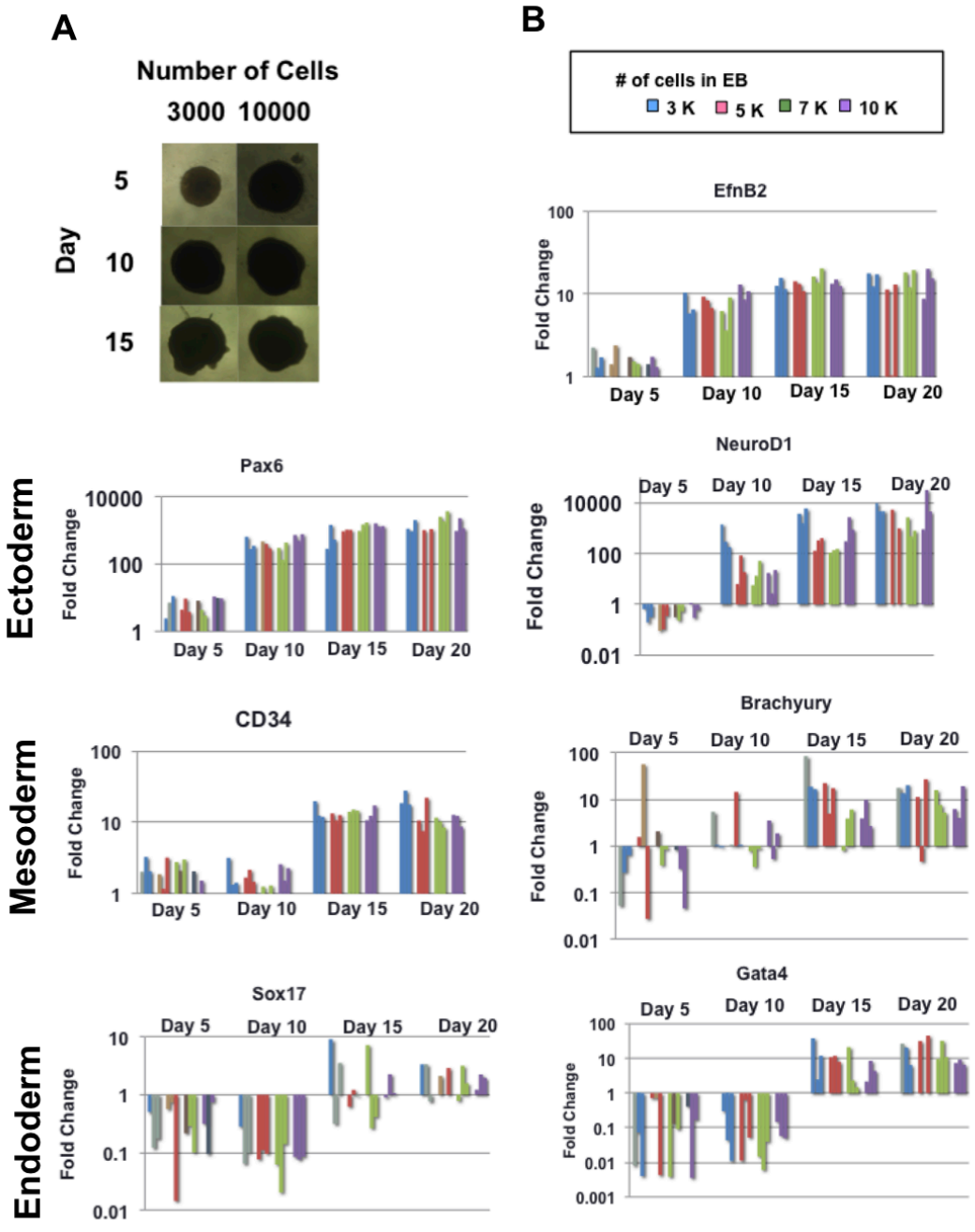

Figure 3-5. Spin EB method results in a differentiation pattern that is more reproducible. **(A)** Uninfected H9 hESCs were trypsinized and various cell densities (3,000, 5,000, 7,000, 10,000) seeded in a 96-well low-attachment plate, as previously described [22,23]. Bright-field images are shown for 2 densities at 3 timepoints. **(B)** Individual EBs were examined for various different differentiation markers across a 20-day time course. Shown here are ectoderm (Pax6 and NeuroD1), mesoderm (CD34 and Brachyury), and endoderm (Sox17 and Gata4) markers. Each bar represents one spin EB.

Figure 3-6

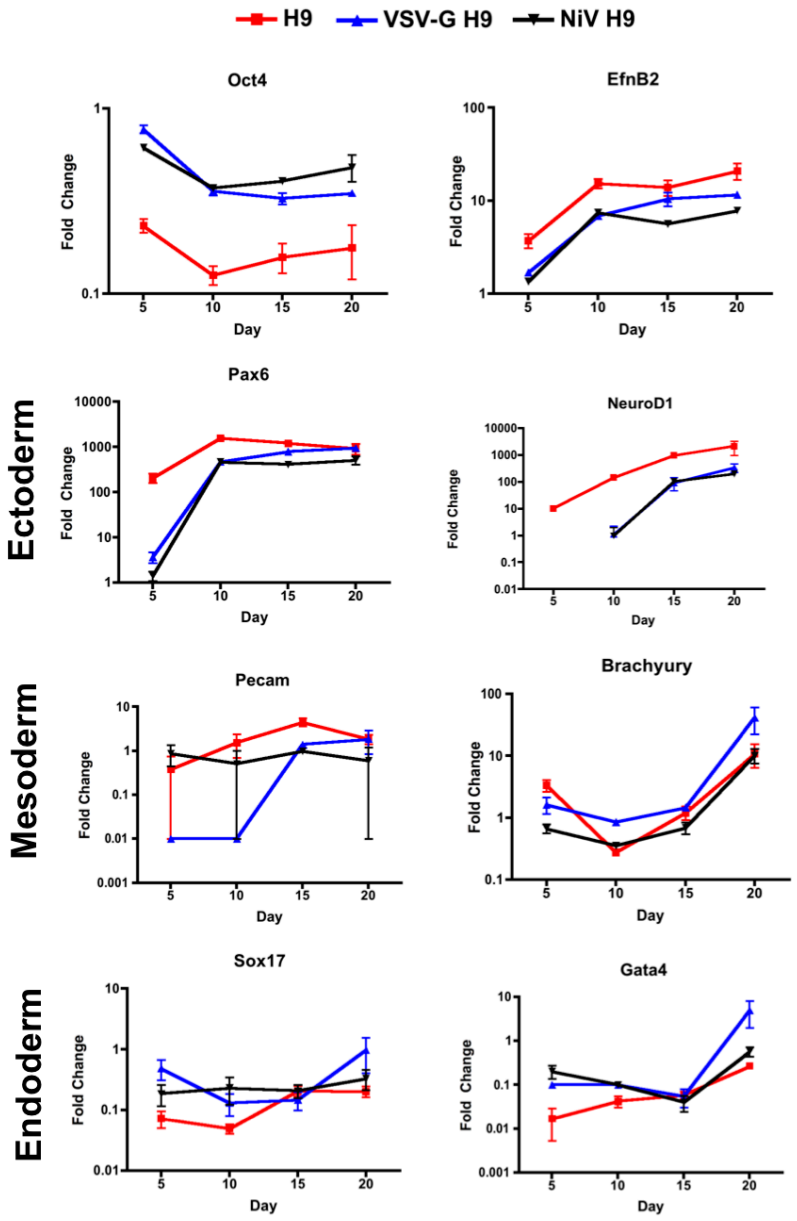

Figure 3-6. EphrinB2+ hESCs exhibit standard differentiation patterns using the spin EB method. H9, NiV, and VSV-G GFP+ H9were trypsinized and either 3,000 or 10,000 cells were seeded in a 96-well low-attachment plate, as previously described [22,23]. Individual EBs were examined for various different differentiation markers across a 20-day time course. Ectoderm (Pax6 and NeuroD1), mesoderm (Pecam and Brachyury), and endoderm (Gata4, Sox17) marker expression was examined using real-time PCR across a 20-day time course. Data shown are averages ± standard deviations from three individual EBs.

Figure 3-7

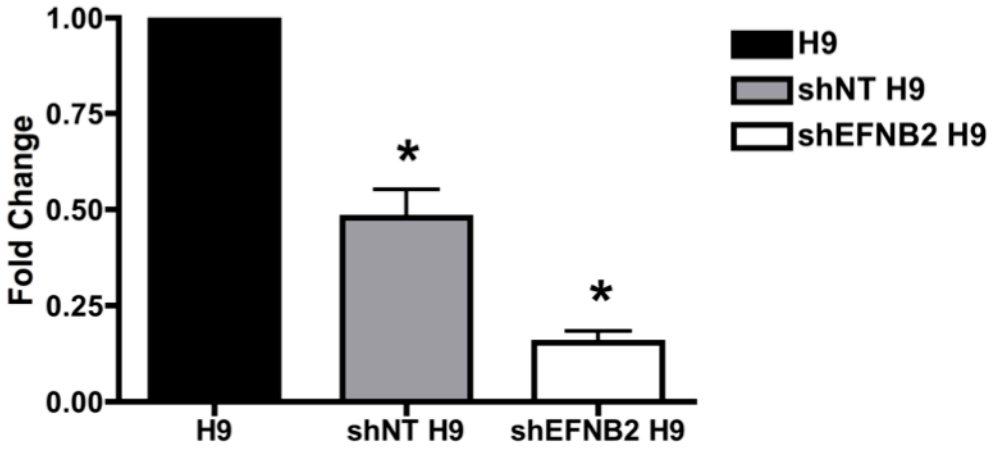

Figure 3-7. Generation of ephrinB2 knockdown H9 hESCs. H9 hESCs were transduced with lentiviruses delivering pGIPZ shRNAmir non-target (shNT) and ephrinB2 (shEFNB2) vectors. 3 days post-infection, the cells were selected with puromycin and expanded. Knockdown of ephrinB2 was confirmed using real-time PCR analysis. Data shown are averages ± standard deviations from 3 independent cell passages. Statistical analyses were performed using a one-way ANOVA with Bonferroni post-test comparison using GraphPad PRISM™. *: $p < 0.01$.

Figure 3-8

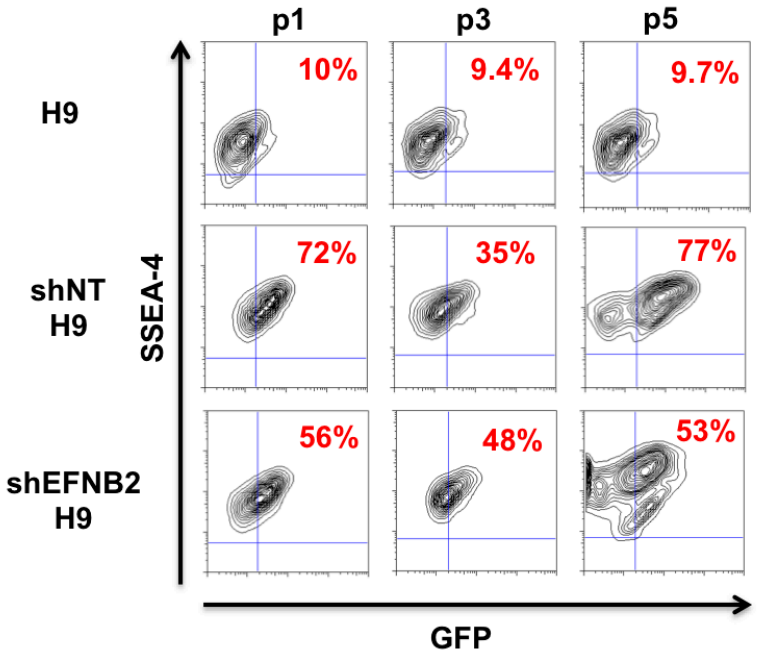

Figure 3-8. EphrinB2-knockdown hESCs self-renew *in vitro*. A self-renewal assay was performed on H9, shNT, and shEFNB2 hESC lines. 500,000 cells were seeded per well of a 6-well plate and cultured for 7 days. The cells were stained with SSEA-4 and the percentage of GFP+ stem cells determined by FACS analysis. Self-renewal was examined over 5 consecutive passages. Shown here is one representative FACS plot of each line at 3 different passages.

Figure 3-9

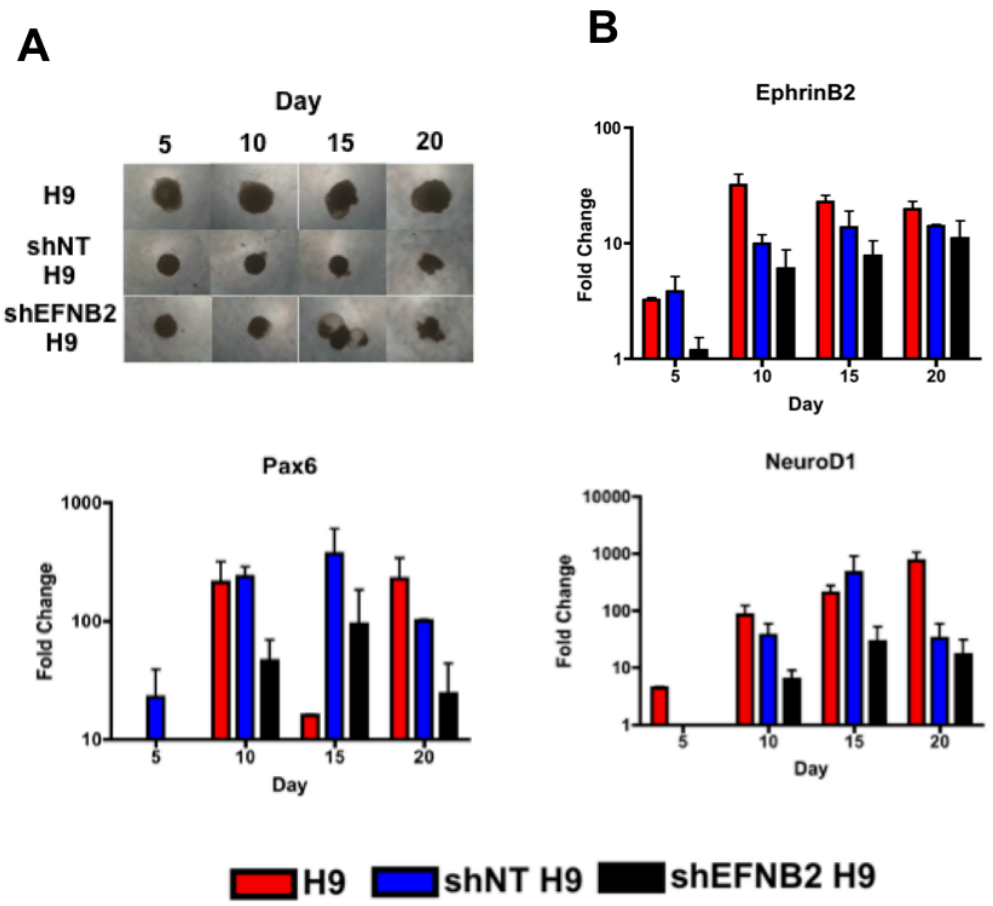

Figure 3-9. Spin EBs derived from efnB2-knockdown hESCs are impaired in neuro-ectoderm formation. (A) H9 shNT and shB2 hESCs were trypsinized and 3000 or 10000 cells were seeded in a 96-well low-attachment plate, as previously described [22,23]. 2 days after spin EB formation, the cells were switched to spontaneous differentiation medium (DMEM/F12 containing 20% KOSR). EBs were collected on days 5, 10, 15, and 20. Bright-field images for each line at the various timepoints are shown. **(B)** Real-time PCR analysis for expression of various differentiation markers was performed. Shown here are ectoderm markers (Pax6 and NeuroD). Data shown are averages ± standard deviations from three pooled EBs from three independent experiments.

Figure 3-9 (continued)

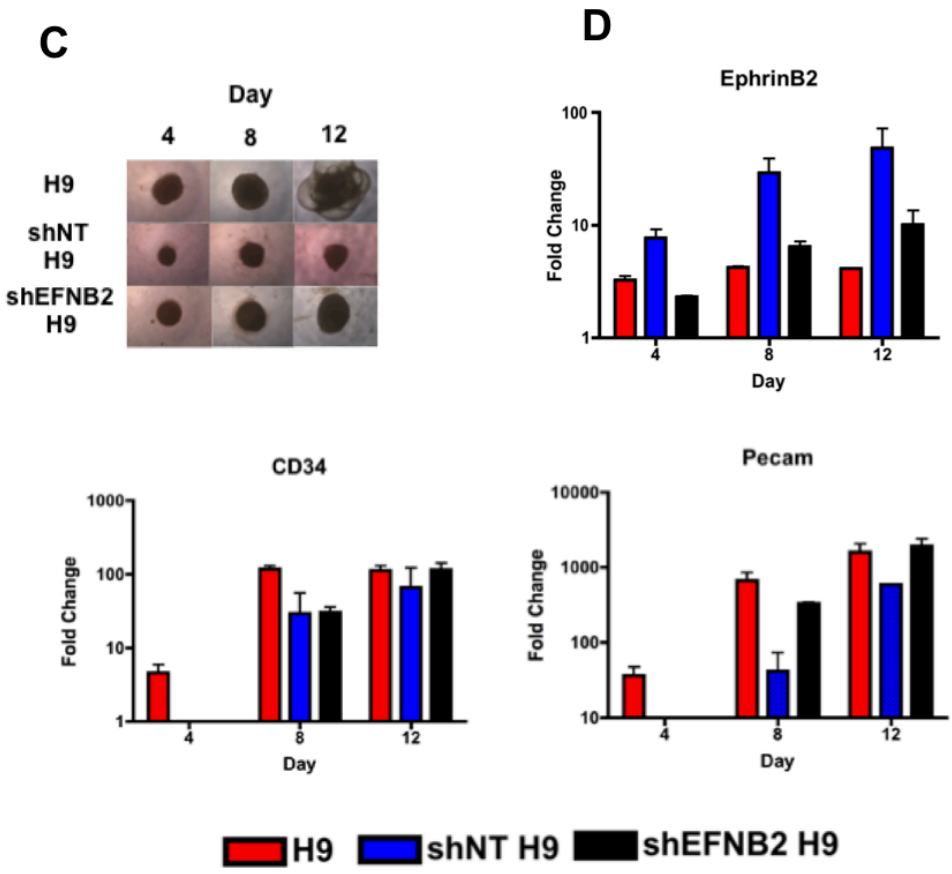

Figure 3-9 (cont.). Spin EBs derived from efnB2-knockdown hESCs are impaired in neuro-ectoderm formation. (C) 2 days after spin EB formation, the cells were switched to mesoderm differentiation medium containing 5ng/ml FGF, 10ng/ml BMP-4, and 20ng/ml VEGF. EBs were collected on days 4, 8, and 12. Brightfield images for each line at the various timpoints are shown. **(D)** Real-time PCR analysis for expression of various mesoderm markers was performed. Shown here are Pecam and CD34. Data shown are averages ± standard deviations from three pooled EBs from two independent experiments.

Figure 3-10

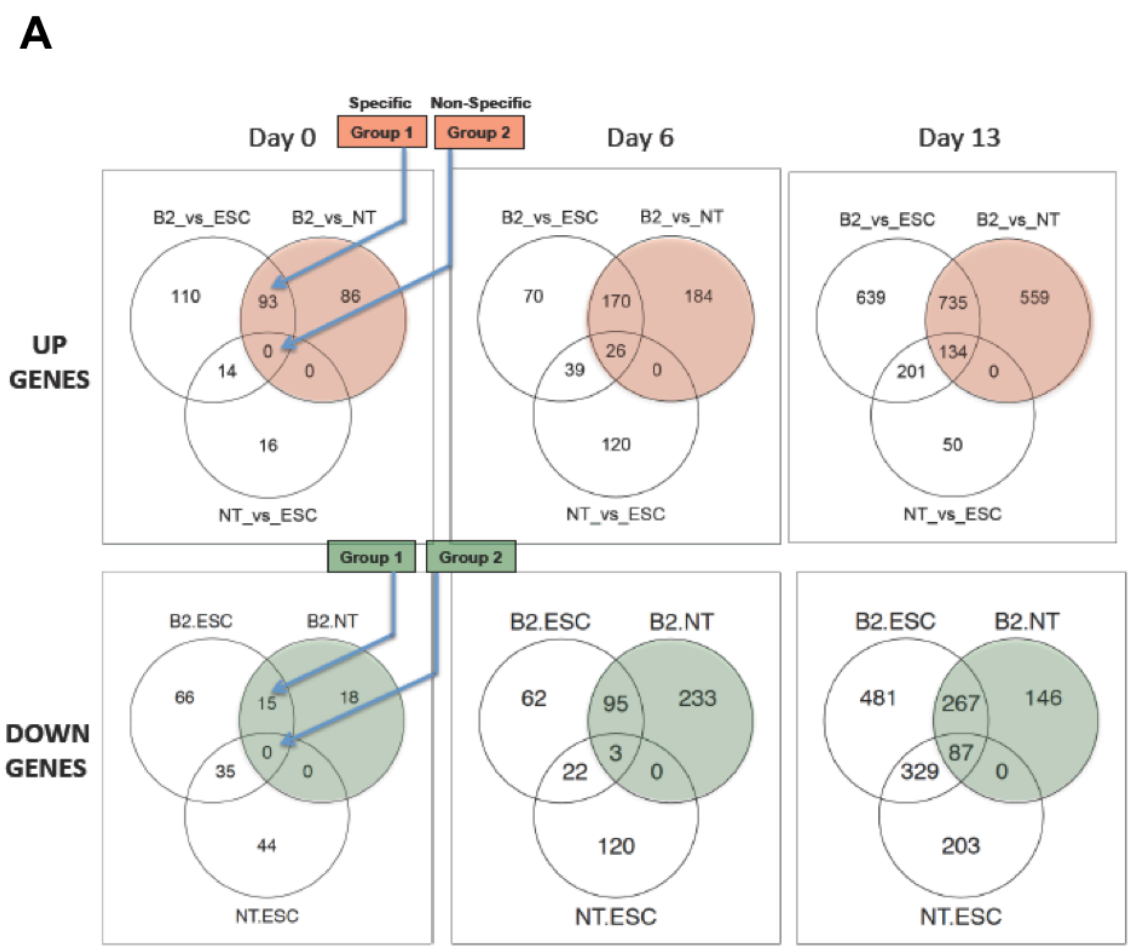

Figure 3-10. Expression analysis of upregulated and downregulated genes in ephrinB2 knockdown hESCs. **(A)** Venn diagrams detailing shared and distinct expression of upregulated (UP) and downregulated (DOWN) genes for H9, shNT, and shEFNB2 hESCs at days 0, 6, and 13. Group 1 consists of genes affected in shEFNB2 compared to H9 and shNT cells (specific), while group 2 also includes genes affected in shNT cells compared to H9 cells (non-specific).

Figure 3-10 (continued)

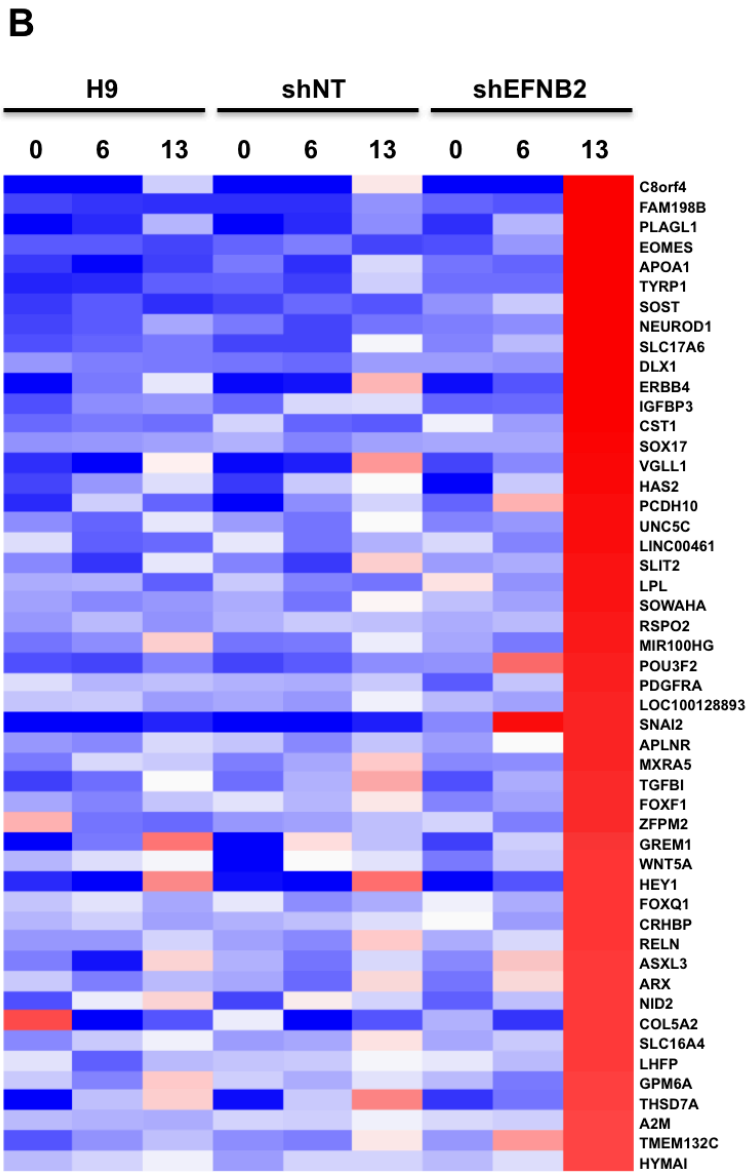

Figure 3-10 (cont.) Expression analysis of upregulated and downregulated genes in ephrinB2 knockdown hESCs. (B) A heat map depicting the top fifty upregulated genes in shEFNB2 hESCs compared to H9 and shNT cells at days 0, 6, and 13. The colors represent the log ratio of averaged replicate values divided by the mean of all samples. Red indicates positive, blue indicates negative, and white indicates zero values.

Figure 3-10 (continued)

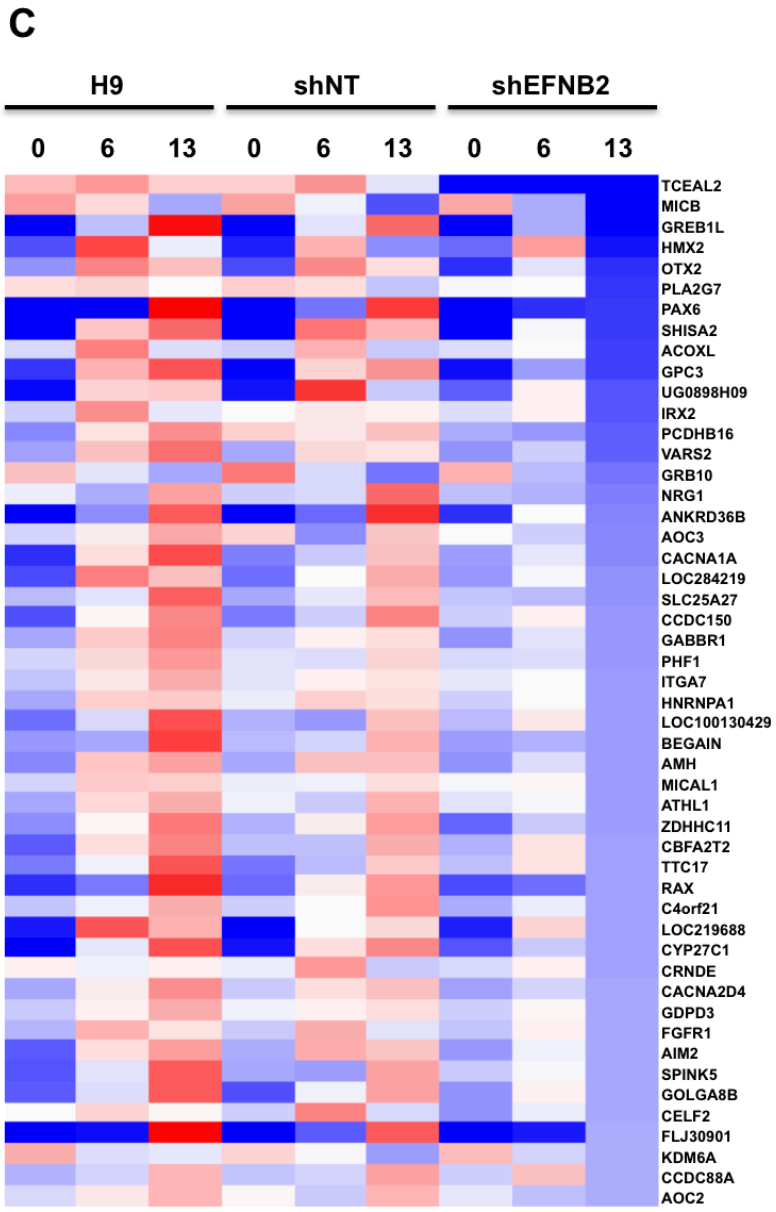

Figure 3-10 (cont.) Expression analysis of upregulated and downregulated genes in ephrinB2 knockdown hESCs. (C) A heat map depicting the top fifty downregulated genes in shEFNB2 hESCs compared to H9 and shNT cells at days 0, 6, and 13. The colors represent the log ratio of averaged replicate values divided by the mean of all samples. Red indicates positive, blue indicates negative, and white indicates zero values.

Figure 3-11

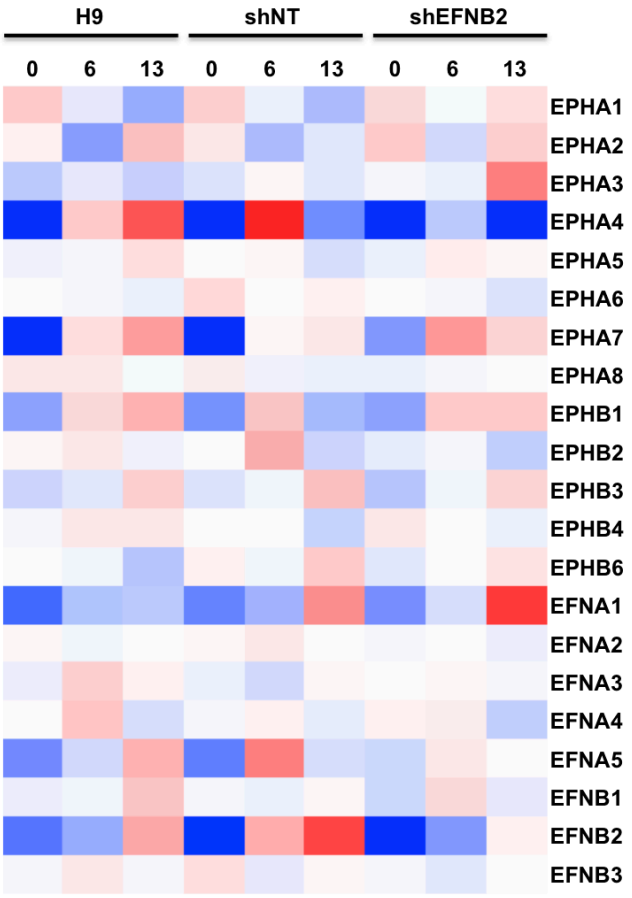

Figure 3-11. EphrinB2 knockdown alters eph-ephrin circuitry. A heat map depicting eph and ephrin gene expression in shEFNB2 hESCs compared to H9 and shNT cells at days 0, 6, and 13. The colors represent the log ratio of averaged replicate values divided by the mean of all samples. Red indicates positive, blue indicates negative, and white indicates zero values.

Figure 3-12

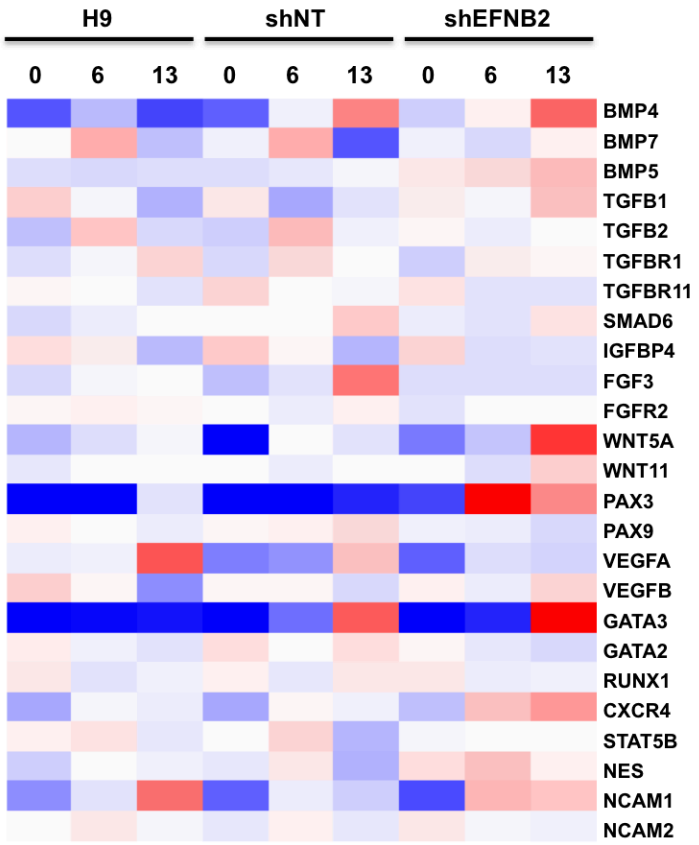

Figure 3-12. EphrinB2 knockdown alters expression of genes involved in mesoderm development. A heat map depicting mesoderm and neuroectoderm gene expression in shEFNB2 hESCs compared to H9 and shNT cells at days 0, 6, and 13. The colors represent the log ratio of average replicate values divided by the mean of all samples. Red indicates positive, blue indicates negative, and white indicates zero values.

Figure 3-13

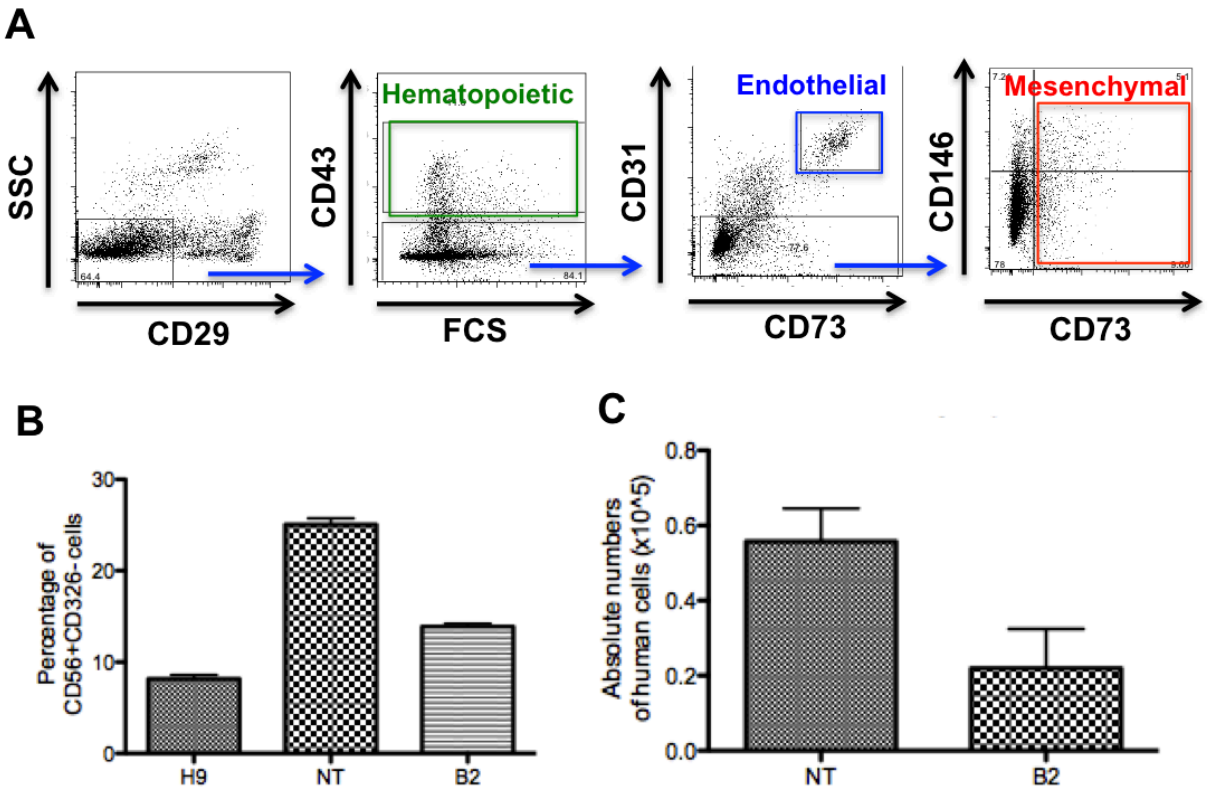

Figure 3-13. EphrinB2 knockdown enhances mesoderm-directed differentiation into mesenchymal cells. (A) Overview of the gating strategy for FACS analysis of differentiation is shown. First, human cells are gated by exclusion of CD29+ mouse OP9 stroma. Next, hematopoietic, endothelial, and mesenchymal lineages are quantified by gating of CD43+, CD31+CD73+, and CD146+CD73+CD31-CD43- populations, respectively. **(B)** Quantification of the percentages of CD56+CD326- cells at day 3.5 of differentiation. Data shown are averages of two replicates ± standard deviation from three independent experiments. **(C)** Quantification of the absolute number of human cells following the 10-day differentiation. Data shown are averages of two replicates ± standard deviation from two independent experiments.

Figure 3-13 (continued)

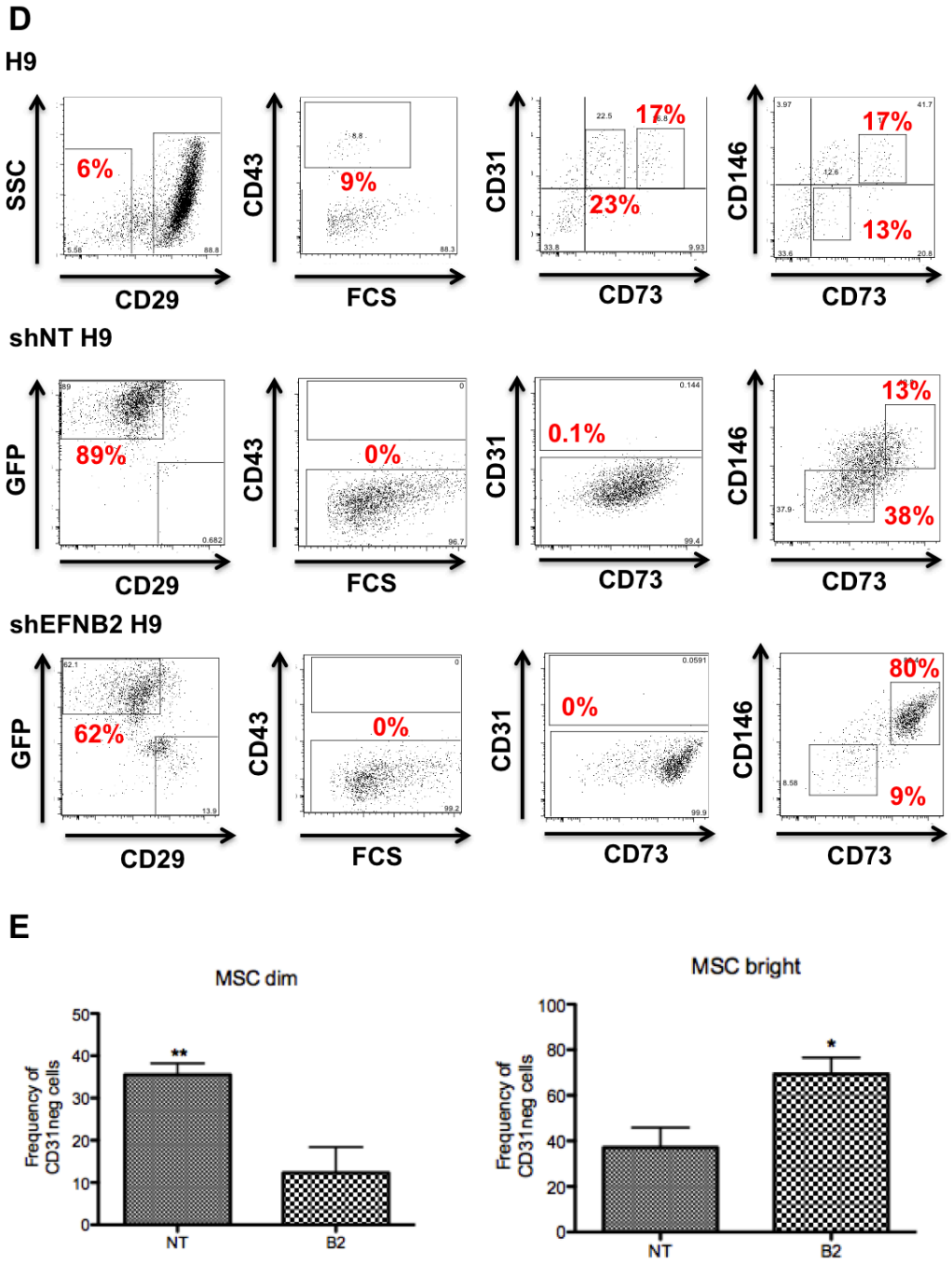

Figure 3-13 (cont.) EphrinB2 knockdown enhances mesoderm-directed differentiation into mesenchymal cells. (D) Following the 10-day differentiation, hematopoietic, endothelial, and mesenchymal lineages were quantified by gating of CD43+, CD31+CD73+, and CD146+CD73+CD31-CD43- populations, respectively, for the H9, shNT, and shEFNB2 lines. **(E)** Quantification of the 2 mesenchymal cell populations, CD73 dim and CD73 bright. Data shown are averages of two replicates ± standard deviation from two independent experiments.

Table 3-1

Gene	Forward primer	Reverse primer
EFNB2	TCCCGATTGAGCCTTACGACACTT	TTCACCTTGACACAGAGCACC
OCT4	ACATCAAAGCTCTGCAGAAAGAACT	CTGAATACCTTCCCAAATAGAACCC
PAX6	CCAGAAAGGATGCCTCATAAA	TCTGCGCGCCCCTAGTTA
NEUROD1	GCCCCAGGGTTATGAGACTA	GTGAGTCCTCCTCTGCGTTC
FOXA2	GGAGCGGTGAAGATGGAA	TACGTGTTCATGCCGTTCAT
GATA4	TCCAAACCAGAAAACGGAAGC	GCCCGTAGTGAGATGACAGG
SOX17	CAGAATCCAGACCTGCACAA	GCGGCCGGTACTTGTAGTT
BRACHYURY	TGCTTCCCTGAGACCCAGTT	GATCACTTCTTTCCTTTGCATCAAG
PECAM	TCTGAACTCCAACAACGAGAA	GCAGGGCAGGTTCATAAATAA
CD34	TGAAGCCTAGCCTGTCACCT	CGCACAGCTGGAGGTCTTAT
GAPDH	ATCAAGAAGGTGGTGAAGCAGG	TCAAAGGTGGAGGAGTGGGTGT

Table 3-1. Primer sequences for real-time PCR

Table 3-2

GO ID	Functional Group	Gene Count	Genes	p Value
GO:0001944	vasculature development	52	ATG5, CD44, HEY1, CXCR4, CTGF, FOXF1, HMOX1, HEY2, CCBE1, RHOB, SEMA3C, SOX17, LOX, CYR61, PDPN, NODAL, SLIT2, THY1, VEGFC, BGN, JUN, COL1A2, ZFPM2, COL1A1, CAV1, COL3A1, ELK3, TCF21, HOXA3, HAND1, THBS1, PLAT, B4GALT1, AIMP1, TBX3,	2.11E-10
GO:0001568	blood vessel development	49	FGF18, NRP1, HTATIP2, ENPEP, CXCL12, CTNNB1, EDNRA, APOB, ATG5, CD44, HEY1, CXCR4, CTGF, FOXF1, HMOX1, HEY2, CCBE1, RHOB, SEMA3C, SOX17, LOX, CYR61, SLIT2, THY1, VEGFC, BGN, JUN, COL1A2, ZFPM2, COL1A1, CAV1, COL3A1, ELK3, HOXA3,	2.57E-09
GO:0048514	blood vessel morphogenesis	41	FGF18, CAV1, NRP1, HTATIP2, ELK3, ENPEP, CXCL12, CTNNB1, EDNRA, APOB, HOXA3, ATG5, HEY1, HAND1, CXCR4, CTGF, HMOX1, FOXF1, HEY2, CCBE1, RHOB, SEMA3C, SOX17, THBS1, CYR61, B4GALT1, PLAT, AIMP1, EPAS1, SMAD7, TGFBR2, COL15A1, SLIT2, THY1, KDR, VEGFC, BGN, JUN, BAX, NTRK2, ZFPM2	1.39E-07
GO:0007507	heart development	39	DLC1, FGF19, SRI, NRP1, ERBB4, COL3A1, EGLN1, PAX3, TTN, ITGB1, CTNNB1, EDNRA, FOXH1, CASP3, ATG5, HAND1, GATA6, GATA4, PPP3CB, SEMA3C, BCOR, NFATC3, ACTC1, TBX3, SMAD7, NODAL, TGFBR2, FBN1, MECOM, COL5A1, SOD2, PKP2, PTCD2, HOPX, TGFBR3, ZFPM2, ADAMTS1, ID3, ADAM19	1.75E-06
GO:0048729	tissue morphogenesis	34	DLC1, BMPR2, PAX3, GREM1, TTN, CTNNB1, PFN1, TCF21, FOXQ1, WNT3, CD44, HAND1, FOXF1, BCL2, TWIST1, BCL10, ACTC1, TBX3, SMAD7, NODAL, GRSF1, EOMES, LEF1, SLIT2, VEGFC, PTCD2, CFL1, PRKAR1A, COL1A2, TGFBR3, COL1A1, CA2, TGFB1I1, BMP7	3.66E-06
GO:0030324	lung development	23	WNT5A, FGF18, CAV2, LIPA, FOXA2, EPAS1, PDPN, NODAL, TGFBR2, BMPR2, ASAH1, CTNNB1, KDR, TCF21, PPP1CA, CTGF, GATA6, FOXF1, PDGFRA, HOPX, ZFPM2, LOX, C11ORF73	6.55E-06
GO:0007389	pattern specification process	41	TSHZ1, NRP1, FOXA2, BMPR2, ZEB1, GREM1, ZIC1, CXCL12, CTNNB1, FOXH1, EDNRA, HOXC6, HOXA2, WNT3, HOXA3, CXCR4, FOXF1, LEFTY2, GATA4, RAB23, BCOR, PITX2, CYR61, TBX3, YY1, NODAL, EMX2, TGFBR2, GRSF1, DLL3, LEF1, HOXB3, DLX2, ASCL1, DLX1, AIDA, HOXB6, NEUROD1, RELN, BMP7, BMP5	5.54E-05
GO:0001525	angiogenesis	27	FGF18, NRP1, HTATIP2, ELK3, ENPEP, CXCL12, CTNNB1, EDNRA, HAND1, CTGF, CXCR4, HMOX1, CCBE1, RHOB, SOX17, THBS1, CYR61, B4GALT1, EPAS1, AIMP1, TGFBR2, COL15A1, SLIT2, THY1, KDR, VEGFC, JUN	8.10E-05
GO:0048762	mesenchymal cell differentiation	13	FGF19, EOMES, KITLG, LEF1, PAX3, CTNNB1, EDNRA, EDNRB, BCL2, CFL1, TGFBR3, SEMA3C, BMP7	4.67E-04
GO:0014031	mesenchymal cell development	13	FGF19, EOMES, KITLG, LEF1, PAX3, CTNNB1, EDNRA, EDNRB, BCL2, CFL1, TGFBR3, SEMA3C, BMP7	4.67E-04
GO:0007498	mesoderm development	16	TBX3, NODAL, EOMES, DLL3, BMPR2, LEF1, SNAI2, SLIT2, FOXH1, TCF21, WNT3, HAND1, FOXF1, EPB41L5, PRKAR1A, BMP7	5.42E-04
GO:0060485	mesenchyme development	13	FGF19, EOMES, KITLG, LEF1, PAX3, CTNNB1, EDNRA, EDNRB, BCL2, CFL1, TGFBR3, SEMA3C, BMP7	5.64E-04
GO:0048332	mesoderm morphogenesis	10	WNT3, HAND1, TBX3, NODAL, PRKAR1A, BMPR2, EOMES, LEF1, BMP7, SLIT2	0.00224
GO:0007369	gastrulation	13	FOXA2, NODAL, EOMES, BMPR2, LEF1, SLIT2, CTNNB1, WNT3, HAND1, DLD, GATA4, PRKAR1A, BMP7	0.00788

Table 3-2. GOstat functional analysis of genes that are up-regulated in shEFNB2 hESCs compared to shNT hESCs at day 13

Table 3-3

GO ID	Functional Group	Gene Count	Genes	p Value
GO:0007423	sensory organ development	25	HMX2, IRX5, FGF9, MYO7A, EDN1, PAX6, PAX2, GLI3, DFNB31, CHD7, MAF, MYO6, RAX, MAFB, SIX3, FZD3, HES1, DDR1, DLX6, DLX5, FOXG1, FOXC1,	8.27E-10
GO:0048666	neuron development	25	FGFR1, IRX5, MYO7A, PAX6, STRN, PAX2, PTEN, ALCAM, DFNB31, MACF1, UNC5A, LHX2, POU4F1, ROBO2, MYO6, OTX2, MAP1B, PTPN11, HES1, EPHA4,	1.49E-06
GO:0030182	neuron differentiation	29	FGFR1, IRX5, MYO7A, PAX6, STRN, RORA, PAX2, PTEN, GLI3, DFNB31, ALCAM, MACF1, UNC5A, PAX7, LHX2, ROBO2, POU4F1, MYO6, OTX2, MAP1B, PTPN11, HES1, SLITRK1, EPHA4, DLX5, FOXG1, EFNA5, CUX1, CACNA1A	1.51E-06
GO:0031175	neuron projection development	21	FGFR1, MYO6, MAP1B, OTX2, PAX6, STRN, PAX2, PTEN, PTPN11, ALCAM, SLITRK1, EPHA4, MACF1, UNC5A, LHX2, DLX5, FOXG1, ROBO2, POU4F1, EFNA5, CACNA1A	2.58E-06
GO:0007409	axonogenesis	16	OTX2, MAP1B, PAX6, PAX2, PTPN11, ALCAM, SLITRK1, EPHA4, MACF1, UNC5A, LHX2, DLX5, FOXG1, ROBO2, POU4F1, EFNA5	4.97E-05
GO:0007416	synaptogenesis	7	MYO6, CADM1, PCDHB6, PCDHB16, MAP1B, POU4F1, CACNA1A	8.55E-05
GO:0001654	eye development	12	MAF, RAX, IRX5, CHD7, MYO7A, SIX3, PAX6, FOXC1, PAX2, MAB21L1, MAB21L2, GLI3	2.74E-04
GO:0060429	epithelium development	16	FRAS1, PAX6, FZD3, FZD2, PAX2, SPINK5, CBFA2T2, GLI3, GPC3, DLX6, DLX5, AHNAK2, MADCAM1, POU3F1, NR2F2, HECTD1	3.02E-04
GO:0007411	axon guidance	9	ALCAM, EPHA4, UNC5A, LHX2, FOXG1, OTX2, PAX6, EFNA5, ROBO2	0.00364
GO:0050767	regulation of neurogenesis	9	HES1, FOXG1, MAP1B, PAX6, ROBO2, CDK5RAP2, ASPM, CACNA1A, RUFY3	0.04181

Table 3-3. GOstat functional analysis of genes that are down-regulated in shEFNB2 hESCs compared to shNT hESCs at day 13

References

1 Thomson, J. A. *et al.* Embryonic stem cell lines derived from human blastocysts. *Science* **282**, 1145-1147 (1998).

2 Pasquale, E. B. Eph-ephrin bidirectional signaling in physiology and disease. *Cell* **133**, 38-52, doi:10.1016/j.cell.2008.03.011 (2008).

3 Batlle, E. *et al.* Beta-catenin and TCF mediate cell positioning in the intestinal epithelium by controlling the expression of EphB/ephrinB. *Cell* **111**, 251-263 (2002).

4 Doetsch, F., Caille, I., Lim, D. A., Garcia-Verdugo, J. M. & Alvarez-Buylla, A. Subventricular zone astrocytes are neural stem cells in the adult mammalian brain. *Cell* **97**, 703-716 (1999).

5 Wang, Z. *et al.* Ephrin receptor, EphB4, regulates ES cell differentiation of primitive mammalian hemangioblasts, blood, cardiomyocytes, and blood vessels. *Blood* **103**, 100-109, doi:10.1182/blood-2003-04-1063 (2004).

6 Wang, Z. *et al.* Receptor tyrosine kinase, EphB4 (HTK), accelerates differentiation of select human hematopoietic cells. *Blood* **99**, 2740-2747 (2002).

7 Palmer, A. & Klein, R. Multiple roles of ephrins in morphogenesis, neuronal networking, and brain function. *Genes Dev* **17**, 1429-1450, doi:10.1101/gad.1093703 (2003).

8 Levroney, E. L. *et al.* Novel innate immune functions for galectin-1: galectin-1 inhibits cell fusion by Nipah virus envelope glycoproteins and augments dendritic cell secretion of proinflammatory cytokines. *J Immunol* **175**, 413-420 (2005).

9 Aguilar, H. C. *et al.* Polybasic KKR motif in the cytoplasmic tail of Nipah virus fusion protein modulates membrane fusion by inside-out signaling. *J Virol* **81**, 4520-4532, doi:10.1128/jvi.02205-06 (2007).

10 Qin, X. F., An, D. S., Chen, I. S. & Baltimore, D. Inhibiting HIV-1 infection in human T cells by lentiviral-mediated delivery of small interfering RNA against CCR5. *Proc Natl Acad Sci U S A* **100**, 183-188, doi:10.1073/pnas.232688199 (2003).

11 Shimizu, S. *et al.* A highly efficient short hairpin RNA potently down-regulates CCR5 expression in systemic lymphoid organs in the hu-BLT mouse model. *Blood* **115**, 1534-1544, doi:10.1182/blood-2009-04-215855 (2010).

12 Damoiseaux, R., Sherman, S. P., Alva, J. A., Peterson, C. & Pyle, A. D. Integrated chemical genomics reveals modifiers of survival in human embryonic stem cells. *Stem Cells* **27**, 533-542, doi:10.1634/stemcells.2008-0596 (2009).

13 Conway, A. E. *et al.* A self-renewal program controls the expansion of genetically unstable cancer stem cells in pluripotent stem cell-derived tumors. *Stem Cells* **27**, 18-28, doi:10.1634/stemcells.2008-0529 (2009).

14 Van Handel, B. *et al.* Scl represses cardiomyogenesis in prospective hemogenic endothelium and endocardium. *Cell* **150**, 590-605, doi:10.1016/j.cell.2012.06.026 (2012).

15 Smyth, G. *Statistics for Biology and Health* (eds Robert Gentleman *et al.*) 397-420 (Springer New York, 2005).

16 Smyth, G. K. Linear models and empirical bayes methods for assessing differential expression in microarray experiments. *Stat Appl Genet Mol Biol* **3**, Article3, doi:10.2202/1544-6115.1027 (2004).

17 Liu, W. M. *et al.* Analysis of high density expression microarrays with signed-rank call algorithms. *Bioinformatics* **18**, 1593-1599 (2002).

18 Ivanova, N. B. *et al.* A stem cell molecular signature. *Science* **298**, 601-604, doi:10.1126/science.1073823 (2002).

19 Negrete, O. A. *et al.* EphrinB2 is the entry receptor for Nipah virus, an emergent deadly paramyxovirus. *Nature* **436**, 401-405, doi:10.1038/nature03838 (2005).

20 Aguilar, H. C. *et al.* N-glycans on Nipah virus fusion protein protect against neutralization but reduce membrane fusion and viral entry. *J Virol* **80**, 4878-4889, doi:10.1128/jvi.80.10.4878-4889.2006 (2006).

21 Bauwens, C. L. *et al.* Control of human embryonic stem cell colony and aggregate size heterogeneity influences differentiation trajectories. *Stem Cells* **26**, 2300-2310, doi:10.1634/stemcells.2008-0183 (2008).

22 Ng, E. S., Davis, R. P., Azzola, L., Stanley, E. G. & Elefanty, A. G. Forced aggregation of defined numbers of human embryonic stem cells into embryoid bodies fosters robust, reproducible hematopoietic differentiation. *Blood* **106**, 1601-1603, doi:10.1182/blood-2005-03-0987 (2005).

23 Ng, E. S., Davis, R., Stanley, E. G. & Elefanty, A. G. A protocol describing the use of a recombinant protein-based, animal product-free medium (APEL) for human embryonic stem cell differentiation as spin embryoid bodies. *Nat Protoc* **3**, 768-776, doi:10.1038/nprot.2008.42 (2008).

24 Norrman, K. *et al.* Quantitative comparison of constitutive promoters in human ES cells. *PLoS One* **5**, e12413, doi:10.1371/journal.pone.0012413 (2010).

25 Davis, R. P. *et al.* Targeting a GFP reporter gene to the MIXL1 locus of human embryonic stem cells identifies human primitive streak-like cells and enables isolation of primitive hematopoietic precursors. *Blood* **111**, 1876-1884, doi:10.1182/blood-2007-06-093609 (2008).

26 Teo, A. K. *et al.* Pluripotency factors regulate definitive endoderm specification through eomesodermin. *Genes Dev* **25**, 238-250, doi:10.1101/gad.607311 (2011).

27 Seguin, C. A., Draper, J. S., Nagy, A. & Rossant, J. Establishment of endoderm progenitors by SOX transcription factor expression in human embryonic stem cells. *Cell Stem Cell* **3**, 182-195, doi:10.1016/j.stem.2008.06.018 (2008).

28 Yang, T. *et al.* Epidermal detachment, desmosomal dissociation, and destabilization of corneodesmosin in Spink5-/- mice. *Genes Dev* **18**, 2354-2358, doi:10.1101/gad.1232104 (2004).

29 Mathers, P. H. & Jamrich, M. Regulation of eye formation by the Rx and pax6 homeobox genes. *Cell Mol Life Sci* **57**, 186-194 (2000).

30 Ghashghaei, H. T. *et al.* The role of neuregulin-ErbB4 interactions on the proliferation and organization of cells in the subventricular zone. *Proc Natl Acad Sci U S A* **103**, 1930-1935, doi:10.1073/pnas.0510410103 (2006).

31 Chung, C. Y. *et al.* The transcription factor orthodenticle homeobox 2 influences axonal projections and vulnerability of midbrain dopaminergic neurons. *Brain* **133**, 2022-2031, doi:10.1093/brain/awq142 (2010).

32 Zhang, X. *et al.* Pax6 is a human neuroectoderm cell fate determinant. *Cell Stem Cell* **7**, 90-100, doi:10.1016/j.stem.2010.04.017 (2010).

33 Zhang, J. & Hughes, S. Role of the ephrin and Eph receptor tyrosine kinase families in angiogenesis and development of the cardiovascular system. *J Pathol* **208**, 453-461, doi:10.1002/path.1937 (2006).

34 Khodosevich, K., Watanabe, Y. & Monyer, H. EphA4 preserves postnatal and adult neural stem cells in an undifferentiated state in vivo. *J Cell Sci* **124**, 1268-1279, doi:10.1242/jcs.076059 (2011).

35 Goldman, O. *et al.* A boost of BMP4 accelerates the commitment of human embryonic stem cells to the endothelial lineage. *Stem Cells* **27**, 1750-1759, doi:10.1002/stem.100 (2009).

36 Magli, A., Schnettler, E., Rinaldi, F., Bremer, P. & Perlingeiro, R. C. Functional Dissection of Pax3 in Paraxial Mesoderm Development and Myogenesis. *Stem Cells*, doi:10.1002/stem.1254 (2012).

37 Ku, C. J., Hosoya, T., Maillard, I. & Engel, J. D. GATA-3 regulates hematopoietic stem cell maintenance and cell-cycle entry. *Blood* **119**, 2242-2251, doi:10.1182/blood-2011-07-366070 (2012).

38 Evseenko, D. *et al.* Mapping the first stages of mesoderm commitment during differentiation of human embryonic stem cells. *Proc Natl Acad Sci U S A* **107**, 13742-13747, doi:10.1073/pnas.1002077107 (2010).

39 Enver, T. *et al.* Cellular differentiation hierarchies in normal and culture-adapted human embryonic stem cells. *Hum Mol Genet* **14**, 3129-3140, doi:10.1093/hmg/ddi345 (2005).

40 Laslett, A. L. *et al.* Transcriptional analysis of early lineage commitment in human embryonic stem cells. *BMC Dev Biol* **7**, 12, doi:10.1186/1471-213x-7-12 (2007).

41 Hough, S. R., Laslett, A. L., Grimmond, S. B., Kolle, G. & Pera, M. F. A continuum of cell states spans pluripotency and lineage commitment in human embryonic stem cells. *PLoS One* **4**, e7708, doi:10.1371/journal.pone.0007708 (2009).

42 Rohani, N., Canty, L., Luu, O., Fagotto, F. & Winklbauer, R. EphrinB/EphB signaling controls embryonic germ layer separation by contact-induced cell detachment. *PLoS Biol* **9**, e1000597, doi:10.1371/journal.pbio.1000597 (2011).

43 Vallier, L. *et al.* Early cell fate decisions of human embryonic stem cells and mouse epiblast stem cells are controlled by the same signalling pathways. *PLoS One* **4**, e6082, doi:10.1371/journal.pone.0006082 (2009).

CHAPTER 4

Generation of additional tools to antagonize the ephrinB2-ephB4 signaling axis in human embryonic stem cells

Introduction

Due to their indefinite proliferation in culture and their ability to differentiate into all the cells of the body [1], human embryonic stem cells (hESCs) serve as a potent source for use in regenerative medicine as a potential therapy for organ and tissue failure. However, there are still some issues that must be addressed before hESCs can be used clinically. Differentiation of hESCs must be tightly controlled to generate the desired cell type, as well as growth factors for expansion of specific populations must be indentified. Hence, efficient methods for differentiation are essential to generate a renewable source of cells for use in regenerative medicine.

In **Chapter 3**, we found that manipulation of the ephrinB2-ephB4 signaling axis altered differentiation kinetics of hESCs *in vitro*. Specifically, lentiviral-mediated ephrinB2 knockdown resulted in an up-regulation of genes involved in mesendoderm cell fate commitment, and drastically inhibited genes involved in neuro-ectoderm formation. Since long-term expression of shRNAs may have off-target effects, here we present additional methods to antagonize the ephrinB2-ephB4 signaling axis (Fig. 4-1). Our lab discovered that the Nipah virus envelope glycoprotein (NiV-G) uses ephrinB2 as an entry receptor [2], and soluble Nipah virus envelope glycoprotein (sNiV-G) has picomolar affinity for ephrinB2 [3]. Thus, soluble NiV-G proteins can potentially act as specific monoclonal antibodies for ephrinB2 and block ephrinB2-mediated ephB4 activation. Here, we generated a H9 hESC line expressing sNiV-G. Preliminary analyses indicate that cells expressing sNiV-G are SSEA4-negative and up-regulate expression of differentiation markers, yet nevertheless demonstrate the ability to self-renew *in vitro*. Further analyses are necessary for the interpretation of these results. In addition, we added the ER retention signal, KDEL, to the C terminus of sNiV-G, which should serve as alternative of down-regulating ephrinB2 at the cell surface. Efficiency of this method will be examined in future experiments.

Materials and Methods

Plasmid construction. Construction of the soluble NiV-G (sNiV-G) plasmid was previously described [2]. To produce the lentiviral sNiV-G-p2A-eGFP vector, the sNiV-G and p2A-eGFP genes were PCR-amplified and subcloned into the *Bam*H1 and *Eco*R1 sites of the FG11F lentiviral vector [4] using an InFusion Cloning Kit (Clontech). To produce the sNiV-G-KDEL construct, the KDEL-ER retention signal was added to the C-terminus of sNiV-G using a QuikChange site-directed mutagenesis kit (Stratagene). The E533Q sNiV-G-KDEL mutant was also made using QuikChange. Construction of all plasmids was verified by digestion with restriction endonucleases (NEB) and DNA sequencing (Genewiz).

Cells and culture conditions. H9 hESCs were cultured on gelatin-coated plates on a feeder layer of mitotically-inactivated murine embryonic fibroblasts (MEFs). hESC medium is composed of DMEM/F:12 supplemented with 20% KnockOut Serum Replacement (KOSR, Invitrogen), 0.1 mM NEAA (Invitrogen), 1 mM L-Glutamine (Invitrogen), 0.1 mM 2-mercaptoethanol (Sigma-Aldrich), 1mM penicillin/streptomycin (Hyclone), and 4 ng/ml basic fibroblast growth factor (bFGF, R&D Systems – obtained via National Cancer Institute Biological Resources Branch). hESCs were passaged in small clumps every 5-7 days using 1mg/ml of collagenase type IV (Invitrogen). H9 hESCs stably expressing soluble NiV-G were generated by lentiviral-mediated transduction of the sNiV-G vector. 3 days post-transduction, SSEA4+GFP+ hESCs were FACS-sorted. 293T cells were cultured in IMDM with 10% FBS, 1% NEAA, 1% Glutamax, and antibiotics. Chinese hamster ovary (CHO) cells expressing ephrin-B2 (CHO-B2) were made as previously described [3], and maintained in DMEM-F12 medium supplemented with 10% FBS and 1 mg/ml of G418 to drive plasmid expression through neomycin resistance.

Lentivirus production. Lentivirus was produced as previously described (**Chapter 2**, manuscript in review). To determine viral titer, serial dilutions of concentrated stocks were added to 2 x 10^5 293T cells and incubated for 2 hours at 37°C. The medium was replaced with fresh medium. 72 hours post-infection, the cells were collected and analyzed by flow cytometry for eGFP expression. Titers were expressed as infectious units per ml (IU/ml).

***In vitro* infection of cells.** For viral transductions, hESCs were transferred to feeder-free conditions. hESCs were dissociated to single cells using 0.05% trypsin (Invitrogen) for counting and then plated on Matrigel- (BD Biosciences) coated plates in hESC medium that was conditioned overnight on MEFs and supplemented with 10 μM HA-1077 (ROCK inhibitor, Sigma-Aldrich) to promote hESC survival [5]. Increasing amounts of virus (based on MOI) and 4ng/ml of polybrene (Sigma) were added to the cells, and centrifuged at 2,000 rpm at 37°C for 2 hours. Following an overnight incubation with virus, the infection medium was removed and replaced with fresh medium. 72 hours post-infection, the cells were harvested, stained with SSEA-4 PE (BD Biosciences), and analyzed by flow cytometry for eGFP expression.

Immunoprecipitation and western blot analysis. sNiV-G was harvested from cell supernatants using an Anti-HA Immunoprecipitation Kit (Sigma). Briefly, 500μl of cell supernatant was incubated on columns containing anti-HA agarose at 4°C overnight. Following the incubation, the columns were washed 5 times with 1X IP buffer. The samples were boiled in 6X sodium dodecyl sulfate (SDS) loading buffer containing 2-mercaptoethanol for 10 minutes, subjected to electrophoresis through a 10% SDS polyacrylamide gel, and transferred onto a PVDF (Millipore) membrane. A mouse anti-HA-tag (Covance) monoclonal antibody was used to detect sNiV-G. A goat anti-mouse IRDye 800CW (LI-COR Biosciences) was used as a secondary antibody. Signals were detected using the Odyssey infrared imaging system (LI-COR Biosciences).

Self-renewal assay. hESCs were rinsed with phosphate-buffered saline solution (PBS), dissociated to single cells using 0.05% trypsin, and passed through a 40 μm cell strainer. MEFs were depleted with feeder removal microbeads (Miltenyi) prior to cell counting. 5 x 10^5 cells were seeded per well of a 6-well plate and cultured for 1 week. This experiment was repeated for five passages. At each passage, the cells were stained with SSEA4-PE (BD Biosciences) and TRA-1-81 antibodies, and FACS analysis was performed to determine the percentage of hESCs.

Real-time PCR analysis. RNA was extracted using a RNeasy kit (Qiagen). cDNA was prepared using a QuantiTect Reverse Transcription kit (Qiagen). Real-time PCR was performed using iQ SYBR Green supermix (Bio-rad) and an iQ iCycler (Bio-rad). Primer sequences are listed in Table 1 (**Chapter 3**).

Cell surface binding assay. CHO-B2 cells were transfected with wild-type or mutant sNiV-G-KDEL constructs using Lipofectamine 2000 (Invitrogen) according to the manufacturer's instructions. 48h post-transfection, the cells were incubated with NiV-G-Fc [6] or ephB4-Fc (R&D Systems) for 1h on ice. Next, the cells were washed with buffer (1% FBS in PBS) and incubated with a mouse monoclonal anti-HA antibody (Covance) for 30 min on ice. Again, the cells were washed and then incubated with an anti-mouse IgG PE antibody (Invitrogen) for 30 min on ice. Data was examined using FACS analysis.

Results

hESCs stably expressing soluble NiV-G are SSEA-4-negative and do not self-renew *in vitro*. Compared to ephB4, NiV-G has a ten-fold higher affinity for ephrinB2 [6]. Here, we generated a H9 hESC line expressing soluble NiV-G (sNiV-G), which is secreted and can thereby potentially antagonize ephrinB2/ephB4 interactions in trans. We designed a lentiviral sNiV-G-P2A-eGFP construct by cloning the sNiV-G gene into a FG11F- based lentiviral vector in which the ubiquitin C promoter drives expression of sNiV-G and eGFP by a P2A self-cleaving peptide sequence (Fig. 4-2A). We transduced H9 hESCs with VSV-G envelope pseudotyped lentiviruses delivering this construct. Next, we FACS-sorted the SSEA-4+GFP+ hESCs and expanded them. Since our sNiV-G protein has a HA tag, we performed an immunoprecipitation of sNiV-G in the culture supernatant to confirm that our cells were indeed producing and secreting the ~80kDa protein (Fig. 4-2B). After staining the cells with SSEA-4, we were surprised to see that even after FACS-sorting and subsequent expansion in culture, only 31% of the cells were GFP+ (Fig. 4-3A). More importantly, the GFP+ cells were SSEA-4-. Further passaging of these cells resulted in a decrease in the GFP+ population and in an increase in both the SSEA4+GFP- and SSEA4-GFP- populations. To try to get a more homogenous population of GFP+ cells, we re-sorted the GFP+ cells. Although we did get a larger population, the GFP+ cells were still SSEA-4- (Fig. 4-3B). To examine the self-renewal capacity of the original and re-sorted sNiV-G H9 lines, 500,000 cells were seeded per well and the percentage of SSEA4+GFP+ cells determined after 7 days in culture. This was repeated for five consecutive passages. For the original sNiV-G line, 21% of the cells were SSEA-4+GFP- while 63% were SSEA-4-GFP+ at passage 1 (Fig. 4-4). By passage 3, the SSEA-4+GFP- population had disappeared, while the SSEA-4-GFP+ population increased to 91%. The re-sorted sNiV-G H9 line did not have any SSEA-4+ populations at any of the passages, but had a SSEA-4-GFP+ population persist throughout. Our results indicate that the cells expressing sNiV-G (SSEA4-

GFP+) have a selective advantage in self-renewal capacity over the cells that are not expressing it (SSEA4+GFP-).

Since the cells stably expressing sNiV-G did not express the pluripotency SSEA-4 marker, we expected them to express differentiation markers and confirmed that using real-time PCR analysis (Fig. 4-5). The re-sorted sNiV-G H9 line expressed less Oct4 and ephrinB2 compared to the original sNiV-G line. Moreover, the re-sorted line demonstrated an upregulation in Pax6, GFAP, and Gata4 markers compared to the original line. Taken together, expression of sNiV-G in hESCs generated a more differentiated population of cells that was still nevertheless able to self-renew over extended passaging in culture.

Expression of an ER-retained version of soluble NiV-G results in downregulation of ephrinB2 at the cell surface. To avoid long-term expression of shRNAs in hESCs, we sought to develop an alternative method of downregulating ephrinB2 at the cell surface. We added the ER retention signal, KDEL, to the C terminus of sNiV-G, which should essentially bind to ephrinB2 during migration through the secretory pathway and lead to accumulation in the ER. To test this construct, we transfected CHO cells over-expressing ephrinB2 with either wild-type sNiV-G-KDEL or E533Q sNiV-G-KDEL. The E533Q mutation abrogates binding to ephrinB2 and ephrinB3 [6]. 48h post-transfection, we stained the cells with NiV-G-Fc and ephB4-Fc to quantify the amount of ephrinB2 at the cell surface (Fig. 4-6). Indeed, the cells transfected with the wild-type construct demonstrated markedly reduced NiV-G-Fc and ephB4-Fc binding. Importantly, the negative control E533Q sNiV-G-KDEL construct did not downregulate ephrinB2, underscoring the specificity of our construct. Thus, the sNiVG-KDEL construct can be used an alternative method to effectively downregulate ephrinB2 expression in hESCs and potentially avoid off-target effects of shRNAs.

Discussion

EphrinB-ephB ligand-receptor interactions are promiscuous, and the lack of highly specific tools has hampered our ability to characterize the role of ephrinB2 in stem cell fate. Here, we exploited the picomolar affinity of NiV-G for ephrinB2 as a method of blocking ephrinB2-mediated ephB4 activation. We designed a FG11F- based lentiviral vector in which the ubiquitin C promoter drives expression of sNiV-G and eGFP by a P2A self-cleaving peptide sequence, which allowed us to track cells expressing sNiV-G. Sorting of the GFP+ cells and subsequent expansion in culture revealed that only 31% of the cells were GFP+ (Fig. 4-3A). Interestingly, the GFP+ cells did not express SSEA-4, and the GFP- cells were SSEA4-. Over the next passages, the GFP+ population decreased and the SSEA4-+GFP- and SSEA4-GFP- populations increased. This suggested that either the cells expressing sNiV-G had poor survival, or the GFP gene was being silenced. To address this, we re-sorted the GFP+ cells to generate a more homogenous population. Indeed, 70% of the cells were now GFP+ (Fig. 4-3B). Surprisingly, this re-sorted GFP+ population did not decrease over several passages as the original population, ruling out the possibility that the GFP marker was being silenced. To determine whether the GFP+ cells had poor survival, we performed a self-renewal assay on the original and re-sorted GFP+ populations (Fig. 4-4). For both lines, the GFP+ populations self-renewed at each passage, also ruling out the possibility that the cells expressing sNiV-G had poor survival. On the other hand, the GFP+ cells appear to have an enhanced self-renewal capacity compared to the standard hESCs in the culture. Further characterization of the cells indicated that the re-sorted GFP+ line up-regulated expression of various differentiation markers (Fig. 4-5). The original GFP+ line did not up-regulate differentiation markers to the same degree, consistent with the FACs profiles showing that the line still contained a population of SSEA+ cells. Also, the original GFP+ line up-regulated ephrinB2 expression by almost ten-fold compared to the re-sorted line. One possible explanation might be that the remaining hESCs in

the culture are up-regulating ephrinB2 as a response to the sNiV-G bound to the ephrinB2 on their cell surfaces.

Based on the current data, over-expression of sNiV-G in hESCs results in a non-stem-cell-like population of cells that nevertheless maintains the ability to self-renew and proliferate in culture. To further characterize these cells, more assays to evaluate the pluripotency potential must be performed, including an *in vitro* differentiation assay and an *in vivo* teratoma assay. In addition, a proper negative control must be added to aid in interpretation of results. We are currently introducing mutations in the sNiV-G gene to completely abrogate binding to ephrinB2. This "ephrinB2-dead" mutant will help us determine whether the observed phenotypes are due to binding of sNiV-G to ephrinB2. Furthermore, it will be interesting to see how the phenotype of hESCs expressing sNiV-G compares to hESCs expressing an shRNA against ephrinB2 (**Chapter 3)**.

Figure 4-1

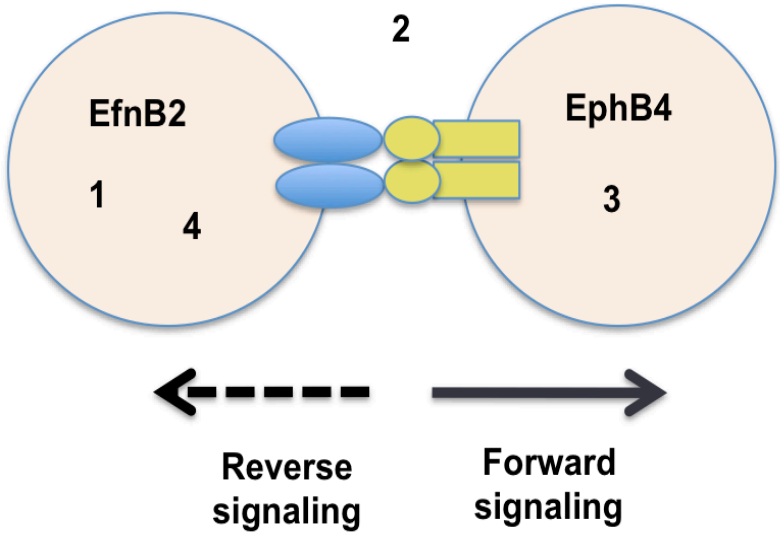

1) shRNA	EfnB2 knockdown
2) Soluble NiV-G	Block EphB4 activation
3) Full-length NiV-G	Block EphB4 activation
4) Soluble NiV-G-KDEL	EfnB2 downregulation

Figure 4-1. Additional methods for interrogating the ephrinB2-ephB4 axis. A schematic of how ephrinB2-ephB4 interactions result in bi-directional signaling termed "reverse" and "forward" signaling as indicated. We propose 3 other methods of interrogating the ephrinB2/ephB4 axis based on unique reagents we have generated. Soluble NiV-G can be used to antagonize ephrinB2/ephB4 interactions *in trans* (method 2), while full-length NiV-G can be used to block ephB4 activation *in cis* (method 3). Finally, in order to avoid long-term high-level expression of shRNAs, we designed an ER-retained version of sNiV-G by appending a KDEL-ER retention signal to the C-terminus of sNiV-G, which should result in ephrinB2 downregulation (method 4).

Figure 4-2

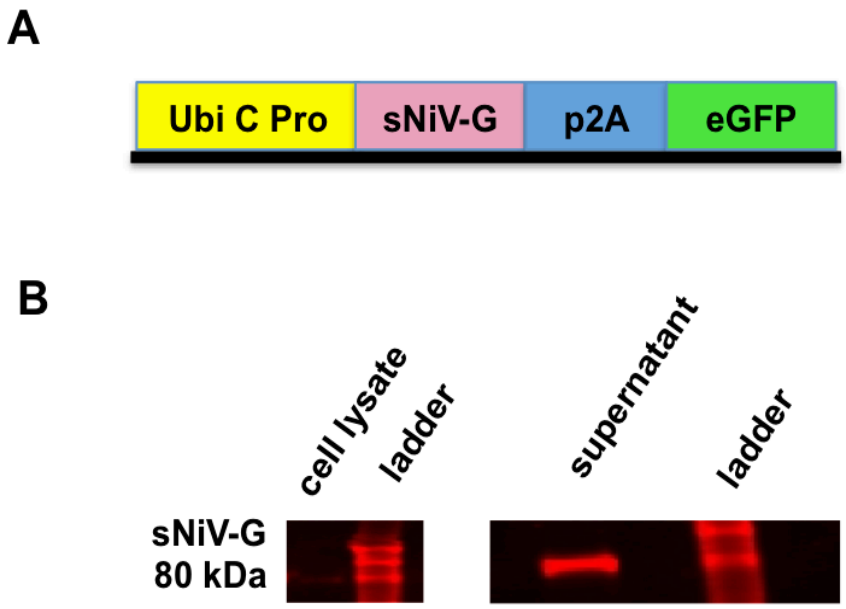

Figure 4-2. Generation of stable H9 hESCs expressing soluble NiV-G. (A) Schematic of the soluble-NiV-G-P2A-eGFP lentiviral construct. The ubiquitin C promoter drives expression of sNiV-G and eGFP by a P2A self-cleaving peptide sequence. (**B)** H9 hESCs were transduced with lentivirus delivering the construct shown in part (A) and SSEA4+GFP+ cells were FACS-sorted 3 days post-infection. To confirm that the cells were secreting soluble NiV-G, an immunoprecipitation with anti-HA beads was performed on the culture supernatant since the protein has an HA tag. The cell lysate and IPs were blotted with an anti-HA antibody.

Figure 4-3

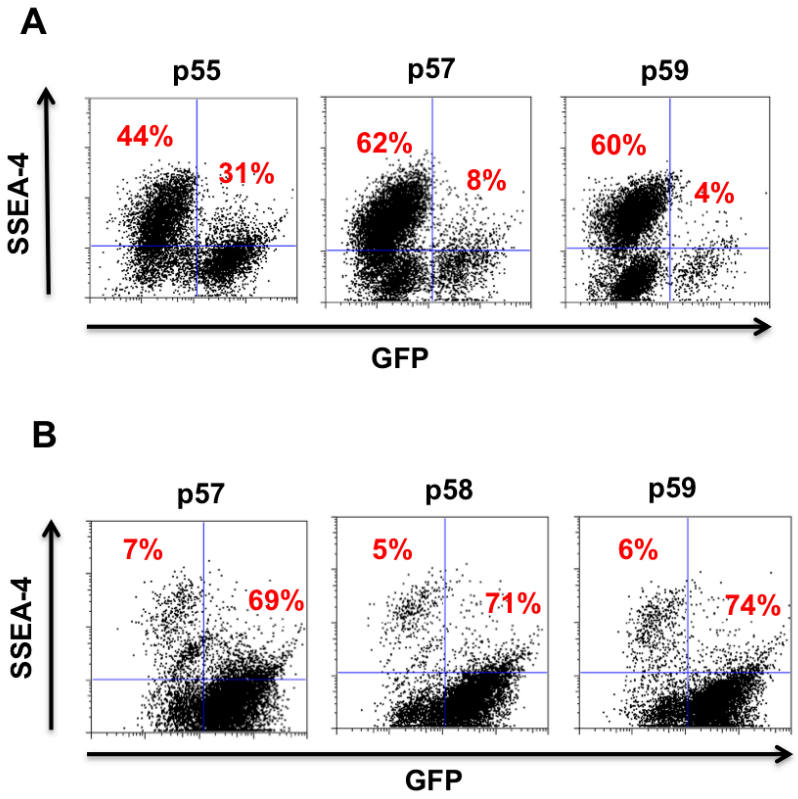

Figure 4-3. H9 hESCs stably expressing soluble NiV-G are SSEA-4-negative. (A) SSEA-4 and GFP expression of the stable sNiV-G H9 line was examined across several passages using FACS analysis. **(B)** From the original sNiV-G H9 population, GFP+ cells were again FACS-sorted to generate a more homogenous population of GFP+ cells. SSEA-4 and GFP expression of these "re-sorted" sNiV-G H9s was examined across several passages as in part **(A).**

Figure 4-4

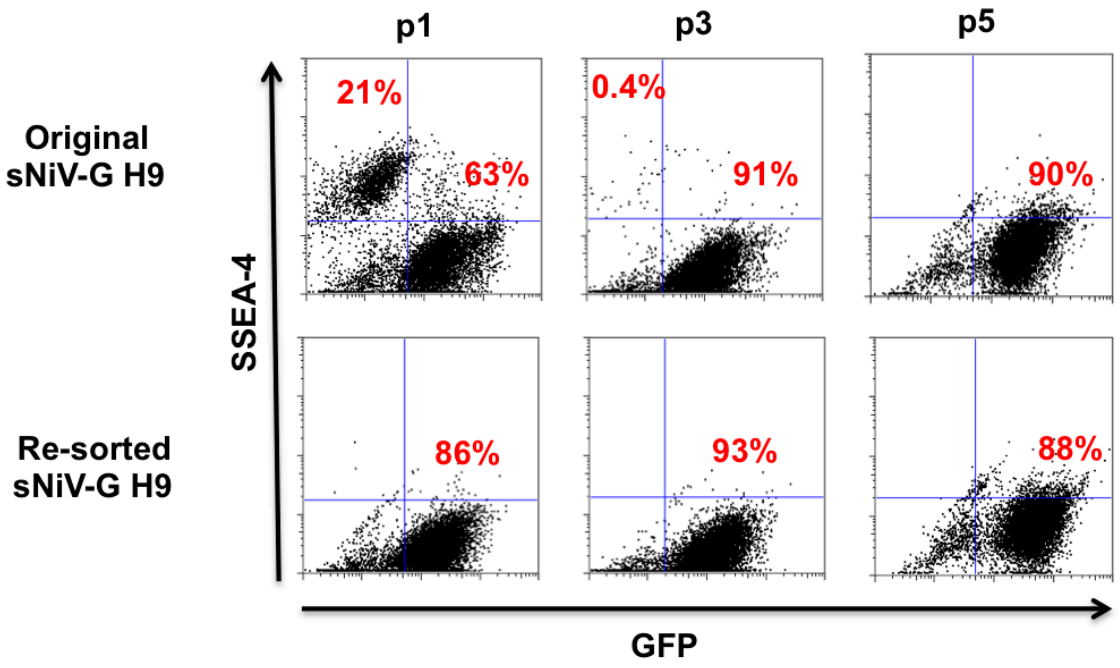

Figure 4-4. H9 hESCs stably expressing soluble NiV-G self-renew. To evaluate self-renewal of the original and re-sorted sNiV-G H9 hESC lines, 500,000 cells were seeded per well of a 6-well plate and cultured for 7 days. The cells were stained with SSEA-4 and the percentage of GFP+ stem cells determined by FACS analysis. Self-renewal was examined over 5 consecutive passages. Shown here are representative FACS plots from 3 different passages.

Figure 4-5

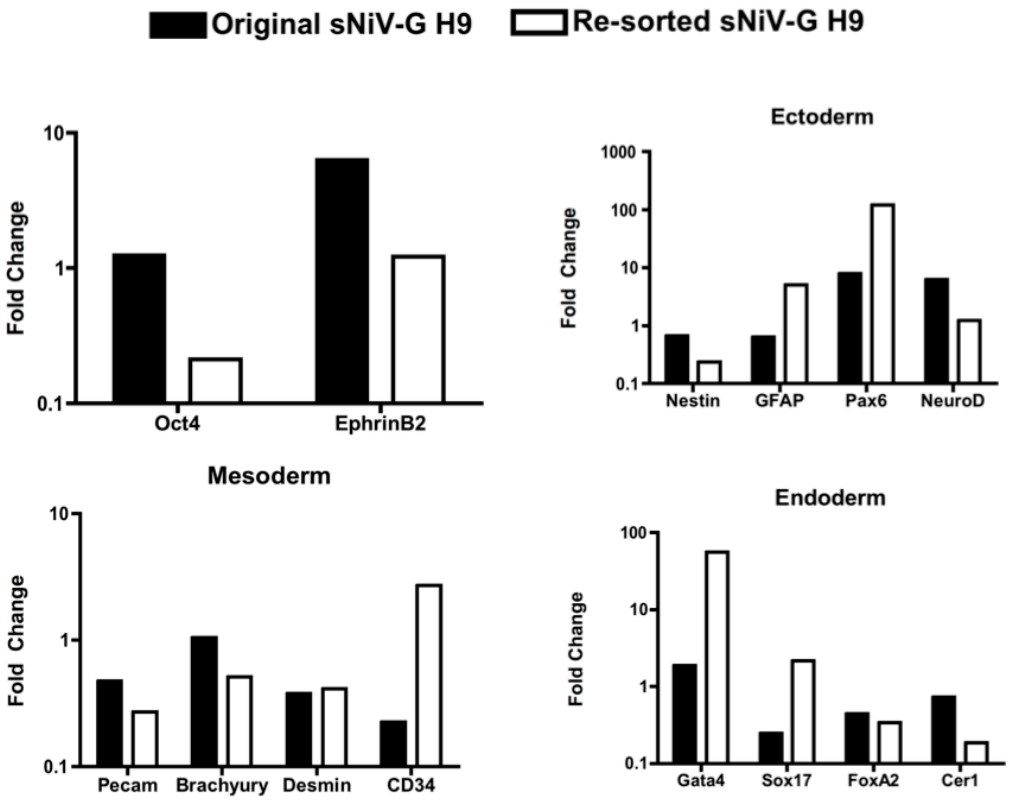

Figure 4-5. H9 hESCs stably expressing soluble NiV-G express various differentiation markers. Expression of pluripotency (Oct4) and various differentiation markers for the original and re-sorted sNiV-G H9s was examined using real-time PCR analysis.

Figure 4-6

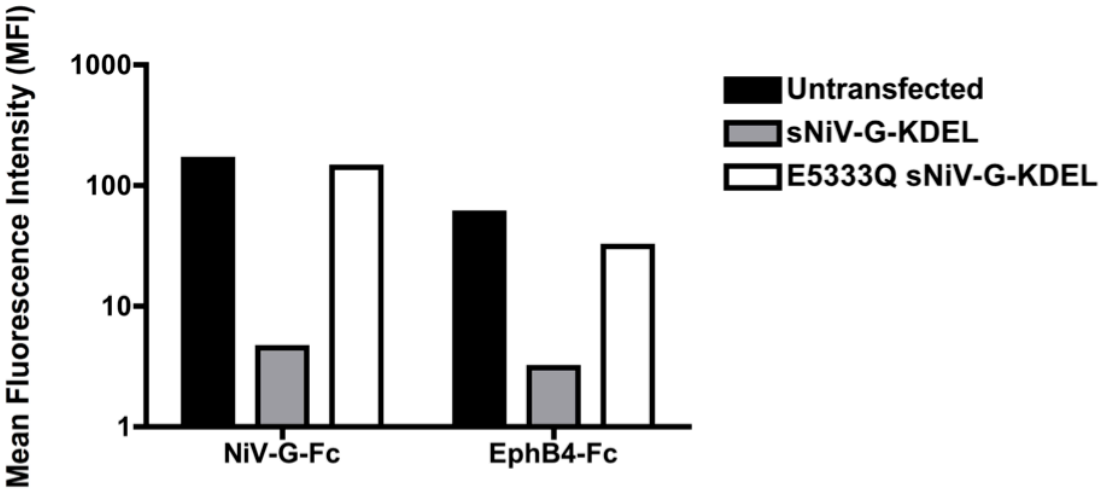

Figure 4-6. Expression of sNiV-G-KDEL results in downregulation of ephrinB2 as the cell surface. CHO cells over-expressing ephrinB2 were transfected with wild-type or mutant sNiV-G-KDEL constructs, and ephrinB2 downregulation was measured by NiV-G-Fc and ephB4-Fc binding 48h post-transfection. The E533Q mutation abrogates binding to ephrinB2 and ephrinB3. Data is presented as raw MFI values.

References

1 Thomson, J. A. *et al.* Embryonic stem cell lines derived from human blastocysts. *Science* **282**, 1145-1147 (1998).

2 Negrete, O. A. *et al.* EphrinB2 is the entry receptor for Nipah virus, an emergent deadly paramyxovirus. *Nature* **436**, 401-405, doi:10.1038/nature03838 (2005).

3 Negrete, O. A. *et al.* Two key residues in ephrinB3 are critical for its use as an alternative receptor for Nipah virus. *PLoS Pathog* **2**, e7, doi:10.1371/journal.ppat.0020007 (2006).

4 Qin, X. F., An, D. S., Chen, I. S. & Baltimore, D. Inhibiting HIV-1 infection in human T cells by lentiviral-mediated delivery of small interfering RNA against CCR5. *Proc Natl Acad Sci U S A* **100**, 183-188, doi:10.1073/pnas.232688199 (2003).

5 Damoiseaux, R., Sherman, S. P., Alva, J. A., Peterson, C. & Pyle, A. D. Integrated chemical genomics reveals modifiers of survival in human embryonic stem cells. *Stem Cells* **27**, 533-542, doi:10.1634/stemcells.2008-0596 (2009).

6 Negrete, O. A., Chu, D., Aguilar, H. C. & Lee, B. Single amino acid changes in the Nipah and Hendra virus attachment glycoproteins distinguish ephrinB2 from ephrinB3 usage. *J Virol* **81**, 10804-10814, doi:10.1128/jvi.00999-07 (2007).

CHAPTER 5

Conclusions

The greatest potential of human embryonic stem cells (hESCs) is to generate a renewable source of cells to replace damaged tissues and organs in patients suffering from various degenerative diseases. Before advancing from the laboratory setting to the clinic, appropriate culture conditions and efficient differentiation methods must be developed to generate homogenous populations of cells. However, the signaling pathways involved in lineage restriction during differentiation of hESCs are still under investigation. In addition, hESCs are more heterogeneous than previously thought, and also have substantially different propensities to differentiate into different lineages [1,2]. This dissertation identified ephrinB2 as another marker of hESCs that is heterogeneously expressed. Furthermore, we demonstrated that manipulation of ephrinB2 signaling during differentiation altered the specification of hESCs to distinct cell types.

EphrinB2 expression is heterogeneous in hESC cultures

Despite widespread expression of key markers of the pluripotent state, previous studies have shown that hESCs consist of a heterogeneous population of functionally distinct cell types [3,4]. Within hESC cultures, various subsets of cells were identified based on their distinct pattern of cell-surface markers and gene expression [5]. Some subpopulations of cells also had distinct differentiation potential *in vitro* and *in vivo*, confirming the existence of cells with pre-determined tissue fates [6]. Taken together, these studies suggested that hESCs expand as a heterogeneous mix of "lineage-primed" cells. Identification of distinct hESC subpopulations with distinct differentiation potentials may contribute to generation of specific cell types for cell-based therapy.

In **Chapters 2** and **3**, we identified ephrinB2 as another cell-surface marker of hESCs and established that it is heterogeneously expressed in cultures. EphrinB2 was previously shown to be a marker of mouse ESCs [7], and its receptor, ephB4, was found to play a role in regulating mesoderm induction during differentiation [8]. Thus, we hypothesized that ephrinB2

must also play a role in hESC fate. However, the promiscuity of ephrin-eph interactions has made it difficult to study this signaling axis. We circumvented this issue by using a unique method of "tagging" ephrinB2+ cells. In **Chapter 2**, we reported that we could efficiently pseudotype a lentiviral vector with the Nipah virus (NiV) envelope glycoproteins. These NiV pseudotyped particles (NiVpp) efficiently targeted ephrinB2+ cells. Further, NiVpp transduced human embryonic, hematopoietic, and neural stem cell populations in an ephrinB2-dependent manner. This was the first functional confirmation that ephrinB2 is expressed on these three populations and that it may be a molecular marker of "stemness." Thus, we established that NiV transduction could be used as a specific method to "tag" ephrinB2+ hESCs.

Examination of NiV-transduced GFP+ cells revealed that ephrinB2 expression is heterogeneous in hESC cultures (**Chapter 3**). Even after FACS-sorting and subsequent expansion in culture, the putative "ephrinB2-expressing" fraction re-established a heterogeneous culture of ephrinB2-expressing and non-expressing cells. The next question was are ephrinB2+ cells poised for self-renewal or differentiation? We performed a self-renewal assay, *in vitro* differentiation assay, and *in vivo* teratomas assay on the NiV-transduced GFP+ cells, but as stated above, the population contains both ephrinB2-expressing and non-expressing cells when cultured. Thus, experiments must be performed immediately after sorting to examine only ephrinB2-expressing cells. For example, gene expression analysis of NiV-transduced cells immediately after sorting would help determine whether ephrinB2+ hESCs express primarily pluripotency genes, lineage-specific genes, or both. If lineage-specific genes are up-regulated, then ephrinB2 heterogeneity could be potentially manipulated to skew hESC differentiation towards a specific cell lineage. Understanding the basis for ephrinB2 heterogeneity seen in hESCs might lead to more robust culture conditions that give rise to more homogenous population of cells suitable for regenerative medicine.

EphrinB2-ephB4 interactions regulate differentiation kinetics of hESCs

Differentiation of hESCs into specific cell lineages is necessary to generate a renewable source of cells for use in regenerative medicine. Nevertheless, the development of methods to control differentiation to favor the generation of one cell type over another is challenging. One efficient strategy to control differentiation is to recapitulate the steps through which cells commit to a specific fate during normal development [9]. Studies that applied knowledge of developmental biology to hESC differentiation identified growth factors and small molecules that can be used to direct the cells along a specific differentiation path [10]. Even with the addition of exogenous growth factors and small molecules, the end product is usually a heterogeneous population of cells that contains only a low percentage of the desired cell type [11]. Understanding the signaling pathways that underlie hESC differentiation is critical if we are to achieve the full potential of this therapeutically useful cell type.

In **Chapter 3**, we generated hESC lines expressing an shRNA against ephrinB2 to directly examine the role of ephrinB2 signaling during differentiation. Embryoid bodies (EBs) derived from ephrinB2-knockdown cells demonstrated a down-regulation of neuro-ectoderm genes under spontaneous differentiation conditions, and an up-regulation of mesoderm markers under mesoderm-directed differentiation conditions. Further microarray analysis of ephrinB2-knockdown EBs confirmed a severe deficiency in expression of neuro-ectoderm markers as well as genes involved in the development of the eye, hair, and skin. On the other hand, genes involved in mesoderm induction and endoderm specification were significantly up-regulated. A previous study with EBs derived from *ephB4*$^{-/-}$ mESCs indicated a down-regulation of mesoderm genes and an up-regulation of neuro-ectoderm genes [8]. Taken together, manipulation of the ephrinB2-ephB4 signaling axis can bias differentiation toward specific derivatives from each germ layer. Understanding the relative contribution of each signaling pathway may result in more optimal conditions for directing the differentiation of specific cell types.

Ephrin-eph circuitry in ESC fate and differentiation

A previous study found that *ephB4*$^{-/-}$ mESCs were associated with a severe deficiency in mesoderm induction genes and an overexpression of neuro-ectoderm genes [8]. Our studies showed that ephrinB2-knockdown hESCs demonstrate the exact opposite phenotype-overexpression of genes involved in formation of mesendoderm progenitors and a severe deficiency in genes specifying neuro-ectoderm formation. Taken together, these studies suggest that ephrinB2 reverse signaling and ephB4 forward signaling most likely play *distinct* roles in germ layer commitment and differentiation. Interestingly, the absence of ephB4 did not affect ephrinB2 expression [8], and ephrinB2 knockdown did not affect ephB4 expression. EphB4 is thought to be the relevant endogenous receptor for ephrinB2, but in this case interactions with other ephB receptors must account for the observed phenotype.

Although ephB4 expression was unaffected, ephrinB2 knockdown resulted in a down-regulation of ephA4. EphA4 is the only receptor that can bind both ephrin-A and ephrin B ligands [12-15], and is highly expressed in the nervous system. The repulsive effects of ephA4 expression guide the growth of developing axons towards their synaptic targets [16,17], and also regulate synaptic morphology and plasticity [18]. In addition, other evidence suggests that ephA4 maintains neural stem cells in an undifferentiated state [19]. Our findings indicate that ephrinB2-ephA4 interactions might also regulate ectoderm germ layer differentiation.

EphrinB2 knockdown also resulted in a significant up-regulation of ephrinA1. In addition to playing an important role in normal cellular processes, ephrinA1 has been intensely studied for its role in human malignancy. EphrinA1 is up-regulated in blood vessels of tumors [20], and it is thought that interactions with its receptor, ephA2, could be critical for vascular sprouting and penetration of vessels into both normal and tumor tissues. Thus, perturbation of ephrinA1-ephA2 interactions could be used in the development of novel anti-cancer therapies to suppress tumor neovascularization. Overall, our study implicates that manipulation of ephrinB2 signaling modulates other eph-ephrin circuitry.

Soluble NiV-G can potentially antagonize ephrinB2-ephB4 signaling

Lastly, in **Chapter 4,** we present unique tools that can be used to potentially antagonize ephrinB2-ephB4 signaling in hESCs. Our group previously demonstrated that the NiV attachment glycoprotein (NiV-G) has picomolar affinity for ephrinB2, which is greater than the affinity of ephB4 [21]. Thus, soluble NiV-G can be essentially used as a monoclonal antibody to block ephrinB2-ephB4 interactions. We generated hESC lines stably expressing soluble NiV-G, but they have not been fully characterized. Preliminary findings suggest that hESCs expressing soluble NiV-G down-regulate expression of pluripotency markers and up-regulate expression of differentiation markers, but further experiments must be performed to confirm this. If soluble NiV-G does indeed increase the propensity of hESCs to differentiate, then this raises the exciting possibility that a reagent made from the most lethal paramyxovirus known can be turned towards the benefit of humankind.

Summary

In sum, this dissertation characterizes the role of ephrinB2 in hESC fate. First, we functionally confirmed that ephrinB2 is a marker of hESCs using a recently engineered NiV envelope pseudotyped lentivirus. Next, we found that ephrinB2 expression is heterogeneous within hESC cultures. Future studies will determine whether ephrinB2 marks hESCs primed towards differentiation into a specific lineage. Lastly, manipulation of ephrinB2 signaling enhanced expression of genes characteristic of mesendoderm progenitors, and inhibited expression of genes involved in neuro-ectoderm specification. Overall, the findings of this dissertation can be used to improve directed differentiation of hESCs into specific cell types for use in regenerative medicine.

References

1 Adewumi, O. *et al.* Characterization of human embryonic stem cell lines by the International Stem Cell Initiative. *Nat Biotechnol* **25**, 803-816, doi:10.1038/nbt1318 (2007).

2 Osafune, K. *et al.* Marked differences in differentiation propensity among human embryonic stem cell lines. *Nat Biotechnol* **26**, 313-315, doi:10.1038/nbt1383 (2008).

3 Laslett, A. L. *et al.* Transcriptional analysis of early lineage commitment in human embryonic stem cells. *BMC Dev Biol* **7**, 12, doi:10.1186/1471-213x-7-12 (2007).

4 Hough, S. R., Laslett, A. L., Grimmond, S. B., Kolle, G. & Pera, M. F. A continuum of cell states spans pluripotency and lineage commitment in human embryonic stem cells. *PLoS One* **4**, e7708, doi:10.1371/journal.pone.0007708 (2009).

5 Enver, T. *et al.* Cellular differentiation hierarchies in normal and culture-adapted human embryonic stem cells. *Hum Mol Genet* **14**, 3129-3140, doi:10.1093/hmg/ddi345 (2005).

6 King, F. W. *et al.* Subpopulations of human embryonic stem cells with distinct tissue-specific fates can be selected from pluripotent cultures. *Stem Cells Dev* **18**, 1441-1450, doi:10.1089/scd.2009.0012 (2009).

7 Ivanova, N. B. *et al.* A stem cell molecular signature. *Science* **298**, 601-604, doi:10.1126/science.1073823 (2002).

8 Wang, Z. *et al.* Ephrin receptor, EphB4, regulates ES cell differentiation of primitive mammalian hemangioblasts, blood, cardiomyocytes, and blood vessels. *Blood* **103**, 100-109, doi:10.1182/blood-2003-04-1063 (2004).

9 Murry, C. E. & Keller, G. Differentiation of embryonic stem cells to clinically relevant populations: lessons from embryonic development. *Cell* **132**, 661-680, doi:10.1016/j.cell.2008.02.008 (2008).

10 Vallier, L. *et al.* Early cell fate decisions of human embryonic stem cells and mouse epiblast stem cells are controlled by the same signalling pathways. *PLoS One* **4**, e6082, doi:10.1371/journal.pone.0006082 (2009).

11 Cohen, D. E. & Melton, D. Turning straw into gold: directing cell fate for regenerative medicine. *Nat Rev Genet* **12**, 243-252, doi:10.1038/nrg2938 (2011).

12 Pasquale, E. B. Eph-ephrin promiscuity is now crystal clear. *Nat Neurosci* **7**, 417-418, doi:10.1038/nn0504-417 (2004).

13 Bowden, T. A. *et al.* Structural plasticity of eph receptor A4 facilitates cross-class ephrin signaling. *Structure* **17**, 1386-1397, doi:10.1016/j.str.2009.07.018 (2009).

14 Qin, H. *et al.* Structural characterization of the EphA4-Ephrin-B2 complex reveals new features enabling Eph-ephrin binding promiscuity. *J Biol Chem* **285**, 644-654, doi:10.1074/jbc.M109.064824 (2010).

15 Singla, N. *et al.* Crystal structure of the ligand-binding domain of the promiscuous EphA4 receptor reveals two distinct conformations. *Biochem Biophys Res Commun* **399**, 555-559, doi:10.1016/j.bbrc.2010.07.109 (2010).

16 Kullander, K. *et al.* Kinase-dependent and kinase-independent functions of EphA4 receptors in major axon tract formation in vivo. *Neuron* **29**, 73-84 (2001).

17 Kramer, E. R. *et al.* Cooperation between GDNF/Ret and ephrinA/EphA4 signals for motor-axon pathway selection in the limb. *Neuron* **50**, 35-47, doi:10.1016/j.neuron.2006.02.020 (2006).

18 Grunwald, I. C. *et al.* Hippocampal plasticity requires postsynaptic ephrinBs. *Nat Neurosci* **7**, 33-40, doi:10.1038/nn1164 (2004).

19 Khodosevich, K., Watanabe, Y. & Monyer, H. EphA4 preserves postnatal and adult neural stem cells in an undifferentiated state in vivo. *J Cell Sci* **124**, 1268-1279, doi:10.1242/jcs.076059 (2011).

20 Ogawa, K. *et al.* The ephrin-A1 ligand and its receptor, EphA2, are expressed during tumor neovascularization. *Oncogene* **19**, 6043-6052, doi:10.1038/sj.onc.1204004 (2000).

21 Negrete, O. A. *et al.* Two key residues in ephrinB3 are critical for its use as an alternative receptor for Nipah virus. *PLoS Pathog* **2**, e7, doi:10.1371/journal.ppat.0020007 (2006).